# Cell-type specific contributions to Rett Syndrome: neuronal and astrocytic signaling and sensory processing

by

Rodrigo I. Garcia

B.S. Biological Sciences
Florida International University, 2008

SUBMITTED TO THE DEPARTMENT OF BRAIN AND COGNITIVE SCIENCES IN PARTIAL FULFILLMENT OF THE REQUIREMENTS FOR THE DEGREE OF

DOCTOR OF PHILOSOPHY IN NEUROSCIENCE
AT THE
MASSACHUSETTS INSTITUTE OF TECHNOLOGY
JUNE 2016



Signature of Author: Signature redacted
Department of Brain and Cognitive Sciences
May 4, 2016

Certified by: Signature redacted
Mriganka Sur
Paul E. and Lilah Newton Professor of Neuroscience
Thesis Supervisor

Accepted by: Signature redacted
Matthew A. Wilson
Sherman Fairchild Professor of Neuroscience and Picower Scholar
Director of Graduate Education for Brain and Cognitive Sciences

# Cell-type specific contributions to Rett Syndrome: neuronal and astrocytic signaling and sensory processing

By

Rodrigo I. Garcia

Submitted to the Department of Brain and Cognitive Sciences on May 20th, 2016
in Partial Fulfillment of the Requirements for the Degree of
Doctor of Philosophy in Neuroscience

## ABSTRACT

Loss of function mutations in the X-linked gene encoding for MeCP2 are the underlying genetic cause for Rett Syndrome (RTT), a devastating neurodevelopmental disorder that primarily affects girls. While the function of this transcriptional regulator remains elusive and complex, recent focus has turned to downstream signaling pathways as putative targets for novel therapeutics. The complexity of MeCP2 function is compounded by the heterogeneity of cell types in the brain, with recent evidence implicating glia cells in RTT pathophysiology. The focus of my thesis has been two-fold: exploring signaling mechanisms downstream of MeCP2 and the potential of IGF-1 as a therapeutic for RTT, and examining functional astrocyte sensory processing in healthy and impaired circuits. I present evidence that IGF-1 levels are reduced in mouse models of RTT and systemic treatment with IGF-1 leads to improvements in lifespan, respiratory patterns, and social behaviors. These effects are accompanied by increased synaptic proteins, activation of signaling pathways, and enhanced excitatory transmission, as well as effects on plasticity in visual cortex circuits. Astrocytes, known to contribute to synapse formation and maintenance, have been implicated alongside neurons as contributors to the RTT phenotype. They express the two most abundant glutamate transporters in the brain responsible for the majority of glutamate clearance from synapses. Indeed, lack of MeCP2 in astrocytes leads to a reduction in signaling pathways and aberrant glutamate transporter expression, with strong implications for synaptic and circuit activity. Efficient processing of visual information requires processing salient features while overcoming the inherent variability in neuronal networks. Natural movies evoke reliable responses from pyramidal neurons in visual cortex and my work reveals that discrete microdomain regions of visual cortex astrocytes also exhibit temporally reliable and spatially correlated responses to natural scenes. I show that glutamate transporters, which influence astrocytic $Ca^{2+}$ signaling and synaptic transmission, regulate the reliability of astrocyte microdomain responses and thus contribute crucially to visual information processing. Finally, I show that in a RTT mouse model, astrocyte microdomains elicited by visual stimuli are reduced in size, consistent with the reduced synaptic transmission and neuronal responses observed in these mice.

Thesis Supervisor: Mriganka Sur, Ph.D.
Title: Paul E. and Lilah Newton Professor of Neuroscience

Acknowledgements

I am very grateful to the many individuals who have provided support and guidance throughout grad school. My thesis advisor, Mriganka Sur, has been a wonderful mentor and staunch supporter of all my endeavors in the lab. His intellect, enthusiasm, and encouragement constantly challenged and shaped my development as a scientist. My thesis committee members, Guoping Feng, Troy Littleton, and Beth Stevens, have provided invaluable insight and feedback throughout this process and have helped shape my thoughts and approaches to my experiments and results. The members of the Sur lab, past and present, have made working here a great experience, and I have benefitted immensely from my interactions with them over the years: Travis Emery, Jorge Castro, and Sally Kwok, and especially Jeremy Petravicz who's knowledge and discussions continuously contributed to my thinking and development. A special thank you to Mandana Sassanfar, without who's tireless efforts I would have never attended the summer internship at MIT which set me on this course.

My parents have made sacrifices that I will never be able to fully appreciate and will never have to experience myself. Their determination to find a better life for my siblings and I lead them to traverse many obstacles and national boundaries. The life and opportunities that I have had would never have been possible without their sacrifices. And to them I dedicate this thesis, which is culmination of many scientific curiosities pursued over many years and through a winding path both geographical and intellectual. We have profoundly different views on how and why we find ourselves on this planet, yet their support has been unwavering and unconditional. They are proud of me and that makes me happy.

Of course, scientific curiosity and intellectual development can only be fostered by the contributions, great and small, of many individuals. I would like to name just a few. My undergraduate advisor, Dr. Lidia Kos at Florida International University, allowed me to explore the foreign realms of laboratory research and nurtured my fascination with biological mechanism that still drive me to this day. Sian Evans was the director of the DuMond Center for Primates and Tropical Forests in Miami, FL. where I worked and cared for a colony of owl monkeys, the only nocturnal new world primate species. I was lured back to academic world by simple and yet profoundly stimulating conversations with a few friends at the time studying philosophy and art. Amanda Brovold, Tony Dennis, and Daniel Clapp convinced me of my desire for intellectual discourse and completely side-railed an otherwise burgeoning career in tech support. For which I am eternally thankful.

Lastly, but certainly not least, are the friendships that I have been fortunate enough to forge and which have been nothing short of my extended family while in Cambridge: Francesca Ramirez, Lawrence De Geest, Christopher Saenz, Laura Lewis, Jakob Voigts, Alix Lacoste, John McCoy, and Sangyu Xu, Brian Sosa

Finally, Danielle Feldman, who is a more important part of my grad school years as any experiment or result will ever be and who made my experiences immeasurably better.

# Table of Contents

# Chapter 1: Introduction

## 1.1 Rett Syndrome

Rett Syndrome (RTT) is a postnatal neurodevelopmental disorder that primarily affects girls. Originally identified by Austrian physician, Dr. Andreas Rett, the disorder did not get much attention until the 1980's with the publication by Hagberg *et al.* that presented 35 patients with a unique developmental disorder and which they chose to name in honor of Dr. Rett (Hagberg et al., 1983). It is estimated that RTT affects every 1 in 10,000 to 15,000 live female births (Chahrour and Zoghbi, 2007). The devastating symptoms of this disorder are preceded by a seemingly initial normal period of development of the patients. At around 12-18 months of age, however, the onset of symptoms is marked by a deceleration of head growth, often leading to microcephaly, followed by growth retardation, weight loss, and muscle hypotonia. Rapid regression follows, with symptoms including social behavioral abnormalities that can be often diagnosed as autistic including a lack of responsiveness to surroundings and social cues, loss of language and motor skills, and mental deterioration. Breathing anomalies and cardiac complications soon develop and most patients will experience mild to severe seizures during childhood and teenage years. Currently, there is no cure for RTT with patients receiving treatment to manage specific symptoms.

A landmark breakthrough was made by the Zoghbi group in 1999 with the identification of mutations in the X-linked gene encoding methyl-CpG-binding protein-2 (MeCP2) as the cause of RTT (Amir et al., 1999). The gene was first isolated in the laboratory of Adrian Bird as a transcriptional repressor that binds to methylated CpG

islands on DNA to change chromatin structure (Lewis et al., 1992). It is estimated that 95% of RTT patients show mutations in MeCP2 that are sporadic in nature, as screenings of the parental genes do not show any mutations. After binding to methyl-CpG islands, it recruits other known corepressors such as Sin3A and histone deacetylases (HDAC1 and 2) through its transcription repressor domain (TRD). However, it is now understood that its transcriptional regulation is much more complex. For example, Chahrour *et al.* demonstrated that MeCP2 could also form a complex with cAMP responsive element binding protein 1 (CREB1) and act as an activator of gene transcription. Gene array analysis of both KO and over-expression of MeCP2 found that many genes are up-regulated after loss of MeCP2 and yet many others are down-regulated with increased expression (Chahrour et al., 2008).

## 1.2 Mouse models of RTT

Several mouse models have been generated that recapitulate most of the phenotypes observed in RTT pathologies. Using the Cre/lox system to control expression, these models have provided insight into the function of MeCP2 through complete or conditional loss of expression, as well as the overexpression of MeCP2 (Chen et al., 2001; Guy et al., 2001; Collins et al., 2004; Luikenhuis et al., 2004; Giacometti et al., 2007). In humans, there is a period of normal development for the first 6 to 18 months, followed by the onset of symptoms. Embryonic knock out models (MeCP2 $^{-/y}$) have a seemingly normal development for the first 4-5 weeks and become symptomatic soon thereafter with stiff gaits, disheveled coats, labored breathing, tremors and seizures. Behavioral phenotypes include increased anxiety, decreased

social interactions, and deficits to learning and memory (Calfa et al., 2011). Male hemizygous mice (MeCP2 $^{-/y}$) have reduced lifespans of ~8 weeks while heterozygous females (MeCP2 $^{-/+}$) have a milder phenotype with a much later onset. In both sexes, the severity of symptoms increases with age. These models provide a robust toolbox for investigation into RTT neuropathology, as many of the clinical features map onto the models and allow for extensive genetic and pharmacological manipulations and measurements. More significant yet, they clearly demonstrate that effects of MeCP2 loss are reversible.

Evidence from human and animal model RTT brains strongly suggests an arrested developmental phenotype. One phenotypic hallmark of RTT patients is decreased head growth with brain weight and volume significantly reduced (Armstrong, 2002). Histological analysis has shown that cortical neurons are also smaller and more densely packed and often have abnormal morphologies (Armstrong *et al.* 1999). Examination of autopsy brains of RTT patients show signs of immature synapses and neuronal maturation. In mouse models, MeCP2 expression increases in postnatal development, with peak expression occurring in maturing neurons and before synaptogenesis (Shahbazian et al., 2002; Armstrong, 2005). In both human patients and in RTT mouse models, there is reduced dendritic arborization and of the dendritic marker MAP2, as well as reduced indicators of excitatory synapses such as PSD-95 – all of which have the hallmark of neuronal connections in an immature or undeveloped state. These findings support the idea that MeCP2 regulates factors and pathways that contribute to neuronal and synaptic maturation.

## 1.3 Signaling Pathways in RTT

Neurotrophins (NT) are selectively expressed in the nervous system and act as a mediators of synaptic development, maturation, and plasticity (Poo, 2001). This group of secretory proteins includes nerve growth factor (NGF), NT3 and NT4/5, and brain-derived neurotrophic factor (BDNF). The binding and activation of their respective tyrosine receptor kinases (Trk) leads to kinase activity initiating downstream effects through the MAPK, PI3K, or PLC-γ signaling pathway. BDNF has been extensively studied and it is known to regulate synaptic proteins, promote maturation of the synapse, and is implicated in proper induction and maintenance of long-term potentiation (LTP) (Korte et al., 1996; Huber et al., 1998; Lu, 2003). It was these observations along with the activity-dependent nature of BDNF that prompted researchers to investigate how MeCP2 could potentially affect these types of genes.

Early studies demonstrated that MeCP2 regulates basal BDNF expression in cultured neurons and that neuronal activity leads to a decreased binding of MeCP2 on BDNF promoter III (Chen et al., 2003). This implies that at basal activity levels, MeCP2 mutant mice should show higher levels of BDNF expression – which turns out not to be the case. Two reasons have been proposed to explain this contradiction. First, the assumption that both a wild type brain and a MeCP2 deficient brain have the same level of neuronal activity has been questioned and there is evidence for reduced cortical activity in mutant mice (Chang et al., 2006). Second, MeCP2 also regulates the transcriptional repressors REST and CoREST that in turn bind to the promoter regions of BDNF. The absence of MeCP2 leads to an increase in REST/CoREST, which in turn down-regulate BDNF levels (Abuhatzira et al., 2007). These lines of research support a

role for MeCP2 in direct and indirect regulation of BDNF expression and help establish the link between signaling transduction pathways and RTT neuropathology.

Indeed, mice deficient in BDNF expression have been shown to demonstrate similar behavioral phenotypes as MeCP2 KO models. Chang *et al.* demonstrated that a double BDNF and MeCP2 KO model had an earlier onset of disease phenotype and that overexpression of BDNF in MeCP2 mutant mice reversed some of these RTT like phenotypes, including locomotor deficits and even extending the lifespan of the mutant mice (Chang et al., 2006). The effects of altered BDNF expression is mediated through the downstream signaling pathways it regulates and the potential to ameliorate the effects of RTT exist in factors that can impact the activation of these pathways. Yet the molecular connection between MeCP2-dependent regulation of BDNF expression and its effect on synaptic function has yet to be explored. As mentioned, BDNF acts through cellular signaling pathways and the evidence presented thus far warrants a closer look at one in particular.

A central molecular pathway implicated in RTT syndrome is the PI3K/Akt pathway. The hallmarks of MeCP2 loss of function – synaptic plasticity, dendritic morphology, and neuronal size - are downstream effectors of this pathway. Activation of this pathway is essential during normal brain development. Its downstream targets include regulation of protein synthesis involved in synaptic plasticity through the mammalian target of rapamycin (mTOR) kinase (Hoeffer and Klann, 2010), control of proper brain growth, promoting growth and branching of dendrites (Jaworski, 2005), and activation of the scaffolding protein and indicator of synaptic maturation, PSD-95. The latter is essential in postsynaptic synapses for anchoring NMDA and AMPA

receptors and is up-regulated through both BDNF and insulin activation of the PI3K/Akt pathway (Lee et al., 2005; Yoshii and Constantine-Paton, 2007). Researchers found that components of this pathway are down-regulated in different regions of MeCP2 deficient brains (Ricciardi et al., 2011) and previous work from the Sur lab has demonstrated that exogenous activation of this pathway can ameliorate some of the RTT phenotype (Tropea et al., 2009). Recently, using induced pluripotent stem cells (IPSc), researchers demonstrated that neurons with mutations in MeCP2 exhibited impaired AKT/mTOR activity along with impaired protein synthesis and a 3 week treatment period with exogenous BDNF was able to ameliorate protein synthesis via activation of AKT/mTOR signaling (Li et al., 2013). Furthermore, reducing PTEN suppression of AKT/mTOR activity with shRNA also demonstrated a rescue of protein synthesis deficit via the AKT/mTOR pathway in MeCP2 mutant cells. Taken together, dysregulation of this pathway is highly implicated in MeCP2 deficient brains and reactivation poses a viable mechanistic therapeutic.

## 1.4 IGF-1 Activation of Signaling Pathways

A major activator of this pathway, and therefore a potential therapeutic, is found in insulin-like growth factor-1 (IGF-1). IGF-1 acts primarily through activation of its cognate receptor (IGF-IR) to initiate signaling through the PI3K/Akt pathway and exert its neurotrophic and neuromodulatory effects (Torres-Aleman, 1999; 2010). The early influence of IGF-1 on the CNS is seen during neuronal development and research has shown its ability to promote neuronal differentiation and maturation, and in the absence of functional receptors, can lead to premature death (Collett-Solberg and

Cohen, 2000; Liu et al., 2009). The receptor for IGF-1(IGF1R) is widely expressed in various brain regions from the brain stem to cortex, IGF-1 sources include neuronal subpopulations, microglia, and into the CNS from serum levels in a neuronal activity-dependent manner (Bondy and Lee, 1993; Lee et al., 1993; Bondy and Cheng, 2004; Nishijima et al., 2010). Studies looking at the roles of serum IGF-1 and brain IGF-1 have indicated separate, but important roles for each in normal brain development (Davila et al., 2007; Liu et al., 2009). Several binding proteins tightly regulate its activity and promote a longer half-life in serum. IGFBP3 is the primary binding protein regulating the activity of IGF-1 in the brain and in $MeCP2^{-/y}$ animals there is a significant increase in levels of this binding protein (Itoh et al., 2007). Furthermore, the activity of IGF-1 can influence the activity of BDNF (McCusker et al., 2006), thereby establishing a potential role in rescuing the effects on BDNF due to MeCP2 loss. Previous work from our lab demonstrated the ability of a shortened, tri-peptide form of this signaling molecule to ameliorate some of the phenotypes observed in RTT models (Tropea et al., 2009). Finally, the therapeutic potential of IGF-1 is bolstered by the fact that, unlike BDNF, it is capable of crossing the blood-brain barrier (BBB) and has been approved for use in human clinical trials.

Thus, the activation of the PI3K/Akt pathway sits at a crucial junction of cellular mechanisms that can be probed as a therapeutic in RTT. Through the regulation of BDNF, MeCP2 directly affects the activation of this pathway. The link between BDNF and maturation of excitatory synapses leading to PSD-95 activity supports the immature synaptic and circuits hypothesis of RTT. IGF-1 can directly activate the

PI3K/Akt pathway, and MeCP2 indirectly regulates the activity of this ligand through control of IGFBP3 expression.

## 1.5 Astrocytes in RTT

PI3K/Akt pathway is also directly linked to the function of non-neuronal cells, specifically astrocytes. Understanding of the role of astrocytes in the function and diseases of the CNS has increased greatly over the last couple of decades (Barres, 2008). During development, astrocytes can promote and regulate synaptogenesis and contribute to the maturation of dendritic spines (Haydon, 2001; Nishida and Okabe, 2007; Theodosis et al., 2008; Perea et al., 2009). One major contribution by astrocytes is the removal of glutamate at the synapse through transporters. In the CNS, glutamate plays a role in excitatory synapses during normal brain function such as learning and memory, and during development in induction and elimination of synapses (Danbolt, 2001; Allen and Barres, 2009; Chung et al., 2015). It is estimated that 90% of the clearance of this neurotransmitter is provided by glutamate transporter-1 (GLT-1).

Initial studies reported a lack of MeCP2 expression in glial cells, however, recent evidence has firmly established its expression in astrocytes and that loss of this MeCP2 expression in astrocytes can induce RTT-like features in neurons. Wild type neurons cultured with MeCP2-null astrocytes developed aberrant dendritic morphologies akin to those seen in MeCP2-null neurons (Ballas et al., 2009; Maezawa et al., 2009). Conversely, MeCP2-null neurons cultured with wild type astrocytes developed normal dendritic morphologies. Recent mouse models in which MeCP2 is selectively re-activated in astrocytes were able to ameliorate several disease

phenotypes and substantially improve survival (Lioy et al., 2011). This evidence strongly suggests that lack of functional MeCP2 in astrocytes has a direct, and as of yet unknown, effect on the proper maturation of neurons and synaptic function that may underlie the pathogenesis of RTT. The role of astrocytes in RTT pathogenesis remains unclear, in particular their contributions in vivo.

## 1.6 Astrocytic Visual Processing

Primary visual cortex integrates simple sensory information into more complex features and is an excellent model system to examine mechanisms of neuronal representations and plasticity. The establishment and efficient functioning of circuits in the visual cortex depends critically on a complex balance of excitatory and inhibitory drive (Gordon and Stryker, 1996; Fagiolini and Hensch, 2000; Hensch, 2005). One mechanism by which astrocytes contribute to the balance of excitatory and inhibitory drive is through the clearance of synaptically released glutamate; indeed, astrocytes in ferret visual cortex are crucial to maintaining orientation-selective responses in neurons and astrocytes. Tuned astrocytes responses reflect those of nearby neurons and pharmacological blocking of GLUTs abolishes orientation selective $Ca^{2+}$ responses to visual stimuli (Schummers et al., 2008). Furthermore, the fine, distal processes of astrocytes can make contacts with thousands of synapses and are implicated in the modulation of neuronal excitability (Bushong et al., 2003; Haber et al., 2006; Witcher et al., 2010), yet the mechanisms by which this carried out, and in particular how sensory-driven $Ca^{2+}$ signals in astrocytes are integrated are not well understood (Khakh and Mccarthy, 2015; Bazargani and Attwell, 2016). Thus an understanding of astrocyte-

specific deficits in normal function and in brain disorders during *in vivo* sensory processing can provide both a better understanding of their contribution to MeCP2-induced deficits as well as their normal interaction with neuronal networks.

## 1.7 Overview of Thesis

In chapter two of this thesis, we present evidence that IGF-1 levels are reduced in MeCP2 mouse models, and that systemic treatment with recombinant human IGF-1 leads to improved lifespan, locomotor activity, heart rate, respiratory patterns, and social behaviors. We also demonstrate that treatment ameliorates deficits at the synaptic, cellular, and circuit level. Chapter three investigates $Ca^{2+}$ signaling in astrocytes of the rodent visual cortex and establishes methods to examine the spatial and temporal coding of astrocytic signaling. We find that discrete structural regions containing microdomain activity respond to visual sensory drive. Furthermore, we report the novel finding that natural scenes can evoke more robust and reliable responses in microdomains of astrocytes as compared to drifting gratings, echoing the effect observed in pyramidal neuronal networks of primary visual cortex. We also show that *in vivo* reduction of GLT-1 modulates these phenomena. Chapter four examines the effects of loss of MeCP2 on astrocyte signaling pathways, glutamate transporter availability, and visually evoked responses in MeCP2 deficient circuits. We report the novel finding that GLT-1 is dysregulated in MeCP2-deficient astrocytes and the demonstrate effects on visually-evoked microdomain $Ca^{2+}$ activity.

## 1.8 References Cited


Abuhatzira L, Makedonski K, Kaufman Y, Razin A, Shemer R (2007) MeCP2 Deficiency in the Brain Decreases BDNF Levels by REST/CoREST-Mediated Repression and Increases TRKB Production. Epigenetics 2:214–222.

Allen N, Barres B (2009) Glia and Synapse Formation: An Overview. Encyclopedia of Neuroscience: Glia and Synapse Formation: An Overview:731–736.

Amir RE, Van den Veyver IB, Wan M, Tran CQ, Francke U, Zoghbi HY (1999) Rett syndrome is caused by mutations in X-linked MECP2, encoding methyl-CpG-binding protein 2. Nature Genetics 23:185–188.

Armstrong DD (2002) Neuropathology of Rett syndrome. Ment Retard Dev Disabil Res Rev 8:72–76.

Armstrong DD (2005) Neuropathology of Rett syndrome. J Child Neurol 20:747–753.

Ballas N, Lioy DT, Grunseich C, Mandel G (2009) Non-cell autonomous influence of MeCP2-deficient glia on neuronal dendritic morphology. Nat Neurosci 12:311–317.

Barres BA (2008) The Mystery and Magic of Glia: A Perspective on Their Roles in Health and Disease. Neuron.

Bazargani N, Attwell D (2016) Astrocyte calcium signaling: the third wave. Nat Neurosci 19:182–189.

Bondy CA, Cheng CM (2004) Signaling by insulin-like growth factor 1 in brain. Eur J Pharmacol 490:25–31.

Bondy CA, Lee WH (1993) Patterns of insulin-like growth factor and IGF receptor gene expression in the brain. Functional implications. Ann N Y Acad Sci 692:33–43.

Bushong E, Martone M, Ellisman M (2003) Examination of the relationship between astrocyte morphology and laminar boundaries in the molecular layer of adult dentate gyrus. J Comp Neurol 462:241–251.

Calfa G, Percy AK, Pozzo-Miller L (2011) Experimental models of Rett syndrome based on Mecp2 dysfunction. Exp Biol Med 236:3–19.

Chahrour M, Jung SY, Shaw C, Zhou X, Wong STC, Qin J, Zoghbi HY (2008) MeCP2, a Key Contributor to Neurological Disease, Activates and Represses Transcription. Science 320:1224–1229.

Chahrour M, Zoghbi HY (2007) The story of Rett syndrome: from clinic to neurobiology. Neuron 56:422–437.

Chang Q, Khare G, Dani V, Nelson SB, Jaenisch R (2006) The disease progression of Mecp2 mutant mice is affected by the level of BDNF expression. Neuron 49:341–348.

Chen RZ, Akbarian S, Tudor M, Jaenisch R (2001) Deficiency of methyl-CpG binding protein-2 in CNS neurons results in a Rett-like phenotype in mice. Nature Genetics 27:327–331 Available at: http://www.nature.com/ng/journal/v27/n3/full/ng0301_327.html.

Chen WG, Chang Q, Lin Y, Meissner A, West AE, Griffith EC, Jaenisch R, Greenberg ME (2003) Derepression of BDNF transcription involves calcium-dependent phosphorylation of MeCP2. Science 302:885–889.

Chung W-S, Allen NJ, Eroglu C (2015) Astrocytes Control Synapse Formation, Function, and Elimination. Cold Spring Harbor Perspectives in Biology.

Collett-Solberg PF, Cohen P (2000) Genetics, Chemistry, and Function of the IGF/IGFBP System. ENDO 12:121–136.

Collins AL, Levenson JM, Vilaythong AP, Richman R, Armstrong DL, Noebels JL, David Sweatt J, Zoghbi HY (2004) Mild overexpression of MeCP2 causes a progressive neurological disorder in mice. Human Molecular Genetics 13:2679–2689.

Danbolt NC (2001) Glutamate uptake. Progress in Neurobiology 65:1–105.

Davila D, Piriz J, Trejo JL, Nuñez A, Torres-Aleman I (2007) Insulin and insulin-like growth factor I signalling in neurons. Front Biosci 12:3194–3202.

Fagiolini M, Hensch TK (2000) Inhibitory threshold for critical-period activation in primary visual cortex. Nature 404:183–186.

Giacometti E, Luikenhuis S, Beard C, Jaenisch R (2007) Partial rescue of MeCP2 deficiency by postnatal activation of MeCP2. P Natl Acad Sci Usa 104:1931–1936.

Gordon J, Stryker M (1996) Experience-dependent plasticity of binocular responses in the primary visual cortex of the mouse. Journal of Neuroscience 16:3274–3286.

Guy J, Hendrich B, Holmes M, Martin JE, Bird A (2001) A mouse Mecp2-null mutation causes neurological symptoms that mimic Rett syndrome. Nature Genetics 27:322–326.

Haber M, Zhou L, Murai KK (2006) Cooperative astrocyte and dendritic spine dynamics at hippocampal excitatory synapses. Journal of Neuroscience 26:8881–8891.

Hagberg B, Aicardi J, Dias K, Ramos O (1983) A Progressive Syndrome of Autism, Dementia, Ataxia, and Loss of Purposeful Hand Use in Girls - Retts Syndrome - Report of 35 Cases. Ann Neurol 14:471–479.

Haydon PG (2001) Glia: listening and talking to the synapse. Nat Rev Neurosci.

Hensch TK (2005) Critical period plasticity in local cortical circuits. Nat Rev Neurosci 6:877–888.

Hoeffer CA, Klann E (2010) mTOR signaling: at the crossroads of plasticity, memory and disease. Trends in Neurosciences 33:67–75.

Huber KM, Sawtell NB, Bear MF (1998) Brain-derived neurotrophic factor alters the synaptic modification threshold in visual cortex. Neuropharmacology 37:571–579.

Itoh M, Ide S, Takashima S, Kudo S, Nomura Y, Segawa M, Kubota T, Mori H, Tanaka S, Horie H, Tanabe Y, Goto Y-I (2007) Methyl CpG-binding protein 2 (a mutation of which causes Rett syndrome) directly regulates insulin-like growth factor binding protein 3 in mouse and human brains. J Neuropath Exp Neur 66:117–123.

Jaworski J (2005) Control of Dendritic Arborization by the Phosphoinositide-3'-Kinase-Akt-Mammalian Target of Rapamycin Pathway. Journal of Neuroscience 25:11300–11312.

Khakh BS, Mccarthy KD (2015) Astrocyte Calcium Signaling: From Observations to Functions and the Challenges Therein. Cold Spring Harbor Perspectives in Biology.

Korte M, Griesbeck O, Gravel C, Carroll P, Staiger V, Thoenen H, Bonhoeffer T (1996) Virus-mediated gene transfer into hippocampal CA1 region restores long-term potentiation in brain-derived neurotrophic factor mutant mice. P Natl Acad Sci Usa 93:12547–12552.

Lee C-C, Huang C-C, Wu M-Y, Hsu K-S (2005) Insulin stimulates postsynaptic density-95 protein translation via the phosphoinositide 3-kinase-Akt-mammalian target of rapamycin signaling pathway. J Biol Chem 280:18543–18550.

Lee WH, Michels KM, Bondy CA (1993) Localization of insulin-like growth factor binding protein-2 messenger RNA during postnatal brain development: correlation with insulin-like growth factors I and II. Neuroscience 53:251–265.

Lewis JD, Meehan RR, Henzel WJ, Maurer-Fogy I, Jeppesen P, Klein F, Bird A (1992) Purification, sequence, and cellular localization of a novel chromosomal protein that binds to methylated DNA. Cell 69:905–914.

Li Y, Wang H, Muffat J, Cheng AW, Orlando DA, Lovén J, Kwok S-M, Feldman DA, Bateup HS, Gao Q, Hockemeyer D, Mitalipova M, Lewis CA, Vander Heiden MG, Sur M, Young RA, Jaenisch R (2013) Global Transcriptional and Translational Repression in Human-Embryonic-Stem-Cell-Derived Rett Syndrome Neurons. Cell Stem Cell 13:446–458.

Lioy DT, Garg SK, Monaghan CE, Raber J, Foust KD, Kaspar BK, Hirrlinger PG, Kirchhoff F, Bissonnette JM, Ballas N, Mandel G (2011) A role for glia in the progression of Rett's syndrome. Nature.

Liu W, Ye P, O'Kusky JR (2009) Type 1 insulin-like growth factor receptor signaling is essential for the development of the hippocampal formation and dentate gyrus. Journal of

Neuroscience.

Lu B (2003) BDNF and activity-dependent synaptic modulation. Learn Mem 10:86–98.

Luikenhuis S, Giacometti E, Beard CF, Jaenisch R (2004) Expression of MeCP2 in postmitotic neurons rescues Rett syndrome in mice. P Natl Acad Sci Usa 101:6033–6038.

Maezawa I, Swanberg S, Harvey D, LaSalle JM, Jin L-W (2009) Rett syndrome astrocytes are abnormal and spread MeCP2 deficiency through gap junctions. Journal of Neuroscience 29:5051–5061.

McCusker RH, McCrea K, Zunich S, Dantzer R, Broussard SR, Johnson RW, Kelley KW (2006) Insulin-like growth factor-I enhances the biological activity of brain-derived neurotrophic factor on cerebrocortical neurons. J Neuroimmunol 179:186–190.

Nishida H, Okabe S (2007) Direct astrocytic contacts regulate local maturation of dendritic spines. Journal of Neuroscience 27:331–340.

Nishijima T, Piriz J, Duflot S, Fernandez AM, Gaitan G, Gomez-Pinedo U, Verdugo JMG, Leroy F, Soya H, Nuñez A, Torres-Aleman I (2010) Neuronal activity drives localized blood-brain-barrier transport of serum insulin-like growth factor-I into the CNS. Neuron 67:834–846.

Perea G, Navarrete M, Araque A (2009) Tripartite synapses: astrocytes process and control synaptic information. Trends in Neurosciences 32:421–431.

Poo MM (2001) Neurotrophins as synaptic modulators. Nat Rev Neurosci 2:24–32.

Ricciardi S, Boggio EM, Grosso S, Lonetti G, Forlani G, Stefanelli G, Calcagno E, Morello N, Landsberger N, Biffo S, Pizzorusso T, Giustetto M, Broccoli V (2011) Reduced AKT/mTOR signaling and protein synthesis dysregulation in a Rett syndrome animal model. Human Molecular Genetics 20:1182–1196.

Schummers J, Yu H, Sur M (2008) Tuned Responses of Astrocytes and Their Influence on Hemodynamic Signals in the Visual Cortex. Science 320:1638–1643.

Shahbazian MD, Antalffy B, Armstrong DL, Zoghbi HY (2002) Insight into Rett syndrome: MeCP2 levels display tissue- and cell-specific differences and correlate with neuronal maturation. Human Molecular Genetics 11:115–124.

Theodosis DT, Poulain DA, Oliet SHR (2008) Activity-dependent structural and functional plasticity of astrocyte-neuron interactions. Physiological Reviews 88:983–1008.

Torres-Aleman I (1999) Insulin-like growth factors as mediators of functional plasticity in the adult brain. Horm Metab Res 31:114–119.

Torres-Aleman I (2010) Toward a comprehensive neurobiology of IGF-I. Dev Neurobiol 70:384–

396.

Tropea D, Giacometti E, Wilson NR, Beard C, McCurry C, Fu DD, Flannery R, Jaenisch R, Sur M (2009) Partial reversal of Rett Syndrome-like symptoms in MeCP2 mutant mice. P Natl Acad Sci Usa 106:2029–2034.

Witcher MR, Park YD, Lee MR, Sharma S, Harris KM, Kirov SA (2010) Three-dimensional relationships between perisynaptic astroglia and human hippocampal synapses. Glia 58:572–587.

Yoshii A, Constantine-Paton M (2007) BDNF induces transport of PSD-95 to dendrites through PI3K-AKT signaling after NMDA receptor activation. Nat Neurosci 10:702–711.

# Chapter 2: Functional recovery with recombinant human IGF1 treatment in a mouse model of Rett Syndrome[1]

## 2.1 Abstract

Rett Syndrome (RTT) is a neurodevelopmental disorder that arises from mutations in the X-linked gene *MECP2*. MeCP2 has a large number of targets and a wide range of functions, suggesting the hypothesis that functional signaling mechanisms upstream of synaptic and circuit maturation may contribute to our understanding of the disorder and provide insight into potential treatment. Here, we show that insulin-like growth factor-1 (IGF1) levels are reduced in young male MeCP2 null ($MeCP2^{-/y}$) mice, and systemic treatment with recombinant human IGF1 (rhIGF1) improves lifespan, locomotor activity, heart rate, respiration patterns, and social and anxiety behavior. Furthermore, MeCP2 null mice treated with rhIGF1 show increased synaptic and activated signaling pathway proteins, enhanced cortical excitatory synaptic transmission, and restored dendritic spine densities. IGF1 levels are also reduced in older, fully symptomatic heterozygous ($MeCP2^{-/+}$) female mice, and short-term treatment with rhIGF1 in these animals improves respiratory patterns, reduces anxiety levels, and increases exploratory behavior. In addition, rhIGF1 treatment normalizes abnormally prolonged plasticity in visual cortex circuits of adult $MeCP2^{-/+}$ female mice. Our results provide novel characterization of the phenotypic development of Rett Syndrome in a mouse model at the molecular, circuit, and organismal levels

[1] The bulk of these findings have been previously described in Castro J, Garcia RI, *et al.* 2014.

and demonstrate a mechanism-based therapeutic role for rhIGF1 in treating Rett Syndrome.

## 2.2 Introduction

Rett Syndrome (RTT) is a devastating, rare neurodevelopmental disorder that primarily afflicts girls. Over 90% of individuals with RTT have sporadic mutations in the X-linked gene coding for methyl-CpG binding protein 2 (MeCP2). Affected girls are initially asymptomatic, but later develop a wide range of symptoms. Mouse models of RTT with deletion of MeCP2 recapitulate many of the key physiological, autonomic, motor, and cognitive aspects of the disorder (Chahrour and Zoghbi, 2007; Banerjee et al., 2012).

MeCP2 binds widely across the genome and has complex roles that encompass activating or inhibiting gene transcription, repressing methylation, regulating chromatin remodeling and altering non-coding RNAs (Chahrour and Zoghbi, 2007; Chahrour et al., 2008; Banerjee et al., 2012). This wide range of functions has led to the proposal that a focus on functional signaling pathways is needed to drive an understanding of RTT and its possible therapeutics (Chahrour and Zoghbi, 2007; Banerjee et al., 2012; Castro et al., 2013). Several lines of evidence indicate an arrested brain maturation phenotype in RTT, suggesting that loss of functional MeCP2 leads to immature synapses and circuits in the brain (Tropea et al., 2009). Importantly, mouse models have suggested reversibility of specific symptoms once MeCP2 function is restored (Giacometti et al., 2007; Guy et al., 2007). One well-documented target of MeCP2 is brain-derived neurotrophic factor (BDNF), which is known to be critical for neuronal

and synaptic maturation and is downregulated in MeCP2 mutant mice and RTT patients (Chang et al., 2006; Zhou et al., 2006). BDNF exerts influence on neurons and synapses mainly via the phosphoinositide 3-kinase (PI3K)/Akt pathway and the extracellular signal-regulated kinase (ERK) pathways (Yoshii and Constantine-Paton, 2010), which are also downregulated in several brain regions of MeCP2 mutant mice (Ricciardi et al., 2011; Schmid et al., 2012). Overexpression of BDNF has been shown to reverse some symptoms of the mutant phenotype, pointing to the importance of BDNF and its downstream signaling pathways as therapeutic targets for RTT (Chang et al., 2006). Recently, using induced pluripotent stem cells (IPSc), researchers demonstrated that neurons with mutations in MeCP2 exhibited impaired AKT/mTOR activity along with impaired protein synthesis and a 3 week treatment period with exogenous BDNF was able to ameliorate protein synthesis via activation of AKT/mTOR signaling (Li et al., 2013). Furthermore, reducing PTEN suppression of AKT/mTOR activity with shRNA also demonstrated a rescue of protein synthesis deficit via upregulating the AKT/mTOR pathway in MeCP2 mutant cells. Unfortunately, little BDNF is able to traverse the blood brain barrier (BBB), making it unsuitable as a therapeutic agent (Wu and Pardridge, 1999).

Another major activator of the these signaling pathways is insulin-like growth factor-1 (IGF1) which is primarily expressed in the liver and acts in an endocrine fashion throughout the body, crossing the BBB in a neuronal activity-dependent manner (Nishijima et al., 2010); IGF1 is also produced in the brain, especially during early stages of development (Bondy and Cheng, 2004; Fernandez and Torres-Aleman, 2012). A previous study showed that administering the tripeptide fragment Glutamate-

Proline-Glycine (GPE) or (1-3)IGF1, the first 3 (of 70) amino acids of IGF1, to MeCP2 KO mice was effective in correcting several symptoms and restoring key synaptic molecules (Tropea et al., 2009). We have now examined for the first time the effectiveness of full-length IGF1 both in MeCP2 null male ($MeCP2^{-/y}$) and older symptomatic heterozygous female ($MeCP2^{-/+}$) mice (Mellios et al., n.d.). We show that administering full-length, recombinant human IGF1 (rhIGF1, Mecasermin DB01277) to the mutant mice increases IGF1 concentration in serum to near-normal levels and ameliorates a wide range of phenotypes, including organismal and behavioral function, synaptic and circuit plasticity, neuronal structure, and molecular signaling pathways. Together with recent and ongoing clinical trials demonstrating the safety and efficacy of rhIGF1 in treating RTT (Pini et al., 2012; Khwaja et al., 2014), and multiple studies documenting the effectiveness of IGF1 in restoring structural, functional and molecular phenotypes in human iPSC-derived RTT neurons and glia (Marchetto et al., 2010; Li et al., 2013; Williams et al., 2014), our results provide strong mechanistic and preclinical support for the therapeutic role of rhIGF1 in RTT.

## 2.3 Materials and methods

### *2.3.1 Mice.*

All experimental protocols were approved by the Animal Care and Use Committee at Massachusetts Institute of Technology and conformed to National Institutes of Health guidelines. *Mecp2* hemizygous null mice and wild type (WT) littermates were obtained by breeding heterozygous females (Guy et al., 2001) supplied by Jackson Lab on a C57BL/6 (B6.129P2(C)-*Mecp2*$^{tm1.1Bird}$/J, Jackson #003890) background with male mice on the

same background (Jackson #000664). Heterozygous females of ages > 6 months used for testing were obtained directly from Jackson Lab. A total of >150 male and female MeCP2 mice were used for the various assays and measurements. All mice were genotyped as described in the vendor website. Where possible, the genotype of the tested mice was concealed from the investigators while testing was performed. For male mice, the loss of weight and hypoactivity post 4 weeks of age presented limitations to complete lack of genotype knowledge. Similarly, older fully symptomatic heterozygous females were strikingly less motile than WT controls.

### *2.3.2 Dosage.*

Homozygous null mice were grouped with their wild type siblings and housed at 24° C and variable humidity in a 12 hour light cycle (7am-7pm). Animals were weighed and injected i.p. once daily starting on postnatal day 14 (P14) with either vehicle (saline) or 0.25 mg/kg full length (70 aa) recombinant human IGF1 (Peprotech) dissolved in saline with 0.01% BSA (w/v). Due to safety concerns, namely the risk of internal organ damage and the volume of injection that could prove fatal, we considered P14 the earliest age to begin safely injecting the animals. Wild type male mice were euthanized at 15 weeks of age. Hemizygous null mice were terminated when they lost more than 20% of body weight in one week. Heterozygous females were kept in individual home cages and injected with a 10x dose of rhIGF-1 daily for 3 weeks.

### *2.3.3 Behavioral analyses: Social assay.*

Mice were tested in a custom-made social approach apparatus (2) consisting of an acrylic box with a white floor for high contrast and three subdivisions. Each side

compartment contained a clear perforated acrylic cylinder that allowed sniffing and visual interaction between the tested and stimulus mouse. Animals were tested at 5 and 8 weeks of age with unrelated, age- and background-matched wild type stimulus mice. Behavior testing was done during the light cycle at least two hours after injection. The animals were acclimatized by exposing them to the apparatus for 5 minutes for two consecutive days prior to the test. The test animal was first placed in the middle chamber and allowed to freely move for 5 minutes while being video recorded. The test mouse was then removed and a stimulus mouse was placed in the cylinder of one of the side chambers for 5 minutes for acclimatization. The test mouse was immediately reintroduced into the middle chamber and its behavior recorded for 10 minutes. The cage was cleaned thoroughly with Quatricide PV (Pharmacal) after each experiment and a second 5-minute test was recorded after 30 minutes with the same stimulus mouse. Different stimulus mice were used each week.

Video recordings were analyzed with custom-made ImageJ macros that measured the total amount of time spent in each chamber and the number of times that the test animal crossed from one chamber to the other. Only animals with more than 8 crosses were included in the analysis.

### *2.3.4 Behavioral analyses: Anxiety assay.*

Anxiety-related behavior was evaluated on a plus-maze. The maze was made of a solid color smooth acrylic plastic and consisted of a center square (5 cm x 5cm) and four arms: two open without walls and two closed with a 15 cm high wall. Each arm of the maze measured 30 cm long and 5 cm wide and was supported by a 40 cm high

leg. Four week-old animals were placed in the center square always facing to the same open arm and allowed to explore the maze freely for 5 minutes while being videotaped. Mice were not pre-exposed to the set up to avoid test-decay effects due to increased acclimatization to the environment. After the test, the mice were removed from the maze and all the surfaces cleaned with Quatricide before testing the next animal. Amount of time spent in each arm and the number of crossings into the center square were analyzed by custom-made ImageJ macros.

### *2.3.5 Behavioral analysis: Spatial novelty recognition.*

Modified from open field assay previously described (3). For the spatial novelty recognition test, mice were placed in an arena for 6 sessions, each lasting 6 minutes. Between each session mice were transferred to their home cages for 3 minutes and the arena cleaned. During the first session, mice explored the empty area, after which four objects of similar size yet different shapes were added inside. Object exploration was monitored and data collected using video recording above the arena. The mice were allowed to explore the objects during sessions 2-5 and average contact duration with each object was assessed. On the $6^{th}$ session, two objects were spatially rearranged. A performance ratio was calculated as the ratio of the time spent in contact with the displaced objects (DO) vs the non-displaced objects (NDO) during the last trial divided by the ratio of the time spent in contact with the DO vs the NDO during the $4^{th}$ trial.

### *2.3.6 Breath rate and cardiac monitoring.*

Each mouse was tested once a week for two weeks and the data were pooled by age for weeks 4-5 or 7-8. Heart and breath rates were monitored using a pulse oximeter collar sensor (MouseOx, Starr Life Sciences). One day before testing, mice were depilated around the neck for improved sensor readings and blank collar clips were used to acclimatize the animal to the oximeter collar clip prior to each test. Mice were awake and restrained in a tube for 10-minute sessions. Heart rate (beats per minute) and breath rate (breaths per minute) were recorded continuously for each animal by the device, and pooled for group-wide comparisons.

### *2.3.7 Plethysmography recordings of breathing patterns.*

Breathing patterns were recorded in unrestrained and unanesthetized mice using a whole-body flow plethysmograph (EMKA Technologies, Paris, France) in which a constant bias flow supply connected to the animal recording chamber ensured continuous inflow of fresh air (0.8 L/min). Mice were habituated in the plethysmograph chamber to reduce any stress prior to measurements. For each female mouse, the inspiratory time ($T_i$), expiratory time ($T_e$), peak expiratory flow (PEF), and breath holds (defined as $T_e$ times lasting longer than 500 ms) were measured during 12 minute periods, once before treatment began and then again after three weeks of treatment.

### *2.3.8 Locomotion assay: Ambulatory movement.*

Spontaneous locomotor activity was measured with the use of an infrared beam device monitoring movement in a cage (PhenoMaster-Activity XY, TSE Systems, Inc.).

For each experiment, a mouse was acclimatized to the cage for at least 1 hour before recordings started. Movement was measured every minute for 11 hours during the 12 hours dark cycle (7 p.m. to 7 a.m.). The number of beam crossings per minute for each animal was pooled for group-wide comparisons.

### *2.3.9 Western blotting.*

Synaptoneurosomes were prepared as described previously (4). MeCP2 null mice and wild-type controls were decapitated, and the brain tissue extracted and immediately dissected on ice cold PBS. For each brain, half the cortex and cerebellum was homogenized in ice cold homogenization buffer (10 mM HEPES, 2 mM EGTA, 2 mM EDTA, 1% SDS, 1x Phosphatase inhibitor cocktail (Roche), Protease inhibitor cocktail (Roche)) while the other half was homogenized in synaptoneurosome buffer (10 mM HEPES, 2.0 mM EDTA, 2.0 mM EGTA, 150 mM NaCl, Phosphatase inhibitor cocktail (Roche), Protease inhibitor cocktail (Roche)), with 20 even strokes in a glass-glass homogenizer. The synaptoneurosome homogenate was first passed through two 105 µm nylon mesh (Sefar America) filters and then through a 5 µm nitrocellulose filter (Millipore), and finally centrifuged at 1,000 x *g* for 10 minutes at 4 °C. The synaptoneurosome pellet was resuspended in buffer. Aliquots of all the homogenized tissue were stored in -20 °C until SDS-PAGE analysis. BCA protein assay kit (BioRad) was used to determine protein concentration of each homogenate and synaptoneurosome sample.

Whole cell (10 µg) or synaptoneurosome (5 µg) samples were loaded on 4-15% polyacrylamide gels (BioRad), transferred to PVDF membranes (Millipore), and

immunoblotted for protein expression using the following antibodies: total Akt (1:1000, Cell Signaling), phospho (Ser473) Akt (1:500, Cell Signaling), PSD-95 (1:1000, Cell Signaling), total ERK1/2 (1:1000, Cell Signaling), phospho (Thr202/Tyr204) ERK1/2 (1:2000, Cell Signaling), GAPDH (1:4000, Abcam) and Tubulin (1:250,000, Sigma-Aldrich) were used for internal controls. Blots were then incubated with appropriate secondary antibodies coupled to HRP (1:4000, Cell Signaling). Immunoreactive bands were detected by enhanced chemiluminescence (Supersignal West, PicoCL or FemtoCL, Fisher Scientific). Optical densities of detected bands were quantified using ImageJ software. A standard sample of wildtype mouse cortical tissue was run on each gel to gauge blot-to-blot variability.

### *2.3.10 Golgi Stain.*

To measure spine density, P42 male mice were used. Animals were decapitated and brains were dissected out and processed using a Golgi-Cox stain kit (FD Rapid Golgistain, FD Neurotechnologies), following kit protocol. Images were taken in a Zeiss Axioscope with a 63x high numerical aperture (1.4) oil immersion objective. Analysis was done with ImageJ.

### *2.3.11 Measurement of recombinant human and endogenous IGF1 levels.*

To quantify levels of recombinant human and mouse IGF1 in blood serum, a solid-phase ELISA test (Quantikine ELISA, R&D Systems Inc.) was used as per kit instructions. Blood samples were obtained through submandibular puncture and collected in serum separating tubes with clot activator (Sarstedt AG & Co.). The tubes were left to sit for 30 minutes, centrifuged at 10000 x *g* for 5 minutes and the collected

serum frozen. For analysis, serum was pretreated to release IGF1 from binding protein and incubated for 2 hours to attach the IGF1 to the plate. A human IGF1 conjugate was added for one or two hours depending on the IGF1 type. Finally, a substrate solution was incubated for 30 minutes to elicit a colorimetric reaction that was stopped with sulfuric acid. The optical density was measured within 10 minutes of the end of the assay using a microplate reader (iMark, Bio-Rad) set at 450 nm and with a wavelength correction of 550 nm.

### *2.3.11 Optical imaging of intrinsic signals.*

Optical imaging of intrinsic signals was used to evaluate the relative strength of responses elicited by the deprived and undeprived eye during the presentation of visual stimuli (5). Imaging experiments were carried out in P28 males and females as well as adult (>P60) female mice as described previously (6). For monocular deprivation, mice were anaesthetized with avertin (0.016 ml/g) and the eye contralateral to the imaged hemisphere was sutured for 4 days before the imaging session.

For imaging, mice were anesthetized using urethane (1.5 g/Kg) and chloroprothixiene (1%). The head was fixed in a stereotaxic frame and the skull exposed and cleaned. The skull was thinned over V1 using a dremel drill. The cortical surface was illuminated with a tungsten halogen light source and a slow-scan video camera equipped with a tandem macro-lens arrangement was used to acquire images of intrinsic signals. First, the cortical surface was illuminated with a green filter (550 nm) to obtain a reference image of the surface blood vessels. Next, the focal plane was adjusted to about 300 microns below the cortical surface and a red filter (630 nm) was

used for the acquisition of intrinsic signals. To measure the relative cortical activation, a drifting bar (4 orientations, spatial frequency of 9 deg/cycle) was presented to each eye individually. Eye patches were used to deliver the stimulation to each eye separately. Image analysis was performed with custom-made software (MATLAB). The Ocular Dominance Index (ODI) was defined as the difference between contralateral and ipsilateral eye responses divided by their sum, and used to evaluate the relative strength of eye-evoked cortical activation.

### *2.3.12 Slice electrophysiology.*

Control and MeCP2 mutant mice (P27-29) were anesthetized by isofluorane inhalation. The brains were rapidly removed after decapitation and submerged into 4°C slicing buffer containing the following in mM: 130 NaCl, 10 glucose, 1.25 $NaH_2PO_4$, 24 $NaCHO_3$, 3.5 KCl, 6 $MgCl_2$, and 0.5 $CaCl_2$ and bubbled with 95% $O_2$ and 5% $CO_2$. Brains were sliced coronally at a thickness of 300 um on a vibratory microtome VT1200 (Leica). After slicing, sections were incubated for 20 min in room temperature artificial cerebral spinal fluid (ACSF), bubbled continuously with 95% $O_2$ and 5% $CO_2$. The ACSF contained the following in mM: 130 NaCl, 10 glucose, 1.25 $NaH_2PO_4$, 24 $NaCHO_3$, 3.5 KCl, 2.5 $CaCl_4$, and 1.5 $MgCl_2$.

For recording of AMPA receptor mEPSCs, whole cell patch clamp of V1 layer 2/3 pyramidal neurons was performed using pipettes (5.0-6.0 Mohm resistance) filled with an internal solution containing in mM: 120 $CsMeSO_4$, 10 TEA-Cl, 5 EGTA, 10 NaCl, 5 Mg-ATP, 0.4 Na-GTP, and 10 HEPES, pH 7.2-7.3 with 1M CsOH. Neurons were identified by their location and morphology and voltage clamped at a membrane

potential of -70mV. Neurons were recorded at room temperature (25°C) in ACSF containing 1 uM TTX and 50 uM picrotoxin. AMPA receptor mEPSCs were blocked with application of 10 uM CNQX.

Membrane currents were recorded using a Multiclamp 700B (Axon Instruments) at 10kHz and filtered at 2kHz. Traces were analyzed for EPSCs in Clampfit 10.2 software (Axon Instruments) using a template constructed from 4-6 mEPSCs intrinsic to each recording. Cumulative probability was calculated for inter-event interval and peak amplitude and subjected to the Kolmogorov-Smirnov test for significance.

#### *2.3.13 Data analysis.*

Analysis for male and female mice were performed separately using student's t-test, paired t-test (females), and one-way ANOVA with either Newman-Keuls or Tukey's post-hoc analysis for multiple comparisons. ODI comparisons were analyzed with Mann-Whitney rank sum test for non-parametric data. Analysis was performed using either MATLAB or Prism.

## 2.4 Results

### *2.4.1 The physiological condition and social behavior of MeCP2-null animals are affected by decreased levels of endogenous IGF1 and are improved with rhIGF1 treatment*

We first examined whether endogenous IGF1 levels were decreased in MeCP2$^{-/y}$ mice (on a C57BL/6J background) and found that there was indeed significantly less serum IGF1 in P28 MeCP2$^{-/y}$ mice compared to age-matched controls (Figure 1A). The difference was less pronounced but still significant at P56, consistent with the fact that

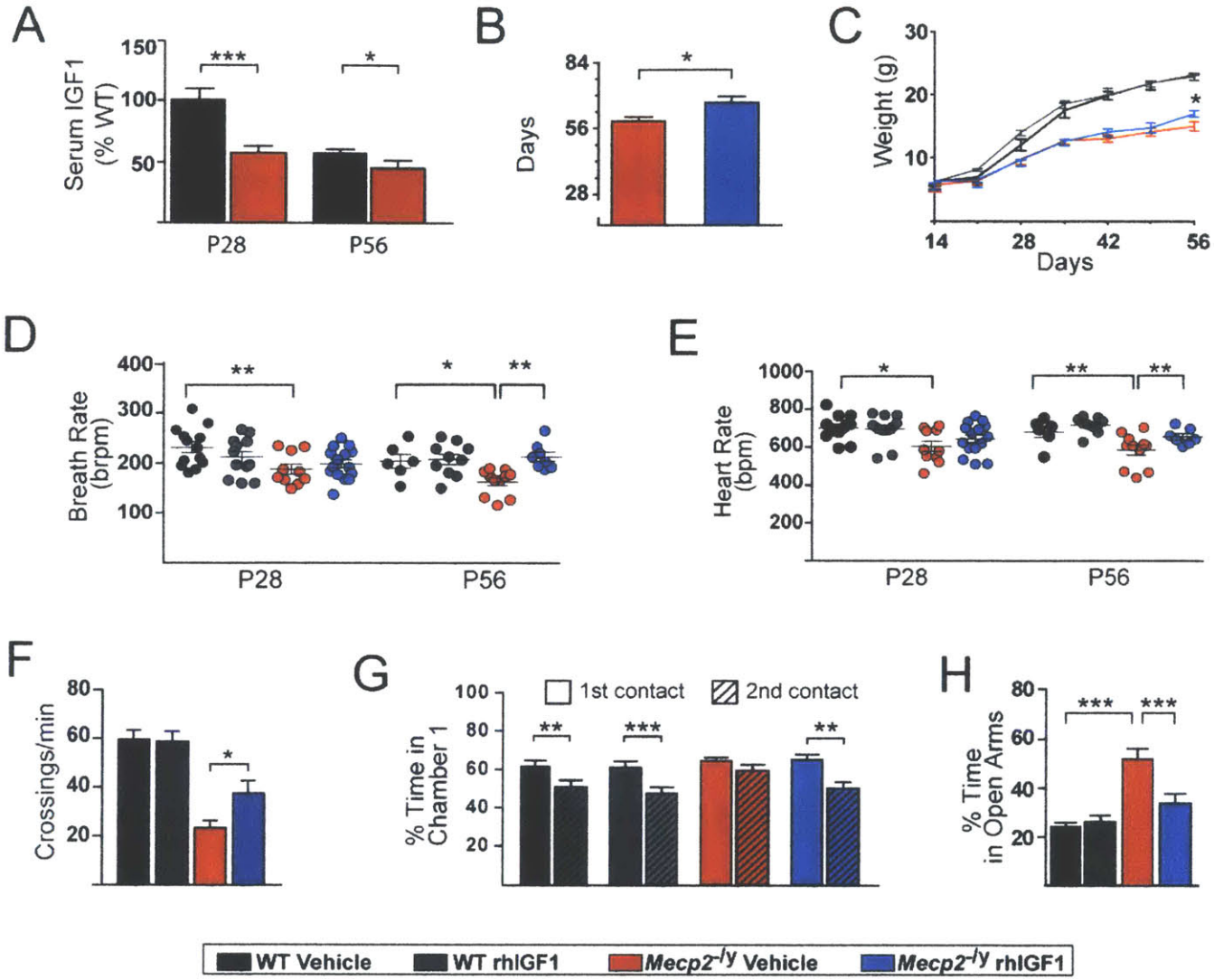


**Figure 1 – rhIGF1 promotes survival, improves physiological condition, and restores normal levels of social and anxiety-related behavior of MeCP2$^{-/y}$ mice.** (A) Serum levels of endogenous IGF1 measured in P28 and P56 mice relative to WT P28 controls (statistical comparisons employed unpaired t-test for equal variances; WT (P28,56) n=12, 10; MeCP2-/y (P28,56) n=10, 9). (B) Mean survival age of MeCP2-/y animals treated with vehicle or rhIGF1 (unpaired t-test; MeCP2-/y vehicle n=27, rhIGF1 n=29). (C) Weight variation from P14 (starting day of injection) to P56. Comparisons between KO Vehicle and Treated were done week by week with an unpaired t-test for equal variances (WT vehicle n=26, rhIGF1 n=22; MeCP2-/y vehicle n=27, rhIGF1 n=29). (D-E) Scatterplot of average breathing (D) and cardiac (E) rates. Each dot represents a single animal; lines indicate population average (ANOVA with Newman-Keuls post-hoc analysis for multiple comparison). (F) Nocturnal locomotor activity expressed as average number of beam crossings per minute (ANOVA with Newman-Keuls post-hoc analysis for multiple comparisons performed at each separate time point; WT vehicle n=25, rhIGF1 n=28; MeCP2-/y vehicle n=21, rhIGF1 n=26). (G) 3-chamber test measurements showing the percentage of time the animals spent socializing with a stranger mouse during the first contact (solid bars) and 30 minutes after the first contact (hatched bars) at P28-35 (paired t-test). (H) Percentage of time spent in the open arms of a plus maze as measurement of anxiety-related behavior at P28-35 (ANOVA with Newman-Keuls post-hoc analysis for multiple comparisons; WT vehicle n=18, rhIGF1 n=16; MeCP2-/y vehicle n=21, rhIGF1 n=23). Error bars represent S.E.M. * $p < 0.05$; ** $p < 0.01$; *** $p < 0.001$.

effects of an increase in systemic IGF1 by administration of rhIGF1, a battery of tests aimed to evaluate the health status, locomotion, and vital signs were carried out on a regular schedule (2A). MeCP2$^{-/y}$ mice that were injected intraperitoneally (IP) starting at P14 with a daily dose (0.25 mg/kg) of rhIGF1 had a very modest increase in lifespan when compared to vehicle-treated MeCP2$^{-/y}$ mice (Figure 1B, 2B). This improvement in life expectancy was accompanied by an increase in weight when measured at P56 – a time point when mutant animals are fully symptomatic (Figure 1C). RTT patients show periods of both apnea and bradycardia, which increases the likelihood of sudden death in some patients. Pulse oximeter monitoring allows for the simultaneous investigations of heart and breath rates from non-anesthetized animals, and MeCP2$^{-/y}$ mice had lower breathing and heart rates as early as P28. Treatment with rhIGF1 improved both metrics after 6 weeks of daily treatment (Figure 1D, E). The shortened lifespan of the MeCP2$^{-/y}$ mice is preceded by a sharp decline in locomotor activity in the form of lethargy and hypokinesia (Stearns et al., 2007). MeCP2$^{-/y}$ mice showed an age dependent decline in their nocturnal movements when compared to their WT littermates; by P56, the untreated mutant mice suffered a pronounced decrease in locomotion, whereas age-matched treated animals showed significantly greater locomotor activity (Figure 1F).

To evaluate social behavior, we selected tests such as the three-chamber test and elevated plus maze that require relatively low motor activity (Figure 2C;). In the three-chamber test (a social preference task), both the WT and MeCP2$^{-/y}$ mice spent more time in the chamber containing a stranger mouse, indicating similar tendencies for social contact. However, when the same stranger animal was presented 30 minutes

after the first exposure, untreated MeCP2$^{-/y}$ mice did not show the usual habituation

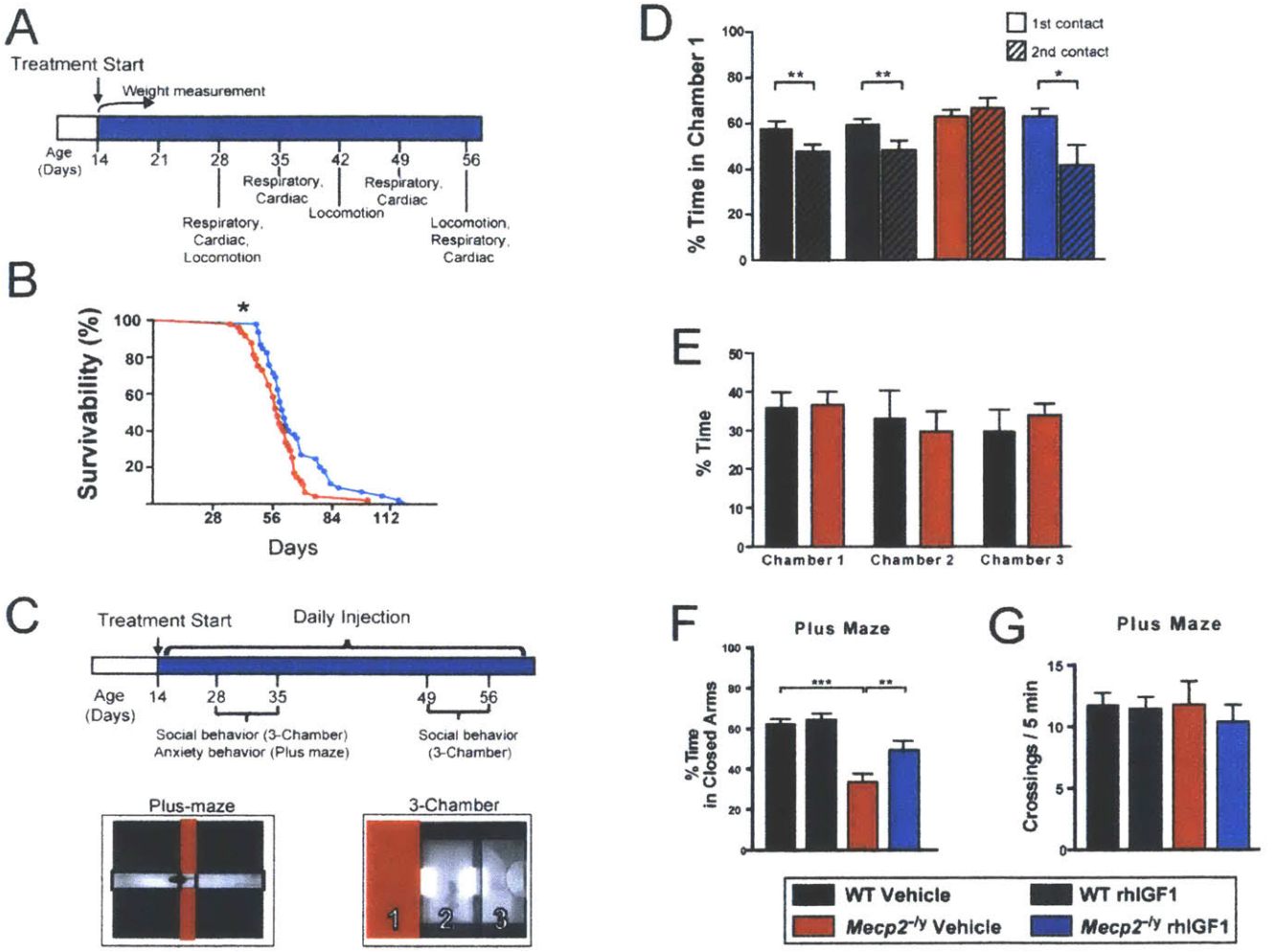


**Figure 2** - (A) Timeline for experimental schedule of physiological measurements. (B) Kaplan-Meier survival plot of MeCP2 mutant animals treated with vehicle or rhIGF1 (Mantel-Cox test). (C) Experimental timeline for behavioral tests (top). Overhead views of the custom-made elevated plus maze apparatus used to measure anxiety with open and closed arms respectively outlined in red and black (bottom left), and 3-chamber apparatus used to test social behavior with first chamber highlighted in red (bottom right). (D) 3-chamber test measurements showing the percentage of time the animals spent socializing with a stranger mouse during the first contact (solid bars) and 30 minutes after the first contact (hatched bars) at P56 (paired t-test). (E) Percentage of time spent in the each chamber in an empty 3-chamber apparatus. Animals do not show any chamber preference when exposed to an empty arena (one-way ANOVA test). (F) Percentage of time spent in the closed arms of the plus maze (ANOVA with Newman-Keuls post-hoc analysis). (G) Basal locomotor activity of the animals during the plus-maze test measured by the number of entries into open arms per session. Please refer to Fig. 1 for number of animals per group in each experiment. Error bars represent S.E.M. * $p < 0.05$; ** $p < 0.01$; *** $p < 0.001$.

and decrease in interest that both age-matched WT groups and treated mutant mice displayed (Figure 1G). This behavior was similarly evident at P56 (Figure 2D). No positional bias was observed (Figure 2E).

In the elevated plus maze, a test used to measure the level of anxiety, we found that untreated MeCP2$^{-/y}$ mice spent more time in the open arms as compared to their WT and treated littermates (Figure 1H). Conversely, the untreated MeCP2$^{-/y}$ mice did not show a preference for the closed arms (Figure 2F) as was seen in WT and mutant treated animals. This behavior was not due to abnormal exploratory activity as the number of crosses to the open arms was similar across groups (Figure 2G).

### *2.4.2 rhIGF1 treatment curtails abnormally prolonged visual cortical plasticity*

RTT symptoms may arise from prolonged immaturity of synapses and circuits in the brain. By using optical imaging of intrinsic signals from layers 2/3 of primary visual cortex (V1) in vivo, we measured the responses driven by eye-specific stimulation in normally-developing animals or after monocular deprivation (MD) of one eye for 4 consecutive days. The ratio between the cortical responses driven by the deprived (contralateral) eye and the non-deprived (ipsilateral) eye, known as the Ocular Dominance Index (ODI), provides a robust measure of the ability of visual cortex circuits to reorganize in response to changes in eye-specific drive (Figure 3A). Such plasticity is prominent during a critical period of development, when synapses and circuits are still maturing - peaking around P28 in WT mice and declining afterwards, due to further cortical maturation (Gordon and Stryker, 1996). We examined cortical plasticity at P28 and P60 (Figure 3B); because MeCP2$^{-/y}$ mice develop severe

symptoms by P60 and often cannot tolerate experiments involving anesthesia, we used

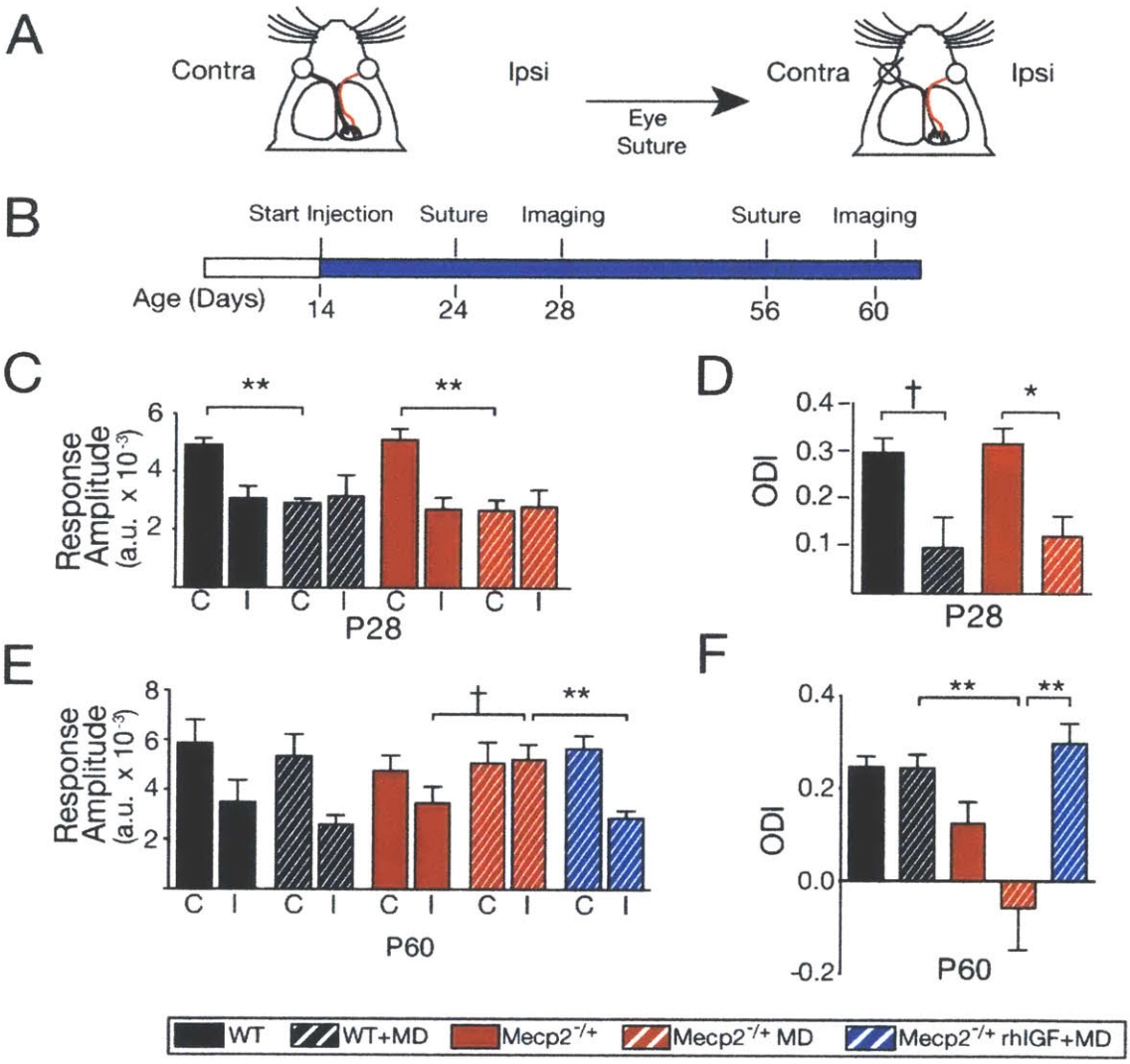


**Figure 3 - Curtailment of abnormal visual cortical plasticity by rhIGF1 treatment.** (A) Schematic showing monocular deprivation (MD) paradigm. Black and red lines respectively depict the contralateral and ipsilateral projections that connect the deprived (contralateral) and non-deprived (ipsilateral) eye to primary visual cortex (V1). (B) Experimental timeline for treatment, eyelid suture and optical imaging. (C) Average response amplitudes measured in V1 from the deprived contralateral (C) and non-deprived ipsilateral (I) eye in P28 female mice (Mann-Whitney test; WT and WT+MD n=3 each; MeCP2-/+ n=4; MeCP2-/+ +MD n=4 each). (D) Average Ocular Dominance Index (ODI) values in P28 females (Mann-Whitney test). (E) Response amplitudes observed in P60 females (Mann-Whitney test; n=5 for each group). (F) ODI representation for P60 females for each condition (ANOVA with Newman-Keuls post-hoc analysis for multiple comparisons). Error bars represent S.E.M. † $p<0.10$; * $p < 0.05$ ; ** $p < 0.01$.

MeCP2 heterozygous female (MeCP2$^{-/+}$) mice, which show much less severe

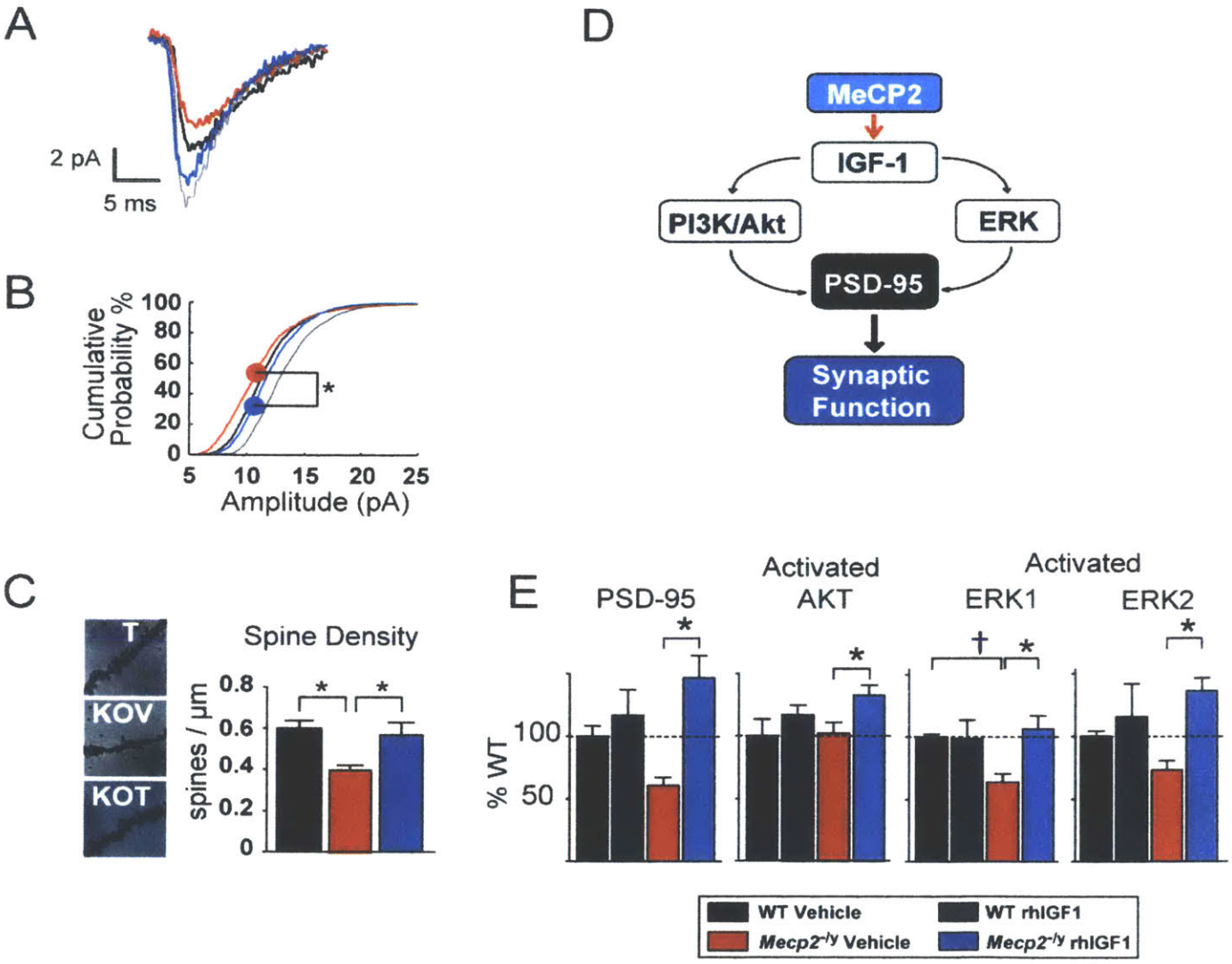


**Figure 4 - Effects of rhIGF1 on excitatory synaptic transmission, spine density and signaling pathways.** (A) Averaged mEPSCs from V1 layer 2/3 cells comparing peak amplitudes (events: WT vehicle n=270; WT rhIGF1 n=816; KO vehicle n=354; KO rhIGF1 n=268). (B) Distribution of mEPSC amplitude across all cells. rhIGF1 treatment significantly shifted the population distribution towards higher peak amplitudes (Kolmogorov-Smirnov test between vehicle and treated MeCP2-/y with pooled data from 5-8 cells from 3-4 animals in each group). (C) Representative micrographs of basal dendrites in supragranular pyramidal neurons at P42 stained with Golgi (scale bar=5⊠m) and their synaptic spine density measurements (one-way ANOVA with Newman-Keuls post-hoc analysis for multiple comparisons). (D) Schematic of proposed signaling pathways downstream of MeCP2-mediated IGF1 activation. (E) Quantification of PSD95 (left) western blots in synaptoneurosomes as a percentage of WT littermate control levels; and the ratios between phosphorylated and total Akt (middle) and ERK1/2 (right) in whole cell homogenates. Ratios are based on western blot protein measurements at P28 (comparisons employed a one-way ANOVA with Newman-Keuls post-hoc analysis for multiple comparisons including WT controls). † $p < 0.1$; * $p < 0.05$; ** $p < 0.01$. Error bars represent S.E.M.

symptoms at these ages. Ocular dominance plasticity at P28 in MeCP2$^{-/+}$ mice was comparable to that in WT mice (Figure 3C, D): MD reduced the response amplitude from the deprived contralateral eye and shifted the ODI towards the non-deprived ipsilateral eye, indicating normal critical period plasticity. By P60, WT mice showed stable visual cortex circuits with no change in eye-specific responses or a shift in the ODI after MD. In contrast, age-matched MeCP2$^{-/+}$ mice still showed a shift in ODI, largely due to an abnormal increase in responses from the non-deprived eye (Figure 3E). This effect was abolished following treatment with rhIGF1, consistent with rhIGF1 curtailing this late-persisting ocular dominance plasticity (Figure 3F).

### *2.4.4 rhIGF1 improves excitatory transmission and spine density in visual cortex neurons while activating signaling pathways and downstream synaptic proteins*

To assess the effect of MeCP2 deletion and rhIGF1 treatment on excitatory synaptic transmission in cortical neurons, we conducted whole cell voltage clamp recordings of mEPSCs from layer 2/3 pyramidal neurons in visual cortex of MeCP2$^{-/y}$ mice. Treatment of MeCP2$^{-/y}$ mice with rhIGF1 induced a significant increase in mEPSC amplitudes and shifted the distribution to a level comparable to that in WT mice (Figure 4A, B and 5A). Application of 10$\mu$M CNQX significantly blocked the occurrence of mEPSCs, indicating that the recorded events were AMPA receptor-mediated (Figure 5B). The frequency of mEPSCs examined by the inter-event interval distributions was unchanged between MeCP2$^{-/y}$ and WT control mice (Figure 5C), indicating that the changes in amplitude were likely to be postsynaptic in nature.

We hypothesized that the observed modifications of circuit level plasticity and

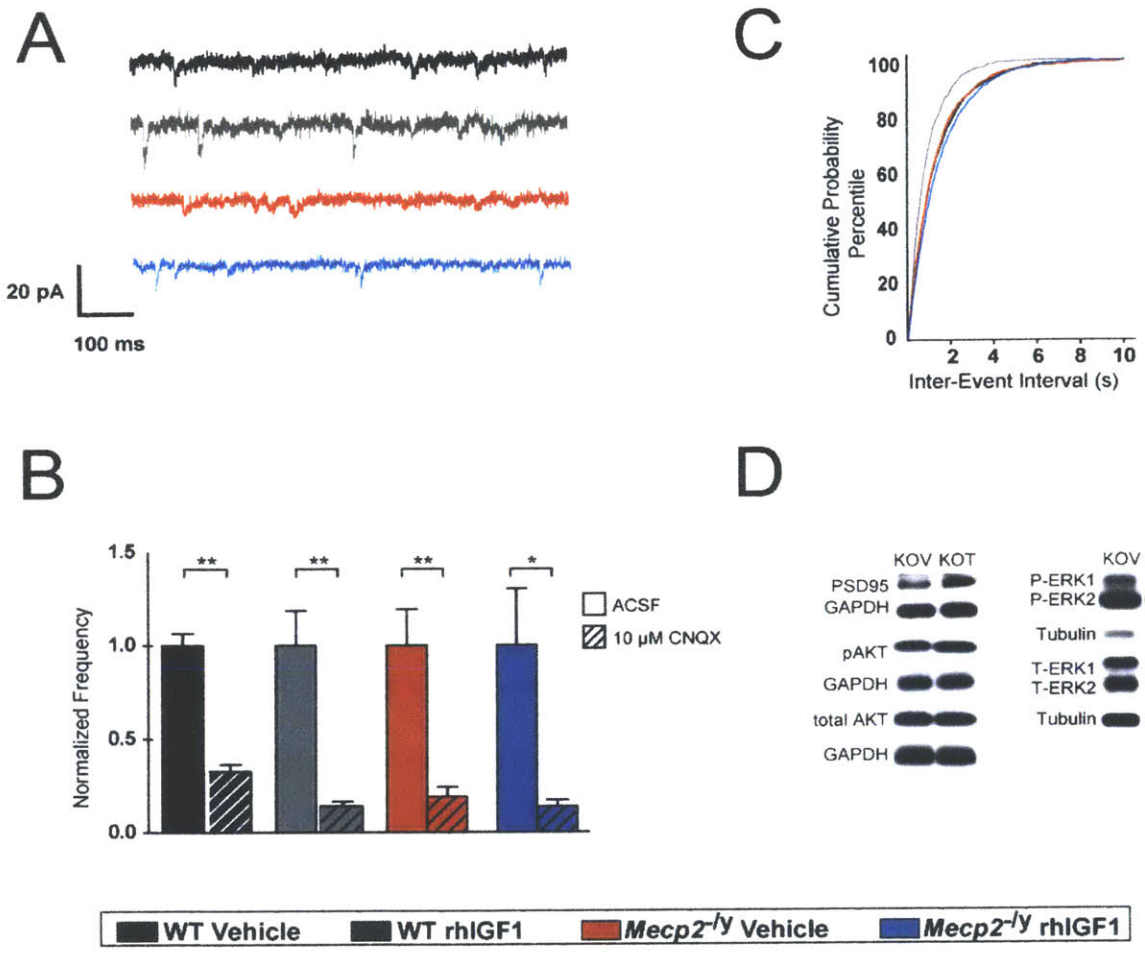


**Figure 5** - (A) Representative trace of mEPSCs recorded from V1 layer 2/3 pyramidal neurons for all groups. (B) Normalized frequencies of mEPSCs recorded from layer 2/3 pyramidal neurons. Populations were normalized to their respective ACSF frequency average value. Incubation with 10 ⊠M of CNQX drastically reduced the activity, indicating that the mEPSCs depend largely on AMPA receptors (paired t-test). (C) Population distribution of the inter-event interval. (D) Representative western blot images of proteins measured. Please refer to Fig. 3 for number of animals per group in each experiment. Error bars represent S.E.M. * $p < 0.05$; ** $p < 0.01$.

changes in synaptic strength could be explained by alterations of synaptic connectivity as well as the molecular underpinnings of these processes. We measured the spine density of layer 2/3 visual cortex basal dendrites in MeCP2$^{-/y}$ mice as a structural correlate of connectivity and functional plasticity. Spine densities showed a significant decrease in the mutant mice and recovery with rhIGF1 treatment (Figure 4C). Cortical synaptic PSD95, a post-synaptic protein necessary for glutamate receptor organization and functional responses to plasticity (Yoshii et al., 2003; Ehrlich and Malinow, 2004), can be regulated by the activation of upstream signaling pathways, in particular the key effectors Akt and ERK1/2 (Yoshii and Constantine-Paton, 2007) (Figure 4D). Quantification of synaptic PSD95 levels measured at P28 from MeCP2$^{-/y}$ mice, after 2 weeks of rhIGF1 treatment, showed a significant increase in treated mice compared to vehicle-treated KO littermates (Figure 4E, left). Consistent with these findings, the ratio of phosphorylated to total Akt and ERK1/2 in cortical whole cell homogenates showed an increase in rhIGF1 treated MeCP2$^{-/y}$ mice compared to the vehicle-treated KO animals (Fig 4E, center and right). Thus, rhIGF1 leads to an increase in neuronal signaling pathways that underlie structural and functional maturation of synapses.

### *2.4.5 rhIGF1 treatment increases the availability of total IGF1*

Because serum IGF1 levels are reduced in MeCP2$^{-/y}$ mice (Figure 1A), we examined whether and how exogenous application of rhIGF1 affected the concentration of IGF1. Previous studies have established a correlation between serum levels of IGF1 and those found in the brain (Yan et al., 2011); therefore, the levels of total IGF1 in serum provide an initial measurement of the potential availability in the

brain. Serum levels of rhIGF1 and endogenous murine IGF1 were measured at P28 and

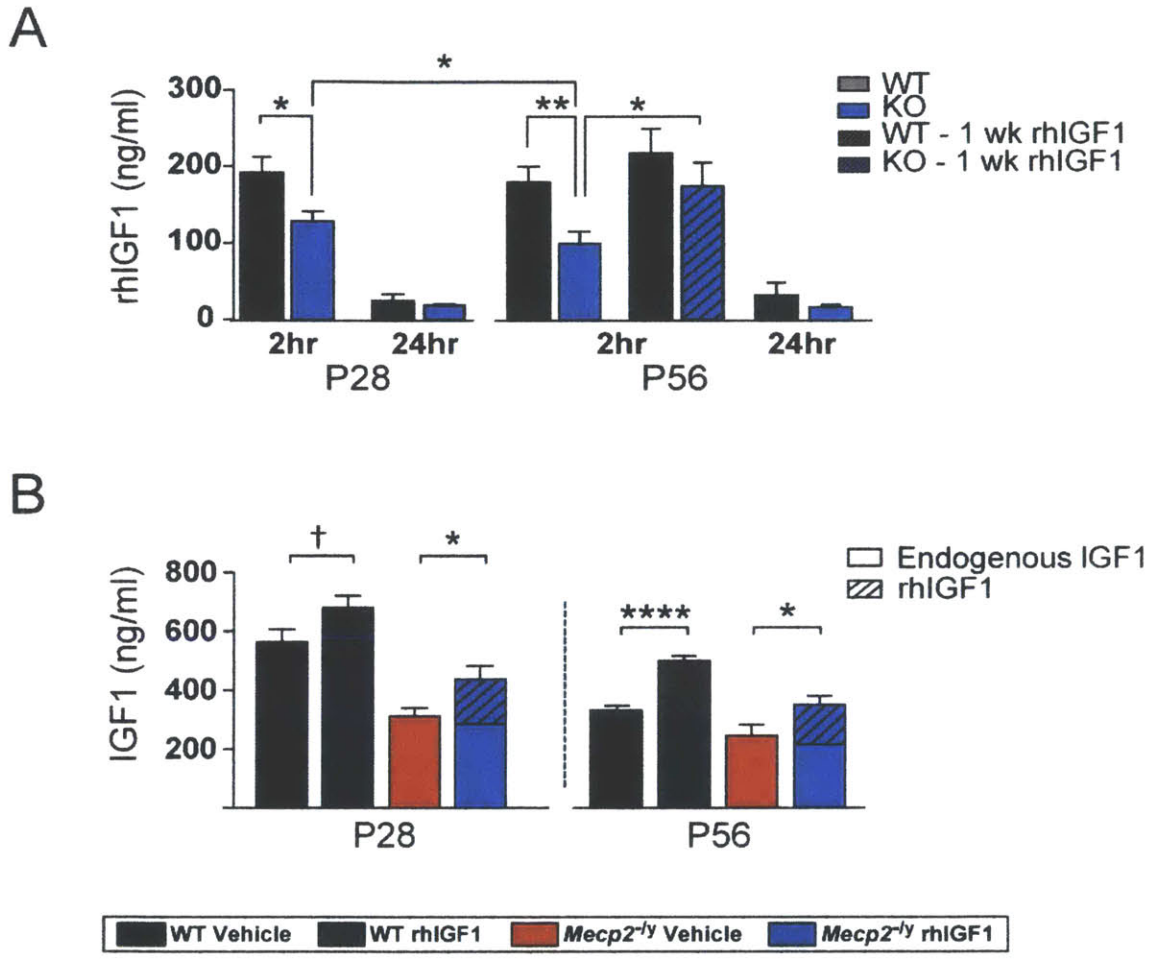


**Figure 6 - Measurement of rhIGF1 levels and IGF1 availability.** (A) Levels of rhIGF1 in serum collected 2 and 24 hours after IP injection of rhIGF1 (unpaired t-test; n of animals at P28, 2 & 24 hrs: WT=14, 7; MeCP2-/y=22, 7; n of animals at P56, 2 & 24 hrs: WT=18, 5; MeCP2-/y=18, 6). See Fig. S3A. Hatched bars show measurements in P56 mice after 1 week of treatment (n=4 each). (B) Total IGF1 concentration in blood serum collected after 2 hours calculated by addition of endogenous IGF1 (filled boxes) and rhIGF1 (hatched boxes) levels for each animal. Statistics were calculated with the summed values (one-way ANOVA with Newman-Keuls post-hoc analysis for multiple comparisons of treatment effects, separate analysis for each age; WT (P28, 56) n=12,10; WT+rhIGF1(P28,56) n=10,15; MeCP2-/y(P28,56) n=10,9; MeCP2-/y+rhIGF1(P28,56) n=11,12). Error bars represent S.E.M. † $p < 0.1$; * $p < 0.05$; ** $p < 0.01$; **** $p < 0.0001$.

P56 using type-specific sandwich ELISA for each species. Samples were taken 2 and

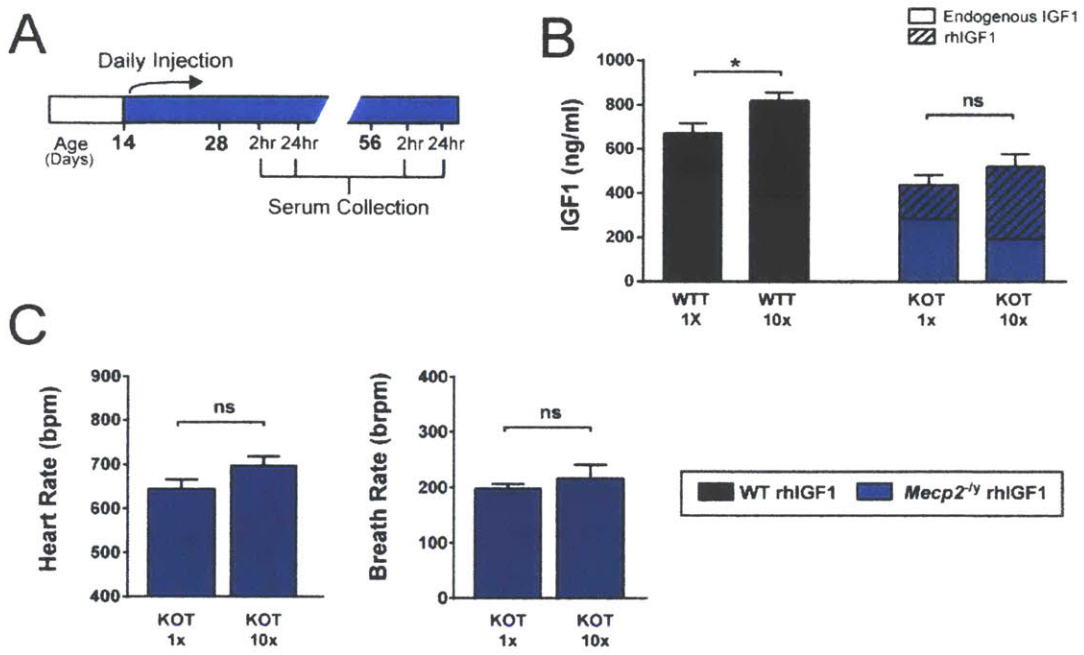


**Figure 7** - (A) Timeline for serum collection. (B) Total IGF1 concentration in blood serum collected 2 hours post-injection when animals were treated with normal dose (.25 mg/kg, 1x) or at 10 times the concentration (2.5 mg/kg, 10x), calculated by addition of endogenous (filled boxes) and rhIGF1 levels (hatched boxes) for each animal. Statistics were calculated with the summed values (unpaired t-test; WT 1x n=10, 10x n=7; MeCP2-/y 1x n=11, 10x n=5). (C) Average cardiac (left) and breathing (right) rates of MeCP2 KO animals treated with the regular or 10x dose (unpaired t-test; MeCP2-/y 1x n=14, 10x n=5 for each). Error bars represent S.E.M. * $p < 0.05$; ns, not significant.

24 hours post-injection, which would allow for the uptake of rhIGF1 into the bloodstream as well as provide an indication of drug clearance time (Figure 7A). In P28 MeCP2$^{-/y}$ mice, following 2 weeks of treatment, we observed a significant increase in serum levels of rhIGF1 two hours post-injection (Figure 6A). However, this increase was lower in treated MeCP2$^{-/y}$ animals when compared to the WT treated animals. A second set of measurements taken at P56, after six weeks of daily treatment, showed a similar pattern of rhIGF1 increase, yet with lower levels in the MeCP2$^{-/y}$ mice; furthermore, the P56 levels were lower than at P28 in the mutant mice. Taken together, these results point to a combined effect of MeCP2 function and treatment length as variables influencing availability of the administered rhIGF1. To further explore these results, we tested P56 animals that received only a one-week treatment and found that rhIGF1 availability in both WT and mutant mice was now comparable to their respective levels at P28 (Figure 6A), implying that the availability of rhIGF1 decreased after prolonged daily injections. Thus, a strategy of intermittent treatment may be effective in elevating serum IGF1. Total levels of IGF1, calculated as a sum of injected rhIGF1 plus endogenous IGF1, were increased in the treated animals across the entire treatment period (Figure 6B). Of note, treated groups, when compared to the corresponding genetically matched untreated groups, did not show a significant decrease in endogenous IGF1 even after six weeks of treatment (Figure 6B, filled boxes). Thus, rhIGF1 treatment contributes significantly to increasing total serum IGF1, and does not reduce endogenous IGF1 production.

We also examined whether a higher concentration of rhIGF1 might be more effective in increasing serum IGF1. Administering a 10-fold higher dose of rhIGF1 (2.5

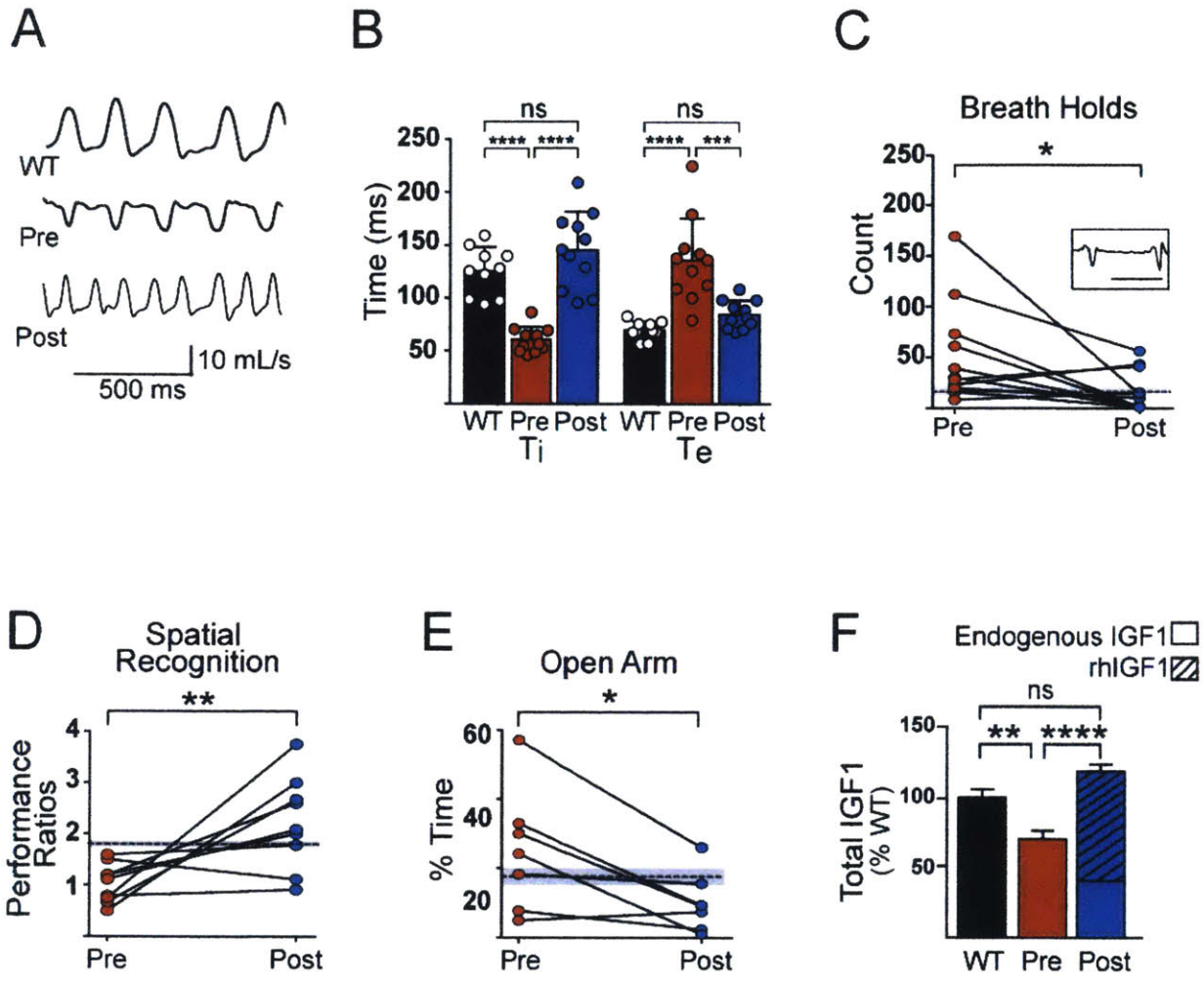


**Figure 8 - Effects of rhIGF1 on MeCP2-/+ breathing patterns, anxiety, and spatial recognition.** (A) Representative breathing pattern traces of WT (top) and MeCP2-/+ females before (middle) and after (bottom) treatment. Downward indicates inspiration (see Fig S4C). (B) Average inspiratory (Ti) and expiratory (Te) times were abnormal in MeCP2-/+ females and treatment restored these to WT levels (paired t-test for post-pre comparison and ordinary one-way ANOVA with Tukey's post-hoc analysis for multiple comparisons). Dots represent individual animals. (C) Total number of breath holds observed during 12 minute recording sessions pre- and post-treatment (paired t-test). Inset shows representative breath hold trace from pre-treatment female (scale bar = 500 ms). (D) Performance ratio of time spent with displaced vs non-displaced objects (see methods for details of assay) pre- and post-treatment (paired t-test). (E) Percent time spent in the open arms of elevated plus maze pre- and post-treatment (paired t-test). (F) Relative serum levels of total IGF1 (murine and rhIGF1) measured pre- and post-treatment (one-way ANOVA with Tukey's post-hoc analysis for multiple comparison). Error bars represent S.E.M., * $p < 0.05$; ** $p < 0.01$; **** $p < 0.0001$. In (C) – (E), dashed line and grey shading represent mean and S.E.M. of WT mice.

regular dose (0.25 mg/kg, 1x) littermates treated for a similar duration. Nevertheless, this high-dosage treatment did not lead to an increase in total serum IGF1 in the MeCP2$^{-/y}$ mice due to a concomitant decrease in endogenously synthesized IGF1 (Figure 7B). Consistent with this finding, autonomic function was similar in the high-dose compared to the low-dose animals (Figure 7C).

### *2.4.6 Short-term treatment with rhIGF1 improves breathing patterns and behavioral deficits in symptomatic MeCP2$^{-/+}$ females*

RTT primarily affects females and the severity of the disease can vary greatly due to the specific mutation and the mosaic expression of MeCP2 caused by X-chromosome inactivation (Amir et al., 2000; Ishii et al., 2001; Xinhua Bao et al., 2007). In order to further examine the therapeutic potential of rhIGF1, we sought to test its efficacy in female heterozygous (MeCP2$^{-/+}$) mice that present a more heterogeneous disease severity as well as a later time of onset (Stearns et al., 2007; Katz et al., 2012; Samaco et al., 2013). We therefore chose to use older, symptomatic females of various ages (> 6 months) and a 10x treatment dose to maximize the potential effects during a 3-week daily treatment regimen. Despite the inherent variability, we were able to test physiological and behavioral parameters pre- and post-treatment on the same animals, allowing for more robust statistical analysis. We first investigated the detailed breathing patterns exhibited by the MeCP2$^{-/+}$ mice by using a whole-body plethysmograph. Previous studies in human patients and mouse models have shown abnormal post-inspiratory times (Viemari et al., 2005; Weese-Mayer et al., 2006; Ogier

et al., 2007). We found irregular patterns with reduced inspiratory and prolonged expiratory times, along with reduced peak expiratory amplitudes, that were strikingly rescued with rhIGF1 treatment (Figure. 8A, B; 9C-E). Apneas and breath holds are a hallmark RTT phenotype and we observed high number of breath holds that were subsequently reduced post-treatment (Figure 8C).

MeCP2$^{-/+}$ mice have been shown to exhibit cognitive-associated deficits in tests for spatial recognition and anxiety (Stearns et al., 2007). We found that female mice had improved performance on recognition of spatial rearrangement following three weeks of treatment (Figure 8D.) Additionally, as with the anxiety-related measurements in younger KO males, females spent more time in the open arms of the elevated plus maze before treatment and had a significant post-treatment reduction (Figure. 8E). In contrast to these improvements in cognitive functions and unlike the effects seen in young males, the short period of rhIGF1 treatment did not improve social recognition performance in the three-chamber test (Figure 9F) or hypoactivity (Figure 9G). Finally, older symptomatic females also showed a relative reduction in serum IGF1 levels as compared to WT controls, and levels of total available serum IGF1 post-treatment were elevated to be similar to WT controls (Figure 8F).

## 2.5 Discussion

We have shown that IGF1 levels are reduced in an established mouse model of RTT (Mecp2tm1.1Bird on a C57BL/6J background) and treatment with full-length rhIGF1 increases serum IGF1 concentration and ameliorates a wide range of phenotypes. RTT patients show a similar reduction of IGF1 levels in CSF (Khwaja et al.,

2014). A treatment regimen with the same dose of rhIGF1 increases IGF1 levels, with a safety profile that yields little negative side effects following administration for 4 weeks or longer, and an efficacy profile that ameliorates specific symptoms including cardiorespiratory function and anxiety (Pini et al., 2012; Khwaja et al., 2014). IGF1 levels are regulated by MeCP2 via the let-7 family of miRNAs (28). Thus, any treatment increasing the level of IGF1 would not only augment the activation of signaling pathways shared with BDNF, a well-known target of MeCP2 that is significantly decreased when MeCP2 is mutated, but also reverse the deficit of IGF1. Our findings stand in contrast to a recent study which examined the effects of full-length IGF1 modified with the addition of polyethylene glycol (PEG-IGF1) treatment in MeCP2 KO mice (Mecp2tm1.1Bird ) on a mixed background (B6129S6F1) and showed variable effects, in particular on body weight, metabolism, and lifespan (Pitcher et al., 2013). However, it is well established that the same genetic manipulation can exhibit profoundly different phenotypes when present on different genetic backgrounds (Sigmund, 2000), and the 129 strains exhibit anomalous glucose and insulin metabolism (Leiter, 2002; Berglund et al., 2008). Indeed, MeCP2 KO mice (Mecp2tm1.1Bird ) when mixed with 129 strains show an increase in body weight, whereas the same KO animals maintained on a C57BL/6 background have lower body weight (Guy et al., 2001; Pratte et al., 2011; Ward et al., 2011). This phenotype would be further exacerbated by the slow pharmacokinetics of PEG-IGF1: serum IGF1 concentration in treated animals was not consistently measured in this study, but would be expected to be abnormally high, particularly at high PEG-IGF1 doses that may lead to buildup effects (Saenger et al., 2011), thus contributing to the

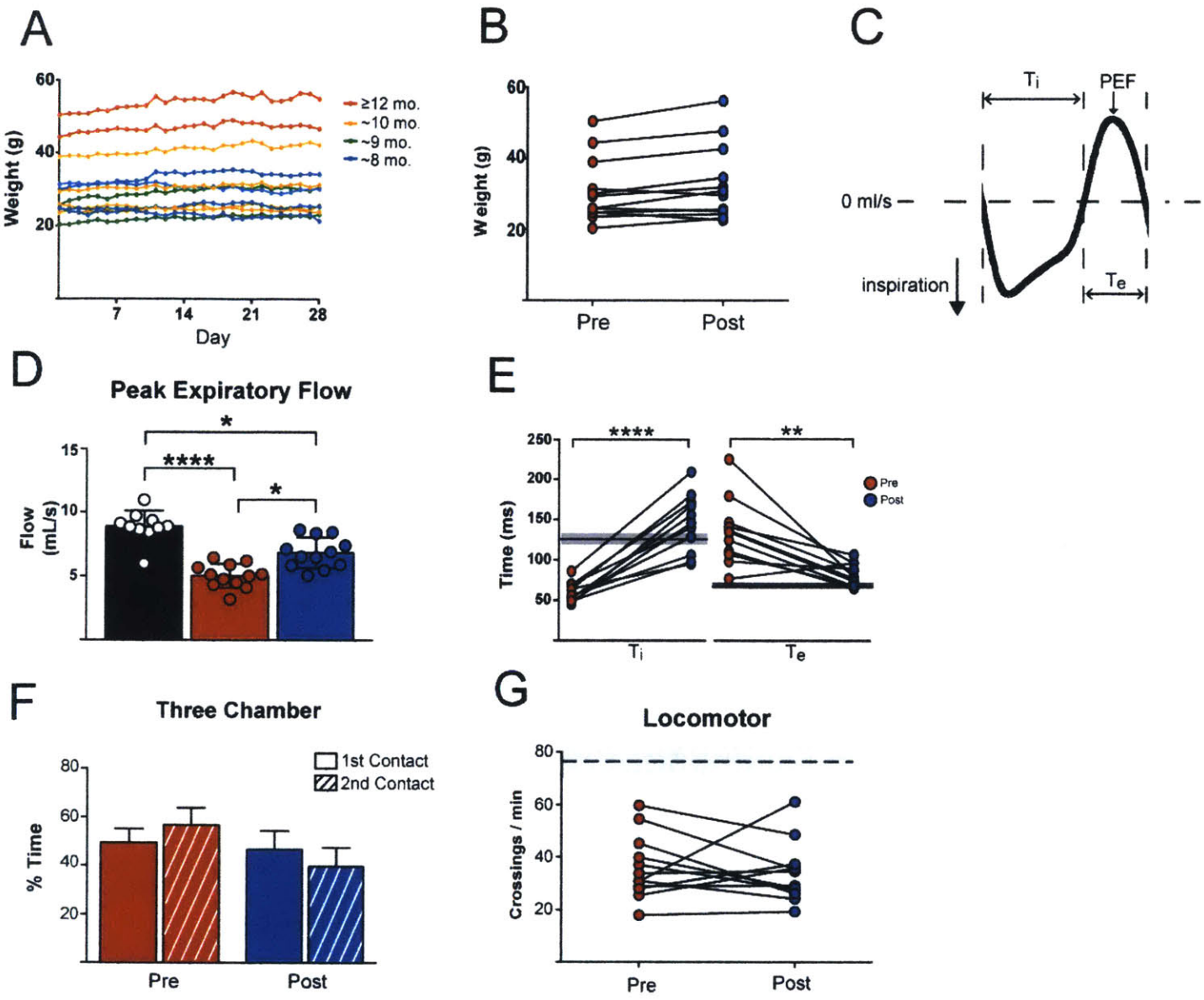


**Figure 9** - Weights of individual animals measured daily from the beginning of treatment until 4 weeks later, one week after treatment ended. Color coded by age of each individual females (see legend). (B) Comparison of weight of each animal at the beginning and end of treatment period shows no decrease or statistical difference (paired t-test). (C) Diagram representing calculation for inspiratory time (Ti), expiratory time (Te), and peak expiratory flow (PEF) of a sample breath. (D) Scatter plots and means of PEF amplitude of female mice in each group showing a significant reduction in MeCP2-/+ mice before treatment and a significant increase post-treatment (ordinary one-way ANOVA with Tukey's post-hoc analysis for multiple comparisons; dots represent individual animals). (E) Individual paired measurements of total Ti and Te (paired t-test). Dashed line and shaded area indicates WT mean and S.E.M. (F) No significant shift in percent time spent in chamber with stranger mouse between first and second exposure pre- and post-treatment. (G) No difference in the average number of beam crossings during paired measurements of nocturnal locomotor activity (paired t-test). MeCP2-/+ mice were considerably more hypoactive than females in WT control group. Dashed line and shaded area indicates WT mean and S.E.M.

not show any significant alterations in weight (Figure 9A, B).

Systemic treatment with rhIGF1 improves organismal function, specific behaviors, cellular pathway activation, and synaptic plasticity. The treatment efficacy and temporal dynamics vary across the different metrics assessed. For example, we observed early effects of the treatment on in MeCP2$^{-/y}$ behavior, but saw efficacy only at later stages in locomotor activity. This variability could partly be due to the contribution of different brain regions to a given endophenotype and region-specific responses to rhIGF1, given the availability of peripheral IGF1 and the heterogeneous expression pattern of IGF1 receptors in the adult mouse brain (Fernandez and Torres-Aleman, 2012). The cortex, choroid plexus, and endothelial cells are regions with highest expression of receptors - the last two are major entry points of systemic IGF1 into the CNS, consistent with the importance of peripheral IGF1 in the maintenance of CNS levels. Nevertheless, the importance of locally synthesized IGF1 in the brain cannot be ruled out, as recent findings show a possible role for environmental enrichment paradigms and active microglia in the production of brain IGF1 (Ciucci et al., 2007; Derecki et al., 2012).

The anxiety measurement we used supports previous findings in mouse models with similar backgrounds and suggests that both sexes of the RTT model have an altered anxiety behavior relative to their WT littermates (Banerjee et al., 2012). Some proposed explanations include abnormal perception of safeness or incapability to interpret danger cues in the mutant mice (Stearns et al., 2007). It is worth noting that the results we obtained for anxiety and social measurements from untreated MeCP2 mutant mice are very similar to those obtained in a PSD95 mutant mouse model,

emphasizing the convergence of signaling pathways and synaptic molecules necessary for these behavioral functions (Feyder et al., 2010). Indeed, IGF1 treatment improves excitatory synaptic transmission and motor behaviors in Shank3 haploinsufficient mice (Bozdagi et al., 2013), and IGF1 application corrects synaptic transmission deficits in iPSC-derived neurons from 22q13 deletion syndrome patients (Shcheglovitov et al., 2013), both of which can be attributed to enhanced PSD95 function.

Measuring response amplitude changes and the corresponding shifts in ocular dominance directly tests visual cortical plasticity and here, for the first time, we describe the effects of a mutated MeCP2 gene on the course of critical period plasticity. Previous data (Tropea et al., 2009) showed that visual cortical plasticity was present in adult MeCP2 mutant mice but whether this was an expansion of the normal critical period or a complete shift in the time window for increased visual cortical plasticity was unknown. Our results support the former explanation, with normal opening of the critical period at P28 as seen by a decreased response from the deprived eye after 4 days of MD, and a persistent state of enhanced plasticity at P60 compared to WT controls, albeit due to enhanced open eye responses. This may represent a form of abnormal synaptic or circuit plasticity following MD (Tropea et al., 2009; Marchetto et al., 2010; Noutel et al., 2011). IGF1 treatment abolishes this plasticity and stabilizes the underlying circuits and synapses – possibly via effects on inhibitory systems in the cortex (Chao et al., 2010) or on homeostatic mechanisms (Blackman et al., 2012). The effect on functional circuits in the adult visual cortex reflects the emerging consensus that the consequences of MeCP2 loss are felt throughout life (Guy et al., 2011; Cheval et al., 2012; Nguyen et al., 2012).

Because serum IGF1 is able to cross the BBB, we attribute the increased activation of brain Akt and ERK to the augmentation of serum IGF1 levels. One correlate of the activation of these pathways is increased synaptogenesis and levels of synaptic PSD95 (Yoshii and Constantine-Paton, 2007; Cuesto et al., 2011). These results are consistent with previous findings of reduced PSD95 transcription and protein expression as well as fewer excitatory synapses and spines in MeCP2 mutant mice (Chao et al., 2007; Tropea et al., 2009; Landi et al., 2011; Ricciardi et al., 2011). The specific mechanisms of IGF1 uptake and clearance in the circulatory system are not completely understood. In normal development, levels of IGF1 peak during puberty (3-4 weeks in mice) and decrease in adulthood. Endogenous IGF1 levels are significantly reduced in young MeCP2$^{-/y}$ and adult MeCP2$^{-/+}$ mice relative to WT mice (Figs. 1A, 8F). This reduction likely plays a role in the development of RTT neuropathology; treatment beginning from 2 weeks of age in MeCP2$^{-/y}$ mice increases the total available IGF1 (endogenous plus rhIGF1) and contributes to the improvement of several phenotypes. In older MeCP2$^{-/+}$ animals, a short period of rhIGF1 treatment similarly increases total IGF1 availability and improves deficits in breathing patterns, spatial recognition and anxiety, yet locomotor and social interaction deficits remain unaltered. It is possible that starting treatment earlier, and extending it for longer durations, may lead to greater efficacy in MeCP2$^{-/+}$ mice.

## Acknowledgements

We thank Alexandra Clemente and Jitendra Sharma, along with members of the Sur laboratory for technical assistance. Supported by a National Science Foundation Graduate Research Fellowship 2388357 (R.G.), a postdoctoral fellowship from the Simons Center for the Social Brain (S.K. and A.B.), and grants from the NIH and the Simons Foundation (M.S.).

**References**

Amir R, Van den Veyver I, Schultz R, Malicki D, Tran C, Dahle E, Philippi A, Timar L, Percy A, Motil K, Lichtarge O, Smith E, Glaze D, Zoghbi HY (2000) Influence of mutation type and X chromosome inactivation on Rett syndrome phenotypes. Ann Neurol 47:670–679.

Banerjee A, Castro J, Sur M (2012) Rett syndrome: genes, synapses, circuits, and therapeutics. Front Psychiatry 3:34.

Berglund ED, Li CY, Poffenberger G, Ayala JE, Fueger PT, Willis SE, Jewell MM, Powers AC, Wasserman DH (2008) Glucose Metabolism In Vivo in Four Commonly Used Inbred Mouse Strains. Diabetes 57:1790–1799.

Blackman MP, Djukic B, Nelson SB, Turrigiano GG (2012) A Critical and Cell-Autonomous Role for MeCP2 in Synaptic Scaling Up. The Journal of Neuroscience 32:13529–13536.

Bondy CA, Cheng CM (2004) Signaling by insulin-like growth factor 1 in brain. Eur J Pharmacol 490:25–31.

Bozdagi O, Tavassoli T, Buxbaum JD (2013) Insulin-like growth factor-1 rescues synaptic and motor deficits in a mouse model of autism and developmental delay. Mol Autism 4:9.

Castro J, Mellios N, Sur M (2013) Mechanisms and therapeutic challenges in autism spectrum disorders: insights from Rett syndrome. Current Opinion in Neurology 26:154–159.

Chahrour M, Jung SY, Shaw C, Zhou X, Wong STC, Qin J, Zoghbi HY (2008) MeCP2, a Key Contributor to Neurological Disease, Activates and Represses Transcription. Science 320:1224–1229.

Chahrour M, Zoghbi HY (2007) The story of Rett syndrome: from clinic to neurobiology. Neuron 56:422–437.

Chang Q, Khare G, Dani V, Nelson SB, Jaenisch R (2006) The disease progression of Mecp2 mutant mice is affected by the level of BDNF expression. Neuron 49:341–348.

Chao H-T, Chen H, Samaco RC, Xue M, Chahrour M, Yoo J, Neul JL, Gong S, Lu H-C, Heintz N, Ekker M, Rubenstein JLR, Noebels JL, Rosenmund C, Zoghbi HY (2010) Dysfunction in GABA signalling mediates autism-like stereotypies and Rett syndrome phenotypes. Nature 468:263–269.

Chao H-T, Zoghbi HY, Rosenmund C (2007) MeCP2 controls excitatory synaptic strength by regulating glutamatergic synapse number. Neuron 56:58–65.

Cheval H, Guy J, Merusi C, De Sousa D, Selfridge J, Bird A (2012) Postnatal inactivation reveals enhanced requirement for MeCP2 at distinct age windows. Human Molecular Genetics 21:3806–3814.

Ciucci F, Putignano E, Baroncelli L, Landi S, Berardi N, Maffei L (2007) Insulin-like growth factor 1 (IGF-1) mediates the effects of enriched environment (EE) on visual cortical

development. PLoS ONE 2:e475.

Cuesto G, Enriquez-Barreto L, Caramés C, Cantarero M, Gasull X, Sandi C, Ferrús A, Acebes Á, Morales M (2011) Phosphoinositide-3-kinase activation controls synaptogenesis and spinogenesis in hippocampal neurons. Journal of Neuroscience 31:2721–2733.

Derecki NC, Cronk JC, Kipnis J (2012) The role of microglia in brain maintenance: implications for Rett syndrome. Trends Immunol.

Ehrlich I, Malinow R (2004) Postsynaptic density 95 controls AMPA receptor incorporation during long-term potentiation and experience-driven synaptic plasticity. Journal of Neuroscience 24:916–927.

Fernandez AM, Torres-Aleman I (2012) The many faces of insulin-like peptide signalling in the brain. Nat Rev Neurosci 13:225–239.

Feyder M et al. (2010) Association of mouse Dlg4 (PSD-95) gene deletion and human DLG4 gene variation with phenotypes relevant to autism spectrum disorders and Williams' syndrome. Am J Psychiatry 167:1508–1517.

Giacometti E, Luikenhuis S, Beard C, Jaenisch R (2007) Partial rescue of MeCP2 deficiency by postnatal activation of MeCP2. P Natl Acad Sci Usa 104:1931–1936.

Gordon J, Stryker M (1996) Experience-dependent plasticity of binocular responses in the primary visual cortex of the mouse. Journal of Neuroscience 16:3274–3286.

Guy J, Cheval H, Selfridge J, Bird A (2011) The role of MeCP2 in the brain. Annu Rev Cell Dev Biol 27:631–652.

Guy J, Gan J, Selfridge J, Cobb S, Bird A (2007) Reversal of neurological defects in a mouse model of Rett syndrome. Science 315:1143–1147.

Guy J, Hendrich B, Holmes M, Martin JE, Bird A (2001) A mouse Mecp2-null mutation causes neurological symptoms that mimic Rett syndrome. Nature Genetics 27:322–326.

Ishii T, Makita Y, Ogawa A, Amamiya S, Yamamoto M, Miyamoto A, Oki J (2001) The role of different X-inactivation pattern on the variable clinical phenotype with Rett syndrome. Brain Dev 23 Suppl 1:S161–S164.

Katz DM et al. (2012) Preclinical research in Rett syndrome: setting the foundation for translational success. Dis Model Mech 5:733–745 Available at: http://dmm.biologists.org/content/5/6/733.long.

Khwaja OS et al. (2014) Safety, pharmacokinetics, and preliminary assessment of efficacy of mecasermin (recombinant human IGF-1) for the treatment of Rett syndrome. PNAS.

Landi S, Putignano E, Boggio EM, Giustetto M, Pizzorusso T, Ratto GM (2011) The short-time structural plasticity of dendritic spines is altered in a model of Rett syndrome. Sci Rep 1:45.

Leiter EH (2002) Mice with targeted gene disruptions or gene insertions for diabetes research: problems, pitfalls, and potential solutions. Diabetologia 45:296–308.

Li Y, Wang H, Muffat J, Cheng AW, Orlando DA, Lovén J, Kwok S-M, Feldman DA, Bateup HS, Gao Q, Hockemeyer D, Mitalipova M, Lewis CA, Vander Heiden MG, Sur M, Young RA, Jaenisch R (2013) Global transcriptional and translational repression in human-embryonic-stem-cell-derived Rett syndrome neurons. Cell Stem Cell 13:446–458.

Marchetto MCN, Carromeu C, Acab A, Yu D, Yeo GW, Mu Y, Chen G, Gage FH, Muotri AR (2010) A model for neural development and treatment of Rett syndrome using human induced pluripotent stem cells. Cell 143:527–539.

Mellios N, Woodson J, Crawford B, Garcia RI, Sharma J, Sheridan SD, Haggarty SJ, Sur M (n.d.) A β-2 adrenergic receptor agonist ameliorates phenotype and corrects miRNA-mediated IGF1 deficits in an animal model of Rett Syndrome. :1–22.

Nguyen MVC, Du F, Felice CA, Shan X, Nigam A, Mandel G, Robinson JK, Ballas N (2012) MeCP2 Is Critical for Maintaining Mature Neuronal Networks and Global Brain Anatomy during Late Stages of Postnatal Brain Development and in the Mature Adult Brain. Journal of Neuroscience 32:10021–10034.

Nishijima T, Piriz J, Duflot S, Fernandez AM, Gaitan G, Gomez-Pinedo U, Verdugo JMG, Leroy F, Soya H, Nuñez A, Torres-Aleman I (2010) Neuronal activity drives localized blood-brain-barrier transport of serum insulin-like growth factor-I into the CNS. Neuron 67:834–846.

Noutel J, Hong YK, Leu B, Kang E, Chen C (2011) Experience-dependent retinogeniculate synapse remodeling is abnormal in MeCP2-deficient mice. Neuron 70:35–42.

Ogier M, Wang H, Hong E, Wang Q, Greenberg ME, Katz DM (2007) Brain-derived neurotrophic factor expression and respiratory function improve after ampakine treatment in a mouse model of Rett syndrome. Journal of Neuroscience 27:10912–10917.

Pini G, Scusa MF, Congiu L, Benincasa A, Morescalchi P, Bottiglioni I, Di Marco P, Borelli P, Bonuccelli U, Della-Chiesa A, Prina-Mello A, Tropea D (2012) IGF1 as a Potential Treatment for Rett Syndrome: Safety Assessment in Six Rett Patients. Autism Res Treat 2012:679801.

Pitcher MR, Ward CS, Arvide EM, Chapleau CA, Pozzo-Miller L, Hoeflich A, Sivaramakrishnan M, Saenger S, Metzger F, Neul JL (2013) Insulinotropic treatments exacerbate metabolic syndrome in mice lacking MeCP2 function. Human Molecular Genetics.

Pratte M, Panayotis N, Ghata A, Villard L, Roux J-C (2011) Progressive motor and respiratory metabolism deficits in post-weaning Mecp2-null male mice. Behav Brain Res 216:313–320.

Ricciardi S, Boggio EM, Grosso S, Lonetti G, Forlani G, Stefanelli G, Calcagno E, Morello N, Landsberger N, Biffo S, Pizzorusso T, Giustetto M, Broccoli V (2011) Reduced AKT/mTOR

signaling and protein synthesis dysregulation in a Rett syndrome animal model. Human Molecular Genetics 20:1182–1196.

Saenger S, Goeldner C, Frey JR, Ozmen L, Ostrowitzki S, Spooren W, Ballard TM, Prinssen E, Borroni E, Metzger F (2011) PEGylation enhances the therapeutic potential for insulin-like growth factor I in central nervous system disorders. Growth Horm IGF Res 21:292–303.

Samaco RC, McGraw CM, Ward CS, Sun Y, Neul JL, Zoghbi HY (2013) Female Mecp2(+/-) mice display robust behavioral deficits on two different genetic backgrounds providing a framework for pre-clinical studies. Human Molecular Genetics 22:96–109.

Schmid DA, Yang T, Ogier M, Adams I, Mirakhur Y, Wang Q, Massa SM, Longo FM, Katz DM (2012) A TrkB small molecule partial agonist rescues TrkB phosphorylation deficits and improves respiratory function in a mouse model of Rett syndrome. Journal of Neuroscience 32:1803–1810.

Shcheglovitov A, Shcheglovitova O, Yazawa M, Portmann T, Shu R, Sebastiano V, Krawisz A, Froehlich W, Bernstein JA, Hallmayer JF, Dolmetsch RE (2013) SHANK3 and IGF1 restore synaptic deficits in neurons from 22q13 deletion syndrome patients. Nature.

Sigmund CD (2000) Viewpoint: are studies in genetically altered mice out of control? Arterioscler Thromb Vasc Biol 20:1425–1429.

Stearns NA, Schaevitz LR, Bowling H, Nag N, Berger-Sweeney J (2007) Behavioral and anatomical abnormalities in Mecp2 mutant mice: a model for Rett syndrome. Neuroscience 146:907–921.

Tropea D, Giacometti E, Wilson NR, Beard C, McCurry C, Fu DD, Flannery R, Jaenisch R, Sur M (2009) Partial reversal of Rett Syndrome-like symptoms in MeCP2 mutant mice. P Natl Acad Sci Usa 106:2029–2034.

Viemari J-C, Roux J-C, Tryba AK, Saywell V, Burnet H, Peña F, Zanella S, Bévengut M, Barthelemy-Requin M, Herzing LBK, Moncla A, Mancini J, Ramirez J-M, Villard L, Hilaire G (2005) Mecp2 deficiency disrupts norepinephrine and respiratory systems in mice. Journal of Neuroscience 25:11521–11530.

Ward CS, Arvide EM, Huang T-W, Yoo J, Noebels JL, Neul JL (2011) MeCP2 is critical within HoxB1-derived tissues of mice for normal lifespan. Journal of Neuroscience 31:10359–10370.

Weese-Mayer DE, Lieske SP, Boothby CM, Kenny AS, Bennett HL, Silvestri JM, Ramirez J-M (2006) Autonomic nervous system dysregulation: breathing and heart rate perturbation during wakefulness in young girls with Rett syndrome. Pediatr Res 60:443–449.

Williams EC, Zhong X, Mohamed A, Li R, Liu Y, Dong Q, Ananiev GE, Mok JCC, Lin BR, Liu J, Chiao C, Cherney R, Li H, Zhang S-C, Chang Q (2014) Mutant astrocytes differentiated from Rett syndrome patients-specific iPSCs have adverse effects on wild-type neurons. Human Molecular Genetics.

Wu D, Pardridge WM (1999) Neuroprotection with noninvasive neurotrophin delivery to the brain. P Natl Acad Sci Usa 96:254–259.

Xinhua Bao, Shengling Jiang, Fuying Song, Hong Pan, Meirong Li, Wu XR (2007) X Chromosome Inactivation in Rett Syndrome and Its Correlations With MeCP2 Mutations and Phenotype. J Child Neurol 23:22–25.

Yan H, Mitschelen M, Bixler GV, Brucklacher RM, Farley JA, Han S, Freeman WM, Sonntag WE (2011) Circulating IGF1 regulates hippocampal IGF1 levels and brain gene expression during adolescence. J Endocrinol 211:27–37.

Yoshii A, Constantine-Paton M (2007) BDNF induces transport of PSD-95 to dendrites through PI3K-AKT signaling after NMDA receptor activation. Nat Neurosci 10:702–711.

Yoshii A, Constantine-Paton M (2010) Postsynaptic BDNF-TrkB signaling in synapse maturation, plasticity, and disease. Dev Neurobiol 70:304–322.

Yoshii A, Sheng MH, Constantine-Paton M (2003) Eye opening induces a rapid dendritic localization of PSD-95 in central visual neurons. P Natl Acad Sci Usa 100:1334–1339.

Zhou Z, Hong EJ, Cohen S, Zhao W-N, Ho H-YH, Schmidt L, Chen WG, Lin Y, Savner E, Griffith EC, Hu L, Steen JAJ, Weitz CJ, Greenberg ME (2006) Brain-specific phosphorylation of MeCP2 regulates activity-dependent Bdnf transcription, dendritic growth, and spine maturation. Neuron 52:255–269.

# Chapter 3: Robust and reliable $Ca^{2+}$ response to complex visual stimuli in astrocytic microdomains

## 3.1 Abstract

Astrocytic intracellular $Ca^{2+}$ signaling has come to light as a prominent feature of neuronal-glial interactions. The majority of astrocyte $Ca^{2+}$ signaling studies are performed in either culture or in situ brain slices, both of which rely on electrical stimulation or pharmacological methods to examine the spatial and temporal coding of astrocyte $Ca^{2+}$ signals. We have investigated visually evoked $Ca^{2+}$ responses in astrocytes of the visual cortex of awake, head-fixed mice using two-photon microscopy. We have found that $Ca^{2+}$ transients in distal processes of cortical astrocytes are more frequent and exhibit a variable relationship with somatic responses. Furthermore, we found discrete structural regions of distal processes of single astrocytes that respond to sinusoidal drifting gratings and are tuned to specific orientations. Lastly, we present the novel finding that natural movies (NM), which are known to evoke sparse but reliable responses from V1 pyramidal neurons, greatly enhance the response probability of astrocyte microdomains to visual stimuli. When compared to sinusoidal gratings, we find that natural movies are significantly more reliable in evoking stimulus-specific responses. We hypothesize that these reliable astrocytic microdomain $Ca^{2+}$ transients are due to the synchronous activation of neighboring ensembles of synapses and are modulated by glutamate transporter activity of perisynaptic astrocyte processes. Using a novel conditional mouse line to down-regulate the expression of GLT-1, we demonstrate that *in vivo* decreases of glutamate transporter expression by astrocytes decreases NM-evoked microdomain

responses. Our results suggest that astrocytes could play an important role in modulating information processing in V1, potentially by modulating response reliability of excitatory synapses through GLT-1 mediated regulation of glutamate availability.

## 3.2 Introduction

Astrocytes comprise one of the largest populations of cells in the brain and have been implicated in a wide range of important functions including structural and metabolic support of neurons (Verkhratsky et al., 2015), neurovascular coupling (Attwell et al., 2010; Carmignoto and Gomez-Gonzalo, 2010; Otsu et al., 2015), clearance of ions and transmitters from synapses (Deitmer and Rose, 2010; Rose and Karus, 2013; Sibille et al., 2014; Kirischuk et al., 2015; Olsen et al., 2015), synaptogenesis and maintenance (Haydon, 2001; Nishida and Okabe, 2007; Theodosis et al., 2008), and more recently, communication with neurons and potential role in information processing (Takata et al., 2011; Ding et al., 2013; Pannasch and Rouach, 2013). Their morphology – domains of extensively ramified processes that overlap minimally with neighboring astrocytes, are motile on the order of minutes, and are responsive to nearby neuronal activity – provides a unique vantage point to carry out some of these particular functions (Bushong et al., 2002; Haber et al., 2006; Wilhelmsson et al., 2006; Reichenbach et al., 2010; Bernardinelli et al., 2014; Perez-Alvarez et al., 2014). Processes in these domains can make contact with thousands of synapses, ensheathing nearly 80% or more of cortical synapses (Ventura and Harris, 1999; Witcher et al., 2007; 2010). These fine-distal processes are densely packed with transporters and mechanisms for the regulation of extracellular ion and

neurotransmitter levels critical to synaptic transmission and neuronal communication (Cheung et al., 2015; Rose and Verkhrastky, 2016)

Astrocytes possess high concentrations of glutamate transporters and are estimated to be responsible for up to 90% of clearance of glutamate from synapses (Tanaka et al., 1997; Danbolt, 2001). Clearance is essential to avoid excitotoxic levels of glutamate and, importantly, can modulate neurotransmission by influencing the duration of synaptic events, the activation of extra-synaptic receptors, and inter-synaptic communication (Tong and Jahr, 1994; Asztely et al., 1997; Huang et al., 2004; Bjørnsen et al., 2013). Glutamate transporter 1 (GLT-1, EAAT2 in humans) is the most prominent transporter expressed in the adult cortex and is largely exclusive to astrocytes. The similar affinities of transporters and receptors for glutamate indicate that competition for glutamate at synapses plays a role in modulating receptor activation (Arriza et al., 1994; Huang et al., 2004), emphasizing the essential function of astrocytic-neuronal interactions.

While the discovery that glutamate and neuronal activity elicits $Ca^{2+}$ elevations in astrocytes has over the years resulted in some controversy, it also unearthed new and vital roles for these cells previously thought to be strictly metabolic players in the brain (Cornell-Bell et al., 1990; Smith, 1994; Porter and McCarthy, 1996; Fiacco et al., 2007; Petravicz et al., 2008; Hamilton and Attwell, 2010; Bazargani and Attwell, 2016). Indeed, recent evidence indicates that they respond to sensory activity and may even contribute to information processing (Wang et al., 2006; Dombeck et al., 2007; Wang et al., 2012; Ding et al., 2013; Kirischuk et al., 2015). Our laboratory has previously shown that astrocyte somata in ferret visual cortex not only respond to visual stimuli and have

spatial receptive fields but also show feature-specific responses such as orientation and direction-selectivity (Schummers et al., 2008). This is partly due to the columnar organization and spatial mapping of neuronal receptive fields; astrocytes in ferret visual cortex receive inputs from synapses sharing receptive field and response features (such as orientation selectivity) of adjacent neurons (Chapman and Stryker, 1993; Yu et al., 2005; Schummers et al., 2008). The rodent visual cortex lacks a similar columnar map and therefore astrocytes receive inputs from a more heterogeneous synaptic landscape. Thus, it is unlikely that astrocyte somata in mouse visual cortex would show orientation-selective responses; rather, astrocyte microdomains would reflect response features of adjacent synapses if microdomain activity could be accurately measured.

Efficient processing of visual information requires the processing of salient features while overcoming the inherent variability of neuronal networks (Shadlen and Newsome, 1994; Azouz and Gray, 1999; Rosenbaum et al., 2014). Previous studies have shown that trial-to-trial variability of neuronal responses is reduced in responses to natural scenes, resulting in both spike trains and subthreshold potentials that are more reliable and sparse (Borst and Theunissen, 1999; Olshausen and Field, 2004; Haider et al., 2010; Baudot et al., 2013). Statistically, natural scenes contain multiple spatial frequencies with a power law distribution that is hypothesized to be used by the visual system to more efficiently encode information (Ruderman and Bialek, 1994; Simoncelli and Olshausen, 2003; Bar, 2004; Barlow, 2009). In contrast, sinusoidal gratings, which contain only one spatial frequency, yield more trial-to-trail variability and evoke less reliable responses (Baudot et al., 2013). At the level of neural populations, it has been shown that movies with naturalistic spectral properties

activate strong local and long-range correlations between neurons, leading to ensembles of synchronously activated neurons (Rikhye and Sur, 2015). This form of population coding helps to minimize shared variability between neurons, and consequentially improves response reliability.

In this study, we asked whether presentation of natural movies evokes reliable $Ca^{2+}$ responses in astrocytic microdomains of rodent primary visual cortex (V1). In order to do so, we have developed methods to investigate the spatial organization of the entire extent of astrocytic microdomains, probing both spatially correlated and reliable responses to visual stimuli. We have used high-resolution in vivo two-photon imaging of single astrocytes in layer 2/3 rodent visual cortex, along with novel reporter lines and the targeted expression of genetically encoded calcium indicators to monitor activity in awake animals. We show that astrocyte microdomains, and not somas, exhibit robust and frequent spontaneous activity, and that natural movies activate larger, more reliable microdomain activity. Furthermore, we find that the response reliability to natural movies, but not to gratings, is modulated by expression of GLT-1. Given the role of glutamate transporters in modulating synaptic activity, this work implicates astrocytes in functional sensory circuit processing.

## 3.3 Methods

### *3.3.1 Mouse lines*

To generate the GFAP-tdTomato transgenic line, a shortened version of the human GFAP promoter (hGFAP, generously provided by the Haydon lab) was cloned together with the red fluorescent protein variant tdTomato (in collaboration with the

Guoping Feng lab) to generate mice expressing tdTomato in astrocytes. Mice kept on a C57BL/6J (Jackson Labs, Maine; Stock#000664) background were generated and used in the initial experiments to identify astrocyte morphology *in vivo* and with viral-mediated expression of calcium indicators.

Transgenic line expressing GCaMP5G in astrocytes was accomplished by using a Cre recombinase inducible system. The GFAP-Cre line (Jackson Labs, Maine; Stock No. 024098) was crossed with the mice expressing the fluorescent calcium indicator protein GCaMP5G variant and tdTomato red fluorescent protein in a Cre recombinase-dependent manner (PC-G5-tdT, Jackson Labs, Maine; Stock No.024477). These mice were used in most experiments testing reliability of visually-evoked $Ca^{2+}$ responses.

For experiments manipulating glutamate transporters, TetO-GLT-1 mice were generously donated by the Kohichi Tanaka lab (Tokyo Medical and Dental University, Tokyo, Japan). Briefly, mice were generated by insertion of Neo-Stop cassette upstream of exon1 of mouse *GLT-1* locus under the regulation of tetracycline trans-activator (tTa). The tetracycline analog, doxycycline, could be used to remove suppression of the stop codon, which decreased transcription of endogenous *GLT-1.*

### *3.3.2 Viruses*

Virus was constructed using the shortened hGFAP promoter to drive expression of the membrane-bound GCaMP5 (Lck-GCaMP5G, AddGene) in an AAV2.5 construct (Virovek). This vector was used in initial experiments with the GFAP-tdTomato transgenic line. To visualize $Ca^{2+}$ activity in mice used in experiments manipulating

GLT-1 protein levels, we used the AAV5.GfaABC1D.Lck-GCaMP6f.SV40 vector (Penn Vector Core, University of Pennsylvania).

### *3.3.3 Surgery*

Experiments were performed under protocols approved by the Massachusetts Institute of Technology's Animal Care and Use Committee and conformed to NIH guidelines. All data in this study were collected from adult (>8 weeks old) mice of either sex (see Mice section above for specific lines and experiments). Mice were anesthetized using isofluorane (3% induction, 1.5–2% during surgery). A custom-built metal head post was attached to the skull using dental cement (C&B-Metabond, Parkell), and a 3-mm-diameter craniotomy was performed over binocular V1 (2–3 mm lateral and 0.5 mm anterior to lambda). Care was taken not to rupture the dura mater. The core body temperature was maintained at 37.5°C using a heating blanket (Harvard Apparatus). Mice were allowed to recover for 2–3 weeks to allow for adequate expression of the virus before imaging commenced. For experiments using the PC-G5-tdT transgenic line, we followed the same surgical procedure for craniotomy, window implantation, and head post attachment without virus injection. Mice were allowed to recover for one week before imaging experiments began.

### *3.3.4 Western Blot Analysis*

Expression of GLT-1 was analyzed via Western blot. Neo- cortex from TetO-GLT-1 mouse brain slices was dissected and homogenized using RIPA buffer (150 mM NaCl, 1% Triton X-100, 0.5% sodium deoxycholate, 0.1% SDS, 50 mM Tris, pH 8.0)

and protease inhibitor cocktail. Samples were then centrifuged at 13,200 rpm for 15 min at 4 °C. 10-15 mg of protein was loaded onto a 10% SDS-PAGE gel and analyzed via electrophoresis (BioRad, Hercules CA). Proteins were detected using guniea pig-anti-GLT-1 (1:10,000, Millipore). Mouse-anti-β-actin (1:2000, Sigma) was used to confirm equal loading. Protein bands were visualized using fluorescently conjugated anti-mouse, or anti-goat antibodies (1:10,000 LiCor Biosciences, Lincoln, NE). Blots were scanned using an Odyssey Infrared Imager (LiCor Biosciences, Lincoln, NE). Quantification of protein expression was conducted using ImageJ (NIH) and expressed in relation to β-actin expression.

### *3.3.5 Two-photon calcium imaging*

Mice were habituated to both imaging environment and visual stimulus prior to imaging sessions. During two-photon imaging sessions, awake animals were head-attached to custom-made stage for two-photon microscopy using a Prairie Ultima two-photon system (Prairie Technologies) driven by a Spectra Physics Mai-Tai eHP laser, passed through a Deep-See module (Spectra Physics / Newport). Excitation laser was tuned to 910 nm and passed through a 25x water-immersion objective (Olympus). Movies were acquired at ~7Hz frame rate.

### *3.3.6 Visual stimulation*

To assess the orientation selectivity and tuning of neurons, we presented oriented gratings on a 23" 1080p LCD monitor (Dell) using custom software (Network Visstim, Sur Lab) written in PsychToolbox-3 (Psychtoolbox.com) on a Windows 7

computer (Dell Precision) with a GeForce 8800 GTS 640MB graphics card (PNY). Gratings were optimized for cellular responsiveness using a contrast of 100%, spatial frequency of 0.002-0.256 cycles/degree, and a temporal frequency of 1-3 Hz. Gratings were then presented by stepping the orientation from 0-360 degrees in steps of 30 degrees, with each grating presentation being preceded for 6 seconds "off" followed by 2 seconds "on'.

Natural movies (n = 5) were selected from the van Hateren natural movie database. Gray scale values of each movie were discretized to 255 values and each frame was normalized to have equal mean luminance (mean of histogram = 128) and contrast (std. deviation of histogram = 32). To slow down the movie from its original 60Hz frame rate, we updated every three frames creating an effective frame rate of close to 20Hz. Movies were presented for 10s and were flanked by 4s gray screens (mean luminance = 128). See also Figure 6.

## 3.4 Results

### *3.4.1 Tools to monitor astrocyte $Ca^{2+}$ activity in vivo*

In order to visualize physiologically relevant $Ca^{2+}$ transients in astrocytic microdomains, we had to overcome several limitations in the field. First, traditional acute preparations would not suffice as previous attempts in the lab and recent evidence has shown that anesthetics can directly dampen astrocytic responses, even more than neuronal ones (Schummers et al., 2008; Thrane et al., 2012). Second, the improvements in genetically encoded calcium indicators was instrumental in allowing visualizing of microdomain transients as previously used organic dyes did not

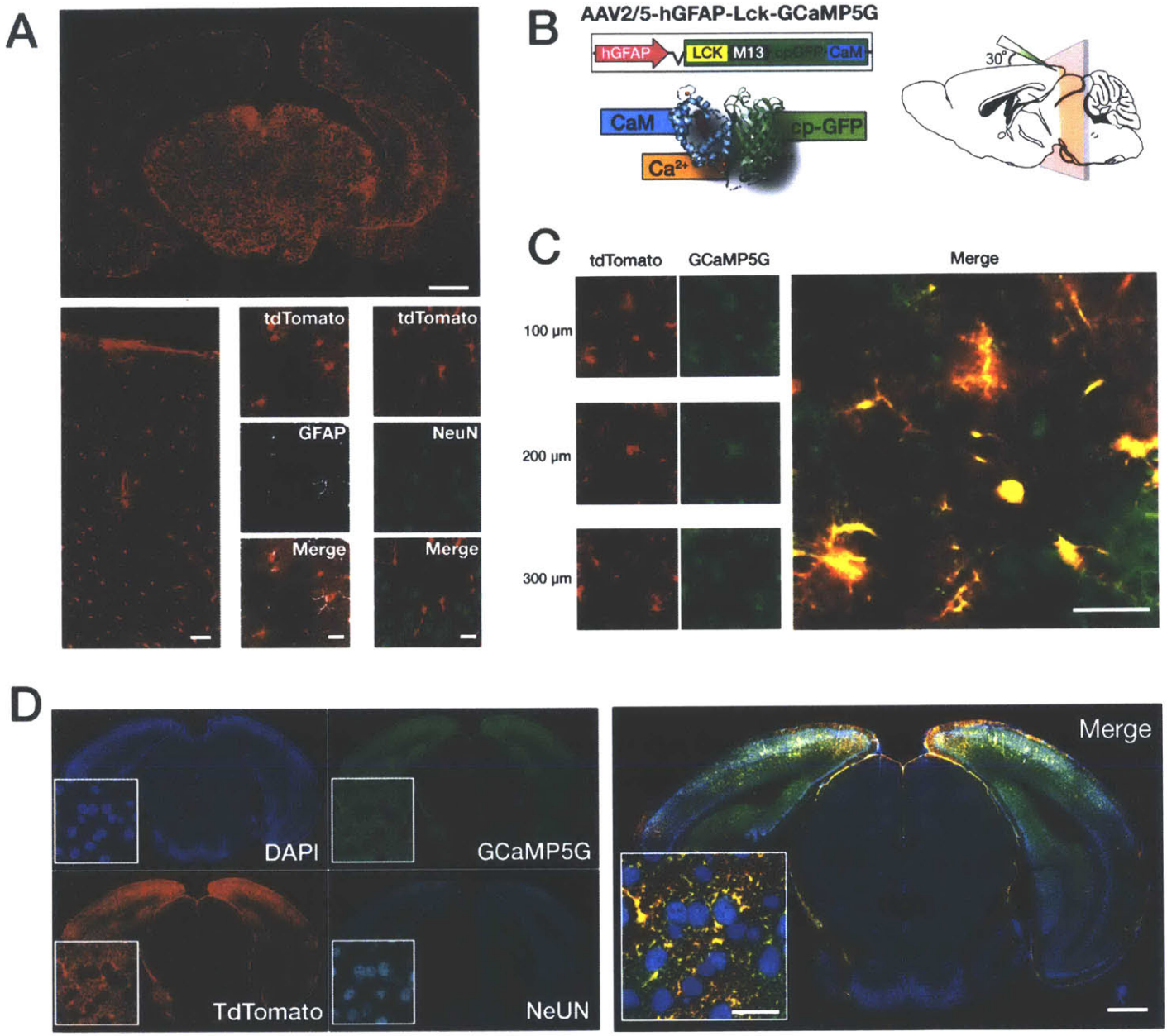


**Figure 1 – Genetically encoded calcium indicators used to monitor astrocyte activity in vivo.** A) Novel reporter line expressing td-Tomato under the human GFAP promoter results in cell-specific expression throughout the brain (top) and all cortical layers (bottom left). Immunostaining shows reporter colocalization with GFAP in astrocytes (bottom, middle). No colocalization is observed with neurons (bottom right). B) Schematic showing AAV2.5 expressing the membrane-bound $Ca^{2+}$ indicator (LCK-GCaMP5G) driven by the shortened human GFAP promoter (left) and diagram of target visual cortex injections in the rodent brain (right). C) In vivo images showing colocalization of the tdTomato reporter with the viral-mediated expression of the $Ca^{2+}$ indicator at different cortical depths (left). Merged z-stack max projection image on the right. D) Newly available floxed transgenic mouse line allows for conditional expression of tdTomato reporter and GCaMP5G by crossing with GFAP-Cre mice for cell-specific expression.

penetrate to the fine distal processes. Third, in order to identify and visualize individual astrocytes in vivo, along with as much of ramified processes, we needed a reporter line that could accomplish this with a fluorescent marker that did not interfere with available GFP-based GECI's.

To overcome these limitations, we generated a novel transgenic mouse line that robustly expresses td-Tomato selectively in astrocytes, confirmed by cell-specific reporter expression using immunohistochemical staining (Figure 1A). No overlap with non-astrocytic markers was observed in situ throughout the cortex. For viral-mediated delivery of a genetically encoded calcium indicator, we used a shortened human GFAP promoter and packaged the membrane-bound version of the GCaMP5 (LCK-GCaMP5G, (Shigetomi et al., 2010a)) into an AAV vector and targeted astrocytes of layer 2/3 visual cortex (Figure 1B-C). We also used a recently published transgenic line that allowed for non-invasive expression of the same reporter and indicators through the use of the cre-flox conditional expression system (Figure 1D; (Gee et al., 2014)).

To image cortical activity in awake behaving animals, we used high resolution two photon imaging of head-fixed animals with cranial windows over primary visual cortex and exposed them to different visual presentations on a screen (Figure 2A). In order to obtain as much information as possible from astrocytes, we imaged at a single-cell resolution with a frame size of ~70 μm x 70 μm. This allowed us to visualize the full extent of a putative single astrocytic domain that included the soma, primary processes, and microdomain regions in the peripheral processes (Figure 2B-C).

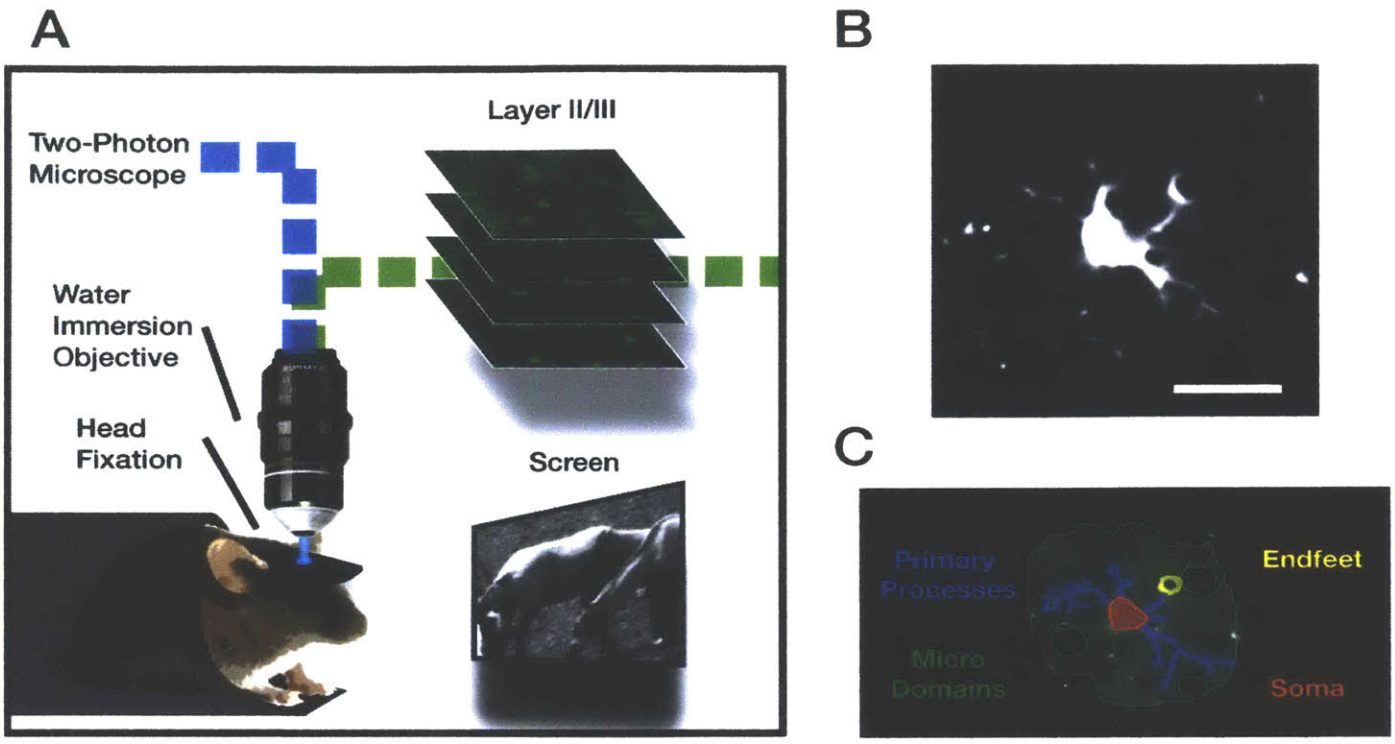


**Figure 2 – In vivo, awake imaging of layer 2/3 astrocytes in rodent visual cortex.** A) Schematic of experimental setup for two-photon imaging with screen for visual stimulus presentation. B) Max projection of single astrocyte (Scale bar = 20 μm). C) Schematic overlaid over same cell in B showing prominent features including negative space of pre-sumptive neuronal cell bodies (black).

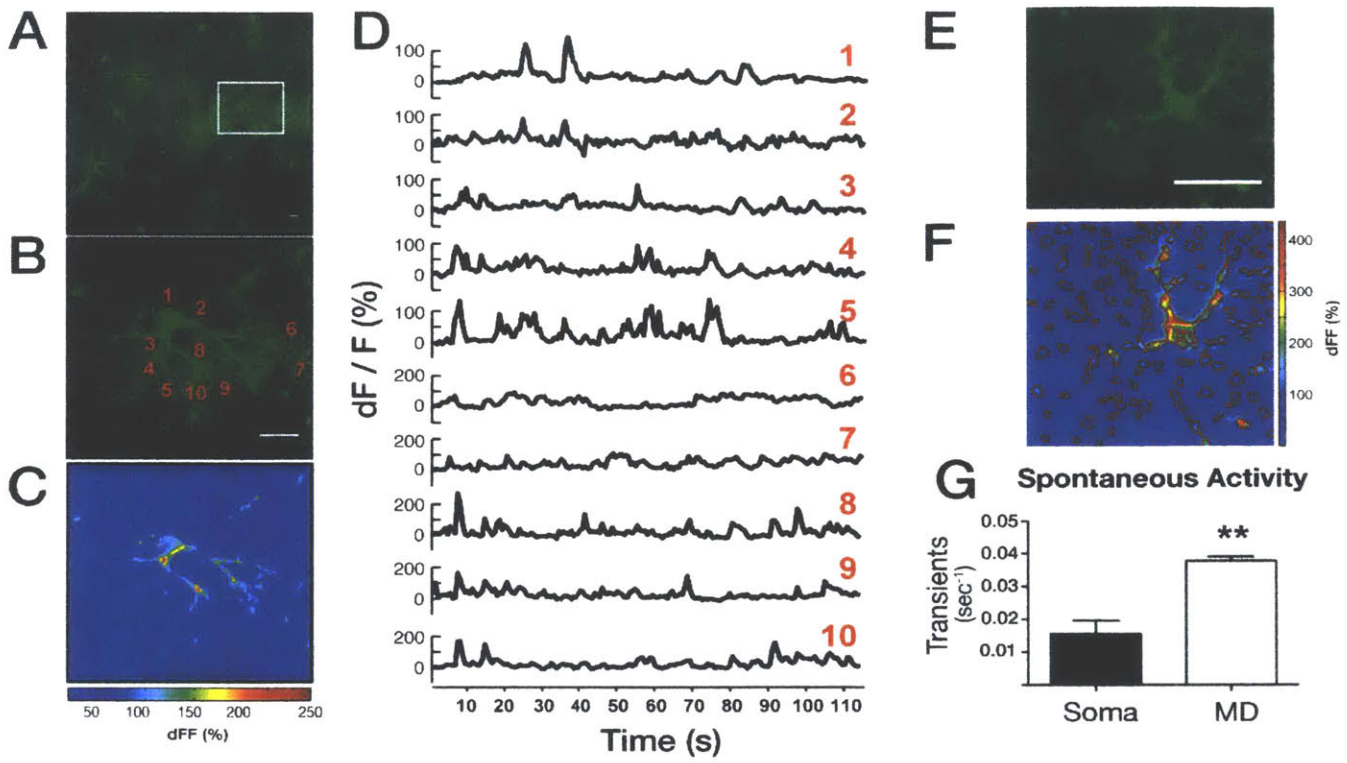


**Figure 3 – Astrocyte microdomains show robust spontaneous transients.** A) Wide field view showing multiple astrocytes expressing GCaMP5G. B) Single astrocyte from (A) with regions of interests including soma, primary processes, and fine distal processes. Scale bar = 10 μm. C) Heat map of dF/F (%) activity on same astrocyte. D) Traces of spontaneous activity from ROIs depicted in B. E) Representative astrocyte expressing GCaMP5G with visible vasculature labeled by endfeet. F) Heat map of calcium activity of same cell with regions of interest overlaid. G) Frequency of spontaneous transients is significantly greater in processes as compared to soma. (**, $P < 0.01$; n = 10 cells, 3 animals). Scale bar = 20 μm.

### 3.4.2 *Astrocyte microdomains show robust spontaneous transients in vivo*

Several studies have previously reported that astrocytic $Ca^{2+}$ responses can be orders of magnitude slower and less frequent than neuronal responses (Kanemaru et al., 2014; Otsu et al., 2015). However, it has become clear that activity in the finer distal processes are both more frequent and have faster rise times than somatic transients (Di Castro et al., 2011; Tong et al., 2012; Shigetomi et al., 2013a);. Our imaging of spontaneous calcium activity corroborates these previous findings: we find that layer 2/3 astrocytes display robust spontaneous $Ca^{2+}$ transients both in soma and in distal processes. Further, the majority of microdomain (MD) transients occurred independent of somatic activity when imaged at single-cell resolution (Figure 3A-D). MD transients were measured and found to occur ~2.5 times more frequently than somatic activity (Figure 3E-G).

### 3.4.3 *Astrocyte microdomains show orientation selectivity*

Since the bulk of the transient activity was found to occur in microdomains located in the peripheral processes, we next wanted to examine visually evoked responses in these microdomains. Figure 4 A & B show two representative astrocytes located about ~150 μm below the pial surface during presentation of drifting sinusoidal gratings. Using custom-written MATLAB algorithms, we were able to identify regions of interest (Figure 4 A & B, insets) that showed calcium increases during the stimulus-on time (Figure C & D, left). We next examined orientation tuning with drifting gratings at different orientations, a common feature of neuronal responses. The right panels in

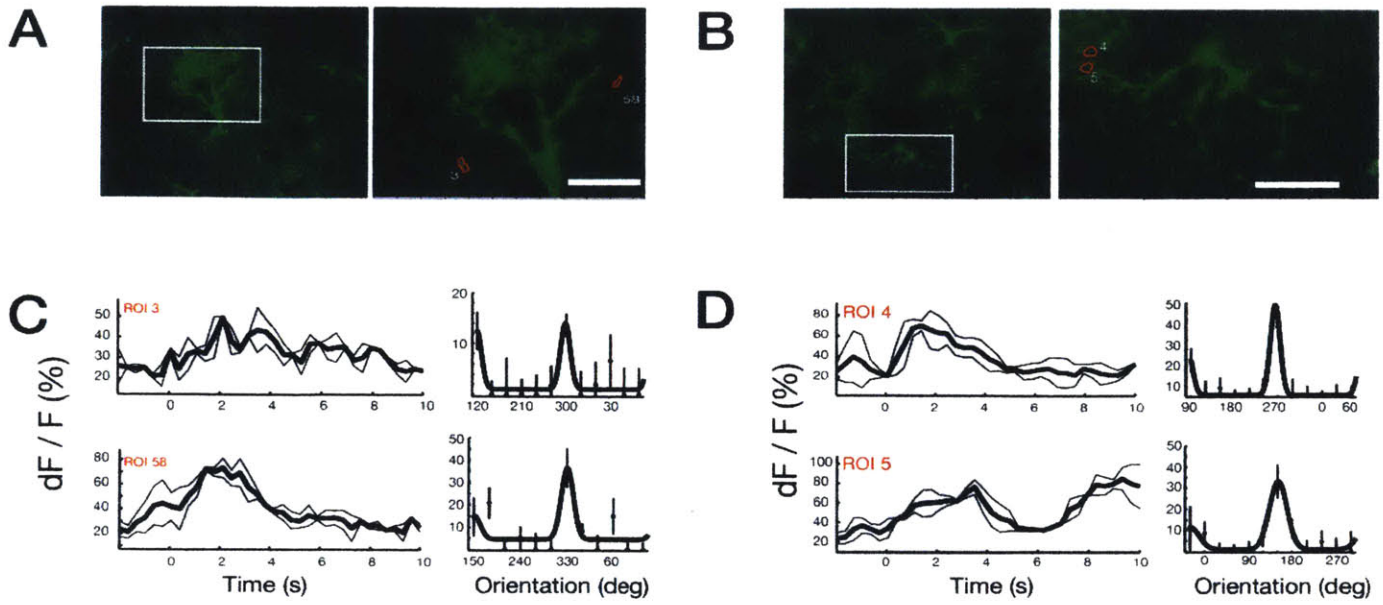


**Figure 4 – Astrocyte microdomains show orientation selectivity.** (A-B) Average projections of cells expressing GCaMP5G in layer 2/3 of visual cortex (left) and individual cells selected with visually responsive regions of interest outlined (right). Scale bars = 20 μm. C-D) Response traces to preferred orientations during visual stimulus (left; shaded box indicates stimulus ON time) and amplitude of responses to preferred orientations.

Figure 4 C & D show the orientation tuning for the regions of interested in the microdomains of the cells depicted above.

### *3.4.4 Natural movies elicit reliable responses*

Only a small percentage of the total microdomains in any given layer 2/3 astrocyte showed regions with orientation tuning. One possible explanation for this is that the surrounding synaptic activity was not sufficient to elicit robust calcium transients in astrocytes. Therefore, we employed a second type of visual stimulus, one which evokes different response properties from the surrounding neuronal network. In contrast to sinusoidal gratings, natural movies (NM) have different stimulus statistics that distinctly activate visual cortex circuits (Figure 5A). Gratings have a single spatial frequency (SF), whereas NMs contain a power law distribution of SFs with broad image features represented by higher power in the low SFs and fine structural details that with weak power in the higher SFs (Bar, 2004). Previous studies have shown that full field natural movies activate neural responses with better signal-to-noise ratio, and hence are processed more efficiently than gratings (Figure 5B). A common measurement of how efficiently a neuron responds is the degree of trial-to-trial variability to a given stimulus, quantified as the reliability of the response, with natural movies evoking more reliable responses compared to gratings (Figure 5C; (Baudot et al., 2013). In the rodent visual cortex, adjacent neurons do not share similar response features – they are not functionally organized into columns and neurons with a given orientation preference seem to be randomly distributed (Ohki and Reid, 2007; Jia et al., 2010). In contrast, full-field stimulation by natural movies elicits highly correlated

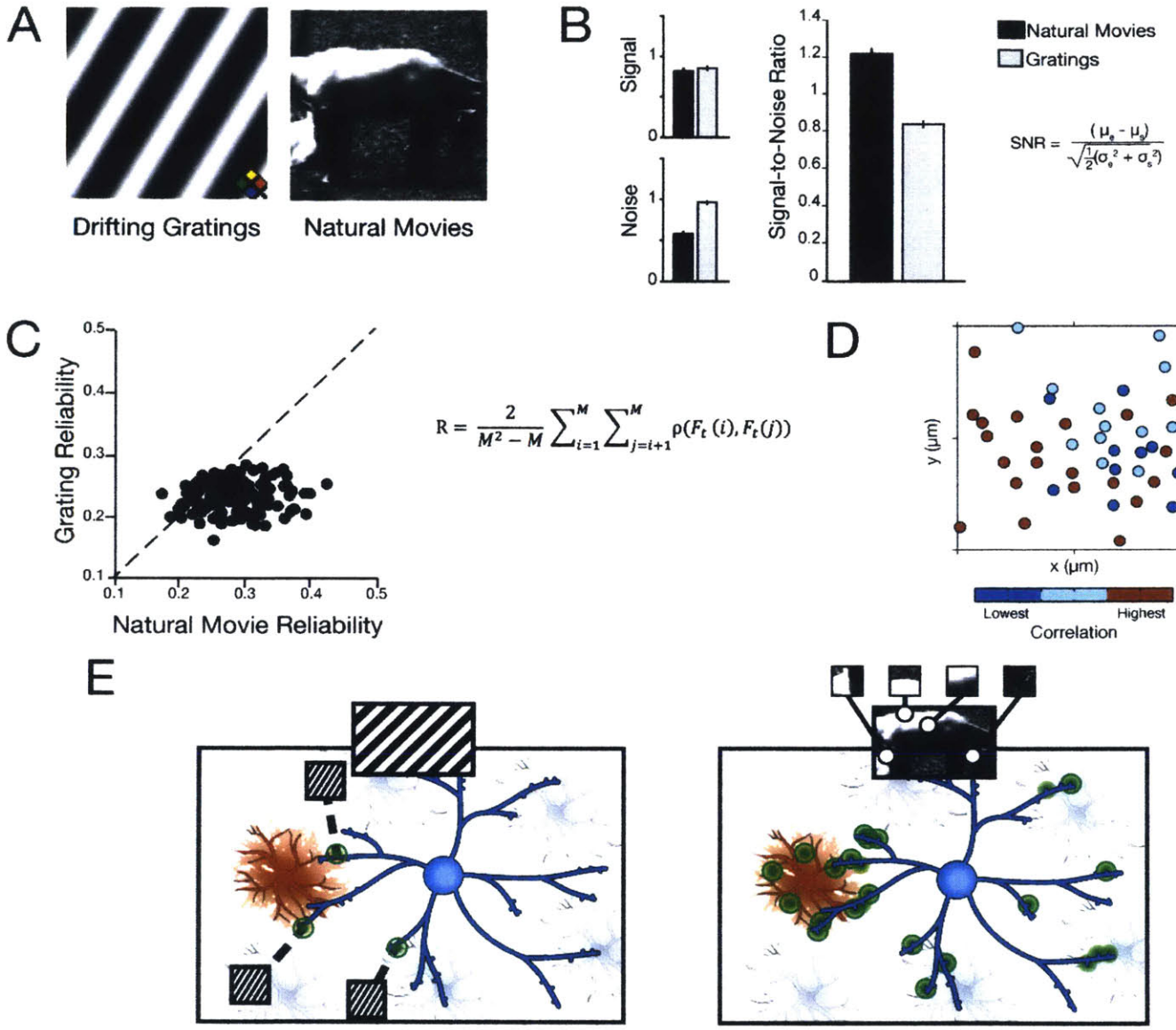


**Figure 5 – Natural movies elicit more reliable and robust responses.** A) Illustrations of simple sinusoidal drifting grating (left) and complex natural movies (single frame, right) stimuli. B) In neurons, natural movies elicit complex interactions and yield greater signal-to-noise ratios than gratings. C) Trial-to-trial variability is also measured by response similarity, or reliability of responses. Neurons respond with higher reliability to natural movies than to simple drifting gratings. D) Illustration representing neurons in a single imaging plane responding to natural movies. Ensembles of neighboring neurons are strongly correlated when stimulated with natural movies. E) Schematic depicting proposed model. Gratings elicit heterogeneous synaptic activation on neuronal dendrites with more variability and will lead to less reliable and sparser astrocyte microdomain activation, left. Natural movies have richer simulus features including multiple orientations and spatial frequencies (top inset on right) that activate larger number of neurons and synapses that we propose will be reflected in larger and more reliable microdomain activation, right.

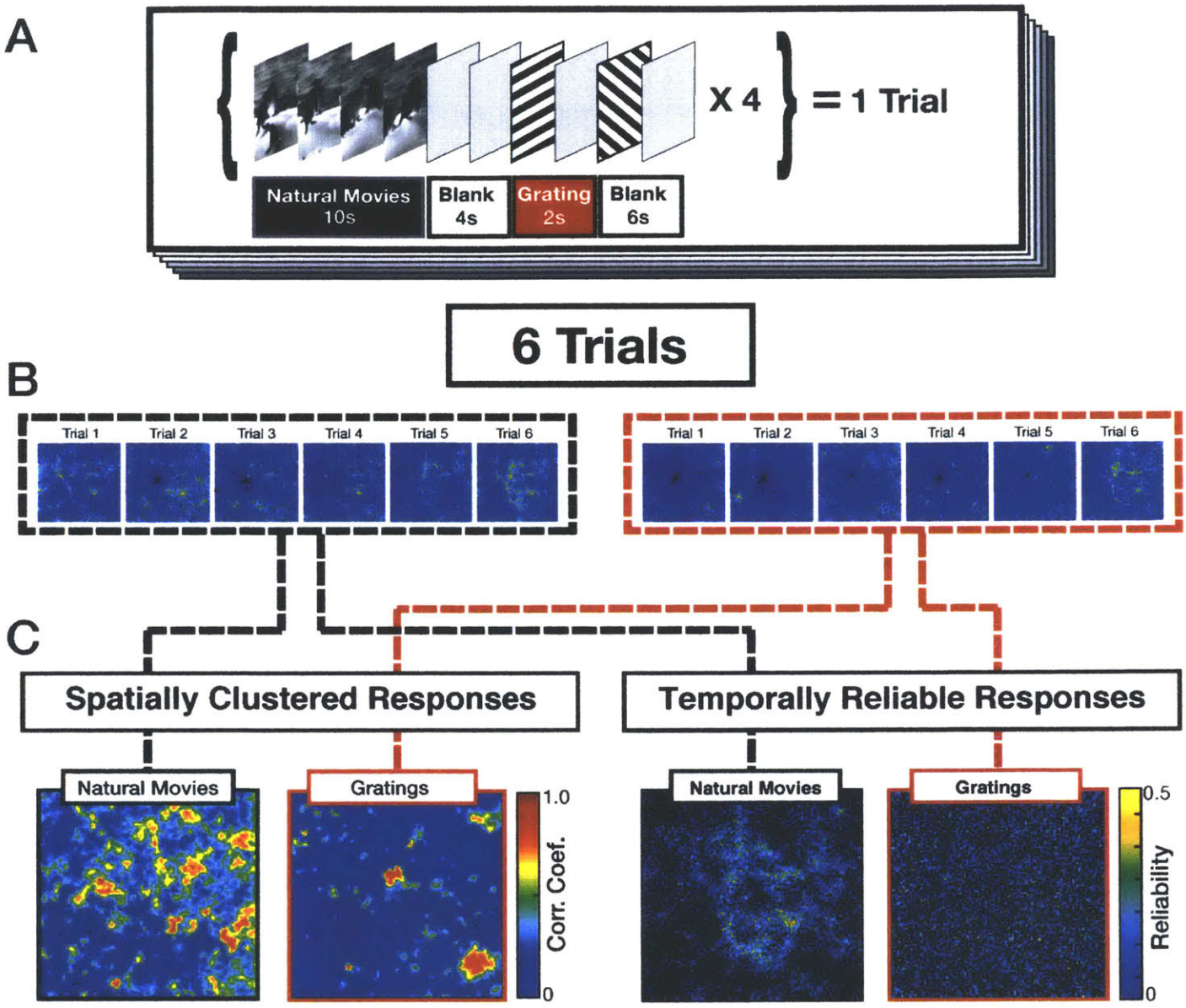


**Figure 6 – Stimulus protocol elicits spatially correlated and temporally reliable responses in microdomains.** A) Schematic of stimulus protocol featuring periods of on and off time for both natural movies and drifting gratings. B) Each trial is repeated 6 times and responses for each pixel are evaluated for spatial correlation of neighboring pixels and trial-to-trial variability. C) Heat maps for the responses for each stimulus are generated for analysis: spatially clustered maps of correlation values (left) and temporally reliable responses (right).

ensembles of neurons in the rodent visual cortex (Figure 5D). Taken together, these features of NMs elicit more reliable responses from neuronal circuits and may be critical for efficient visual information processing. This offered an opportunity to test the hypothesis that if astrocytes play a more active role in information processing, than they should reflect the response features evoked by NMs in the neuronal circuits they are interacting with (Figure 5E). Therefore, we hypothesize that astrocytes will display increased microdomain activity in response to NMs. We conducted awake in vivo measurements of single astrocytes to determine if NMs elicited more coordinated microdomain activation reflective of the corresponding neuronal ensemble activity.

We developed a protocol to investigate the visually driven responses in the microdomains of single astrocytes in response to both gratings and NMs (Figure 6A). There is a growing body of literature on the diversity of $Ca^{2+}$ signals in astrocytes, and an effort to understand the dynamics of microdomain activity (Khakh and Mccarthy, 2015; Khakh and Sofroniew, 2015). Our primary goal was to first characterize the response properties of astrocytes in circuits responding to sensory information. With this in mind, we employed two pixel-based approaches to identify and analyze relevant, visually-evoked activity. The first is based on signal correlation of neighboring pixels that identifies spatially clustered microdomains that are activated during various stimulus conditions, i.e. gratings, NMs, or spontaneous transients (Figure 6C, left). The second is aimed at identifying microdomains that have reliable responses to the different stimuli: temporally correlated responses with low trial-to-trial variability that yields maps of pixels based on their similarity of responses across trials (Figure 6C, right).

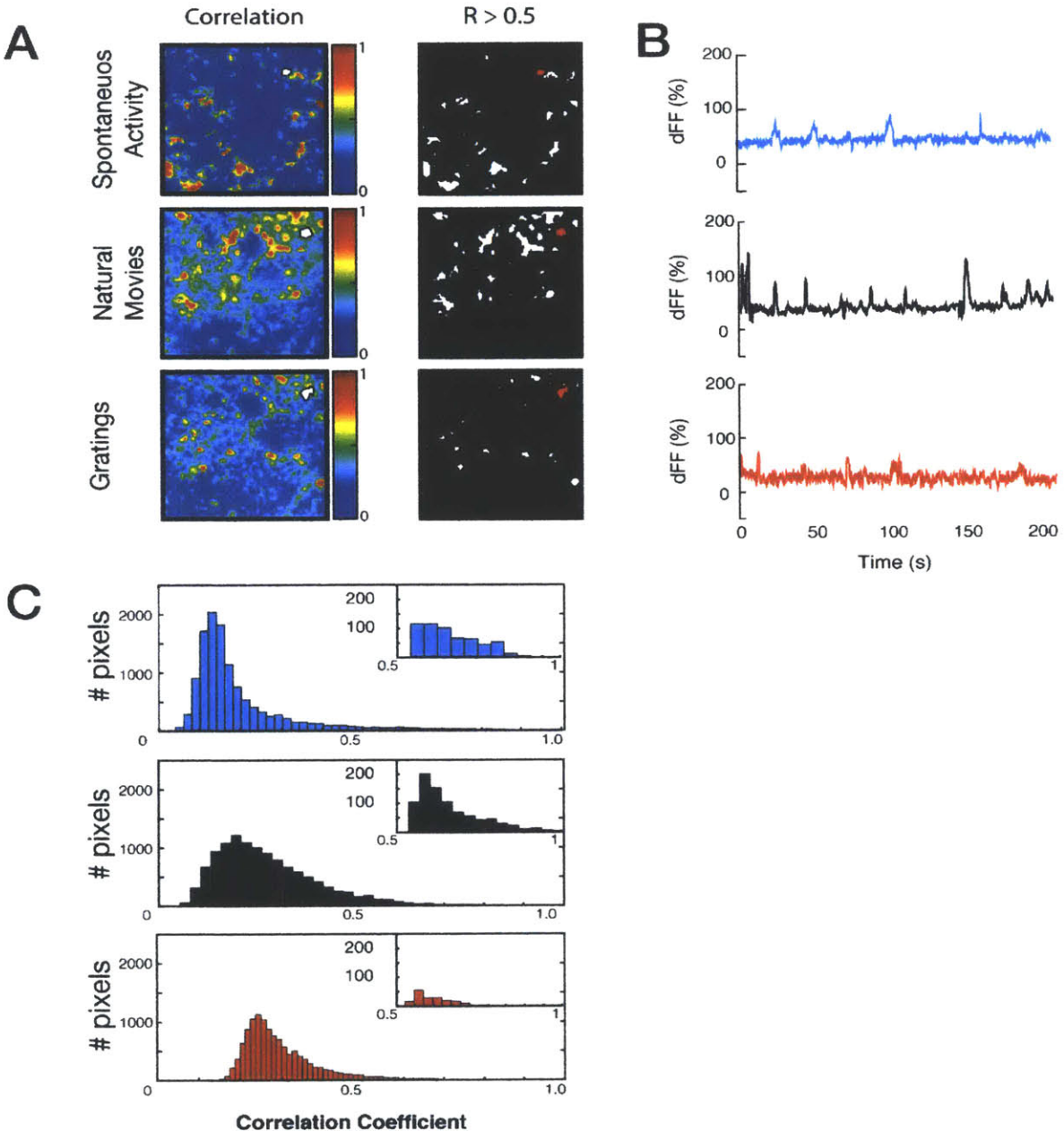


**Figure 7 – Spatially clustered responses in microdomains.** A) Representative heat maps of the same astrocyte to different visual response states depicting clusters of spatially correlated microdomains (left) and same maps thresholded showing regions of pixels with significant correlations (R > 0.5, right). B) Example response traces for regions of interest in (A, right) for each condition: spontaneous activity (top), natural movies, and gratings. C) Distribution of pixels with corresponding correlation values of representative maps in (A, left). Inset shows distribution for significant pixels.

### *3.4.5 Spatially clustered responses in microdomains*

We analyzed the activity of microdomains of single astrocytes under different stimulus conditions. First, we examined the spatially correlated regions activated by NMs and gratings, and also determined the level of activity of spontaneous $Ca^{2+}$ transients. Figure 7A shows representative heat maps for each condition generated based on the correlation of neighboring pixels. From these maps we were able to identify regions that were highly correlated ($R > 0.5$; Figure 7A, right) and compare the response amplitudes to the different stimulus conditions (Figure 7B). We observed that spontaneous activity in the microdomains was more frequent when compared to somatic activity, so we therefore wished to determine how this activation was distributed throughout the astrocyte processes (Figure 7C). Our results indicate that the average response amplitude of microdomains did not differ in response to different stimulus conditions (Figure 8A). However, the total area of the responding microdomains was significantly larger with NMs (Figure 8B). These data are in agreement with the activation of larger numbers of correlated neuronal responses evoked by NMs (Rikhye and Sur, 2015). While this analysis provided insight in to the spatial and temporal profile of visually evoked microdomain responses, it did not address the question as to how reliably astrocyte microdomain activity is elicited by the two differing stimulus sets.

### *3.4.6 Natural movies elicit larger microdomains of reliable responses*

In order to determine the reliability of responses to gratings and NMs and the corresponding degree to which microdomain regions were being activated by the

different stimulus conditions, we employed the second analysis method. We hypothesized that if astrocytes were responding to neuronal activity with microdomain increases in $Ca^{2+}$, then we would expect their responses to exhibit reduced trial-to-trial variability and as well as show greater area of microdomain activation under stimulus conditions such as NMS that evoked similarly reliable responses from neurons. We first quantified the response reliability of every image pixel across stimulus trials and generated activity maps depicting areas with highly reliable pixels. This generated maps of pixel reliability that showed that while a few cells displayed highly active somatic responses during the visual stimulus presentation, most of the highly reliable regions corresponded with process microdomains (Figure 9A, see second representative cell). To quantify the microdomain structures exhibiting high reliability, we performed a power spectrum (PS) analysis of the reliability maps (Figure 9B). Larger clusters of reliable pixels yield higher power in the lower spatial frequencies (SF) and weak power in the higher SFs. Maps with no discernable clustering of areas with reliable pixels result in power spectra traces with low to zero slope, reflecting weak power values across most spatial frequencies. NMs consistently produced reliability maps with higher power in the lower SF indicating that more microdomains were reliably activated as compared to those elicited by gratings stimuli (representative traces in Figure 9B, all cells plotted in Figure 9C). Measuring the slopes of the power spectrum traces confirmed that reliability maps contained larger domains of reliable activity in response to NMs than to gratings (Figure 9D).

### *3.4.7 Glutamate transporters influence reliability of astrocyte responses*

One of the main functions carried out by astrocytes is the clearance of glutamate from the synaptic cleft via glutamate transporters, which can localize to distal processes that are in contact with active synapses and are capable of modulating synaptic transmission (Jackson et al., 2014). Astrocytic clearance of glutamate has been shown in other brain regions to modulate synaptic transmission (Scanziani and Hausser, 2009) and our own lab has demonstrated that blocking of glutamate transporters can modulate visually-evoked $Ca^{2+}$ transients in astrocytes and response properties of neurons (Schummers et al., 2008). Therefore, we hypothesized that altered glutamate transporter expression, and presumably altered synaptic cleft clearance rates, would influence the reliability of responses that we have observed. In collaboration with the Tanaka lab, we obtained a novel transgenic mouse line that uses the tetracycline (Tet) inducible expression system to control the expression of GLT-1 in astrocytes (Figure 10A). Activation of the Tet-off system with doxycycline (dox), a Tet analog, in the chow fed to the animals leads to a down-regulation of the expression of GLT-1. Western blot analysis of brain lysates of animals before and after they were given dox in their diet confirmed the reduction GLT-1 levels. We observed a ~50% reduction in total GLT-1 protein by two weeks, and nearly a ~75% reduction by four weeks (Figure 10C). This protein analysis provides us with a dose response curve that allows us the ability to predict the loss of GLT-1 by astrocytes and examine in the same animal alterations to response properties. This model represents a powerful tool

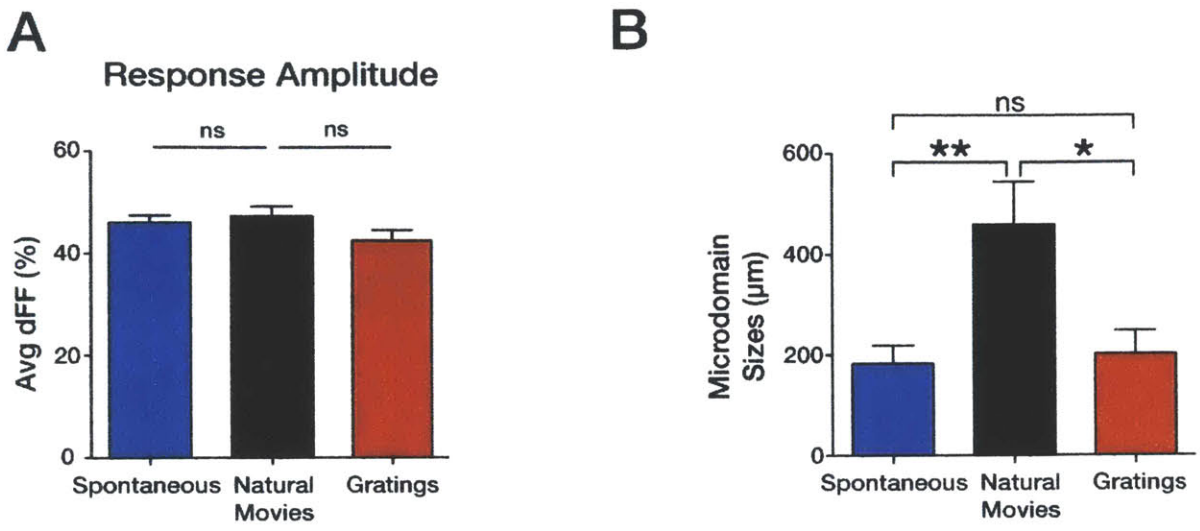


**Figure 8 – Response amplitudes and microdomain sizes.** A) Average response amplitudes for the different conditions show no significant differences in microdomains. B) Average microdomain areas of clustered responses.

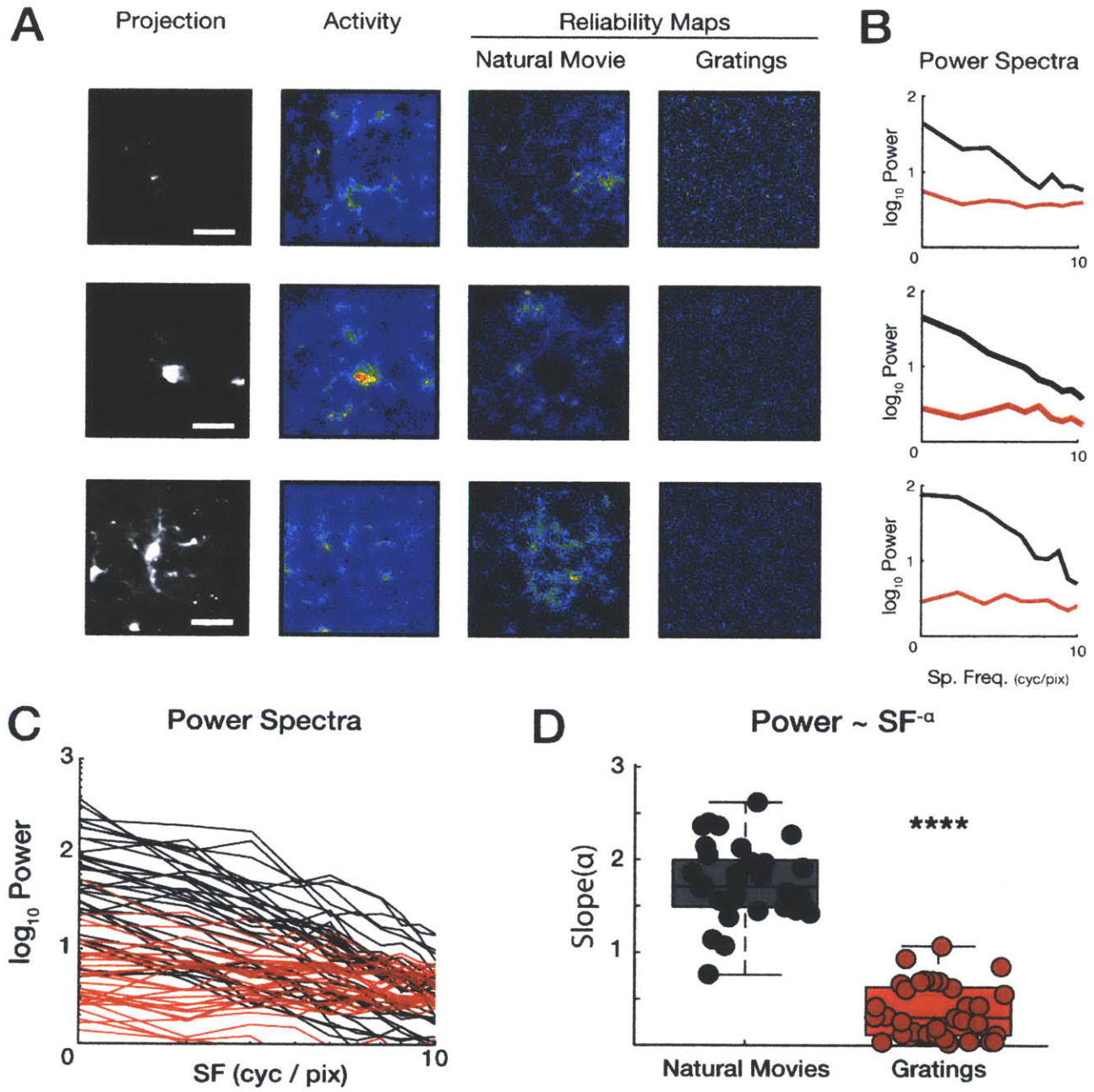


**Figure 9 – Natural movies elicit larger clusters of temporally reliable microdomains.** A) Representative cells depicting max projection of time series, max dFF activity, and reliability maps of microdomain clusters for responses to natural movies and drifting gratings (Scale bar = 20 μm). B) Power spectra (PS) of reliability maps for cells in (A) showing larger power (amplitude of trace) in the lower spatial frequencies (left on x-axis) which correspond to larger clusters of reliable pixels in natural movies as compared to gratings. C) Power spectra traces aof all recorded cells. D) Average slopes of PS traces for all cells are greater for natural movies than for gratings, indicating larger clustering of reliably activated microdomains. (n = 34 cells, 10 animals)

in which we may temporally control the level of GLT-1 expression by astrocytes while avoiding developmental issues associated with a germline knockout model.

Using this conditional mouse model, we conducted experiments to determine the contribution of GLT-1 to visually-evoked response reliability of astrocyte microdomains. To provide an in-animal control, we replicated our findings from WT animals in which NMs evoked larger microdomain areas of reliable responses than the drifting grating stimulus. We found that prior to dox treatment and reduction of GLT-1 protein levels, astrocytes showed reliability maps with significant differences in the sizes of microdomains that were activated by NMs and gratings (Figure 11A & B, left). This difference between NM and grating responses was qualitatively reduced by two weeks of dox treatment and further by four weeks of treatment (Figure 11A, middle and right). Correspondingly, there was a progressive reduction in the difference between the slopes of the NM and grating responses (Figure 11B, middle and right). While the reliability maps showed significant differences in slopes at all time points between NM and grating stimuli, there was a marked trend towards reduced activation of microdomains by NMs with suppression of GLT-1 (Figure 11C). This trend was due to the reduction in the NM-evoked response reliabilities, but with no corresponding change in gratings-evoked response reliabilities, at 2-week and 4-week dox treatment time points. Closer inspection found that the sizes of microdomains reliably activated by gratings were not significantly affected, as measured by the slopes of the power spectrum results. Instead, only the sizes of microdomains reliably evoked by NMs diminished significantly as GLT-1 expression was reduced at both the 2-week and 4-week time points (Figure 11D). Collectively, this evidence argues that GLT-1 is involved

in the modulation of astrocyte $Ca^{2+}$ microdomain activity during stimuli such as NMs that evokes highly reliable neuronal responses, but not during the more sparse synaptic activity generated by sinusoidal gratings.

## 3.4 Discussion

Through the use of awake *in vivo* imaging and novel mouse models, we present the findings that astrocytes *in vivo* display robust $Ca^{2+}$ transients, with the majority of activity occurring in the major branches and fine process microdomains. Furthermore, we find that astrocyte microdomains exhibit orientation tuned responses; however, these responses are sparse and exhibit unreliable activation profiles. Additionally, using a novel visual stimulation paradigm that previously had been found to elicit increased neuronal reliability *in vivo* (Rikhye and Sur, 2015), we show that astrocytes microdomain activity displays significantly increased reliability when stimulated with natural movies (NMs) compared to sinusoidal gratings. Furthermore, NMs evoke significantly larger $Ca^{2+}$ microdomains relative to those elicited by drifting gratings. Lastly, utilizing an *in vivo* conditional knockdown of GLT-1, we find that there is a significant decrease in the size of reliably responding microdomains that are elicited by NMs. Collectively, the evidence presented in this chapter indicates that contrary to previous reports that astrocytes do not respond to visual stimuli in vivo (Bonder and McCarthy, 2014; Paukert et al., 2014), astrocyte process microdomains do exhibit sparse orientation tuning and respond reliably to coordinated neuronal activity elicited by NM stimuli. Further, astrocytic GLT-1 is a key modulator of this response reliability.

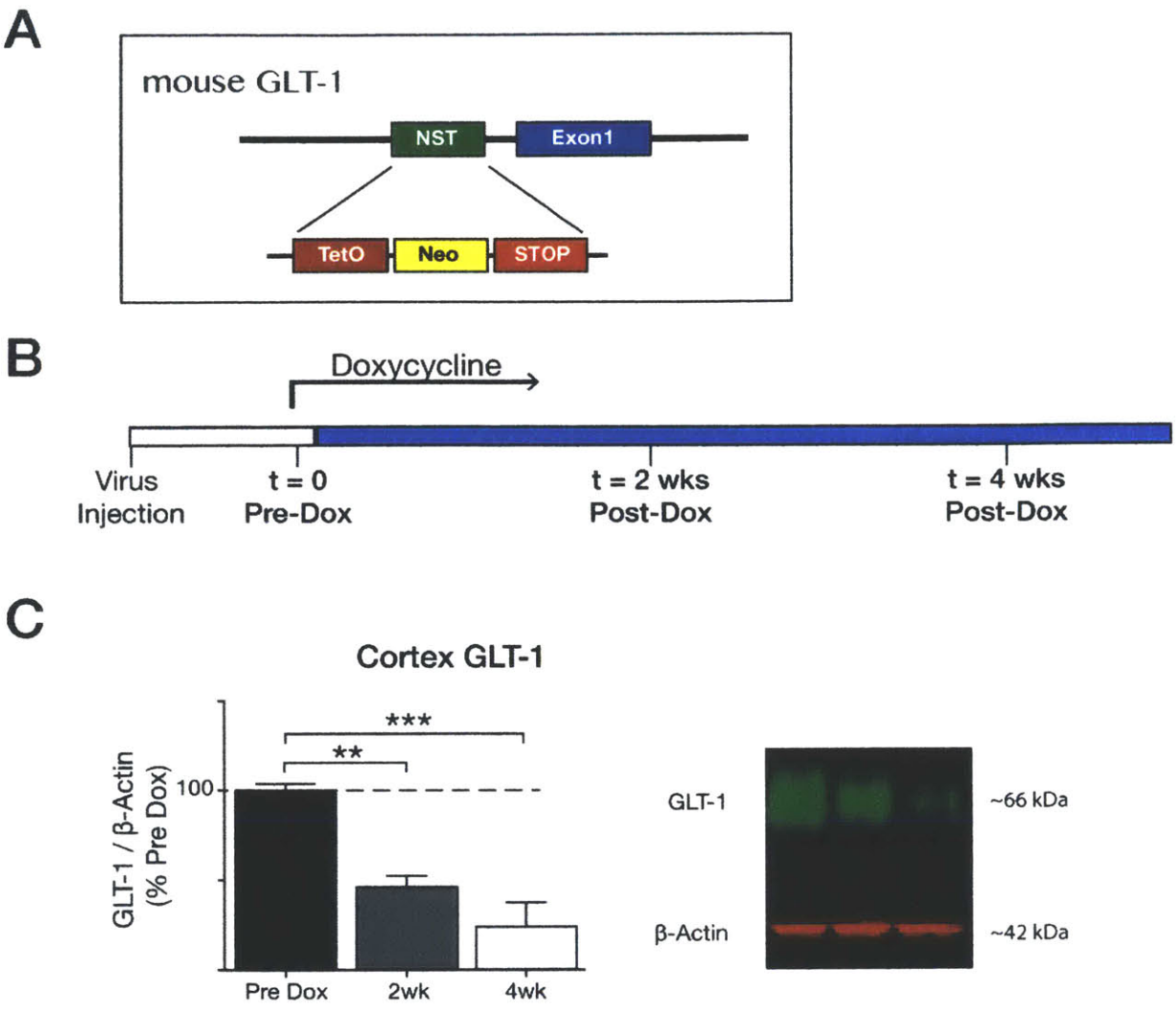


**Figure 10 – Doxycycline-dependent down-regulation of glutamate transporter.** A) Schematic of transgenic line with NeoStop cassette insertion upstream of exon 1 of GLT-1. Doxycycline (Dox) introduced in chow diet leads to expression of stop codon and down-regulation of GLT-1 protein. B) Time course for GLT-1 experiments. Transgenic mice are injected with virus targeting expression of GCaMP in astrocytes of visual cortex two weeks prior to first imaging session (t=0, Pre-Dox). Two subsequent imaging sessions are performed two and four weeks post exposure to Dox. C) Western blot analysis of GLT-1 protein in cerebral cortex of transgenic animals two and four weeks post Dox show a ~50% and ~75% reduction in GLT-1. Bands of GLT-1 or β-actin are shown.

This evidence is in agreement with previous work from the Sur lab using the ferret visual system, where it was shown that blocking glutamate transporters in ferret visual cortex modulates neuronal and astrocytic $Ca^{2+}$ elevation and feature specific responses in a visual stimulus specific manner (Schummers et al., 2008). These finding place astrocytes as integral components of visual cortex circuits, and implicate glutamate transporters as potential modulators of astrocyte-neuron interactions via $Ca^{2+}$ microdomain activity.

The best currently available method to monitor astrocytic activity are indicators showing fluxes of $Ca^{2+}$ elevations. While tools such as genetically encoded calcium indicators (GECIs) have matured in recent years, many questions regarding astrocyte calcium signaling remain unanswered (Bazargani and Attwell, 2016; Shigetomi et al., 2016). This is partly due to the variable potential sources of calcium that have been identified and the many mechanisms that contribute to the regulation of calcium signals (Porter and McCarthy, 1996; Hirase et al., 2004; Wang et al., 2006; Shigetomi et al., 2010b; Tong et al., 2012; Haustein et al., 2014). Structurally, astrocytes are a dense collection of ramified processes stemming from the cell body and a few primary processes (Bushong et al., 2002; 2003). The fine distal processes have been shown to make contact with synapses and exhibit a range of channels, pumps, receptors, and exchangers that not only monitor ion and transmitter concentrations, but also play a role in regulating $Ca^{2+}$ concentrations in astrocyte processes (Allen and Barres, 2009; Perea et al., 2009; Eroglu and Barres, 2010). The use of GECIs *in vivo* and in awake animals, such as the work carried out in this chapter, has identified spotty $Ca^{2+}$ transients that are localized to the fine distal processes, which have come be known as

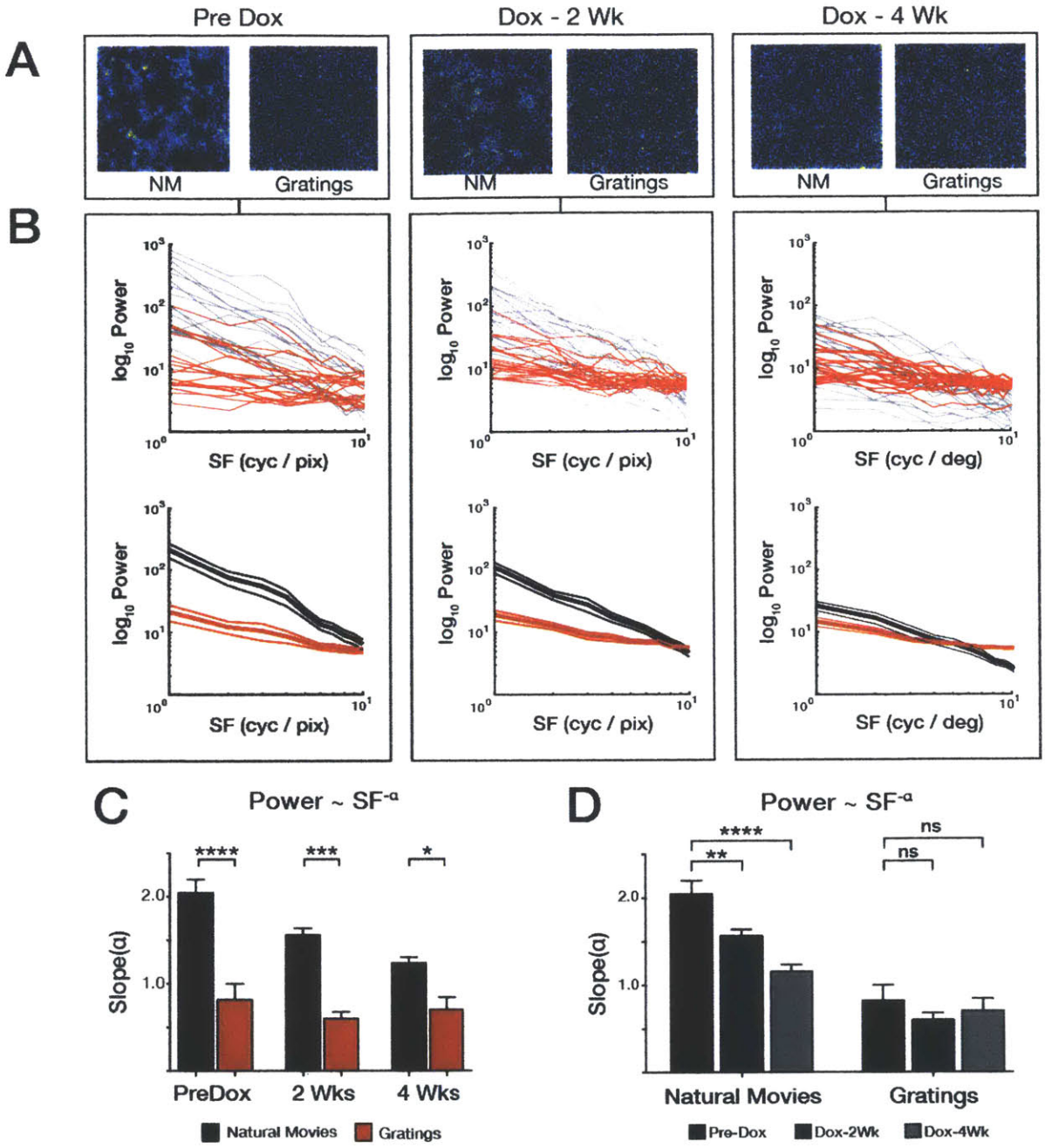


**Figure 11 - Glutamate transporter influences astrocyte responses to natural movies.** A) Representative maps reliable microdomain activation before and after manipulation of GLT-1 expression. B) Individual (lower) and population mean (bottom) power spectra (PS) traces. C) Population averages for the slopes of the PS shows reduced activation of reliable microdomains that correlates with reduction of GLT-1 expression. D) Comparison of effects of GLT-1 reduction on activation of microdomain responses to natural movies and gratings. Significant differences only observed in the reduction of PS slopes for natural movies, no significant difference to the response reliability to gratings.

microdomains – they represent a functional unit that may reflect nearby synaptic activity. The molecular mechanisms governing microdomain activity is still under investigation, and different mechanisms may underlie these transients depending on the circuits that the astrocytes are found in as similar mechanisms have been shown to differentially affect microdomain activity in the hippocampus (Shigetomi et al., 2013b; Haustein et al., 2014). The work reported here examines the activation of microdomains to complex visual stimuli and provides evidence that GLT-1 mediates these responses.

In neuronal recordings of visual circuit activity, the increased reliability to natural movies has been attributed to the low spatial frequency content in natural scenes. These features are believed to contribute to fast and efficient extraction of salient features in the natural world and assist in scene recognition and motion discrimination. Previous work has demonstrated that only neurons that are highly correlated reliably process natural movies and these ensembles are clustered together (Rikhye and Sur, 2015). Conversely, the orientation preference of synapses on dendritic arbors of individual pyramidal neurons revealed that synapses responding with the same orientation preference are widely distributed and often on different branches (Jia et al., 2010). This may be in part a reflection of the rodent visual cortex which does not show columnar organization for orientation preference, as is observed in cats and ferrets (Ohki and Reid, 2007). The structural and functional nature of the mouse visual cortex therefore is a plausible explanation for the sparse orientation tuning we observed in astrocyte microdomains. Therefore, we hypothesize that the required coordinated input onto astrocytes to generate significantly large process $Ca^{2+}$ transients to elicit a

tuned somatic $Ca^{2+}$ response is unlikely to be generated by the mouse visual cortex in response to sinusoidal gratings. In contrast to sinusoidal gratings, we hypothesize that the activation of ensembles of correlated neurons in response to NM stimulation provides sufficient coordinated input on to astrocytes to generate the robust and increased $Ca^{2+}$ microdomain activity observed in the data presented in this manuscript. This stance gains support from previous publications in acute slices and in vivo where changes in input stimulus or synaptic strength is reflected by changes in astrocyte Ca2+ activity (Xie et al., 2012; Zhao et al., 2012; Sibille et al., 2015). Furthermore, impairment of glutamate uptake during periods where many neurons are firing together and reliably may impose noise by way of prolonged presence of glutamate at the synapses.

In the future, experiments examining how neuronal reliability is altered in response to reduced glutamate transporter expression will be crucial in determining the impact of the $Ca^{2+}$ microdomain alterations observed in these experiments. If neuronal reliability is found to be unaltered, it may be hypothesized that the changes in activity reflects cell autonomous alterations in pathways governing the generation of astrocytic $Ca^{2+}$ microdomains. Conversely, if neuronal reliability is demonstrated to be altered, it would implicate GLT-1 and glutamate clearance as a key contributor. Indeed, in a mouse model of Rett Syndrome, we show that GLT-1 expression is altered (increased following MeCP2 reduction); in this model, spatially correlated astrocyte microdomains are reduced in size (Chapter 4), and neuronal responses show reduced reliability (Banerjee et al., submitted). A potential experiment that would provide valuable insight would be to overexpress GLT-1 in visual cortex astrocytes and examine the effect on

both neuron and astrocyte responses. Lastly, new genetically encoded indicators sensitive to glutamate are being developed in collaboration with Dr. Loren Looger's laboratory that would allow us to directly visualize glutamate transport into astrocytes, while simultaneously measuring $Ca^{2+}$ microdomain activity, to determine the relationship between the two processes.

In conclusion, the data presented in this manuscript provides evidence that astrocytes receive and respond to neuronal input and activity elicited by visual stimuli. The nature of microdomain responses is an ongoing research topic in the field of astrocyte signaling, yet it is becoming clear that astrocytes situated in different circuits will have unique responses. It may be that the underlying mechanisms giving rise to microdomain activity may differ and be tuned to the structure and function of nearby synapses. Furthermore, my work supports the notion that astrocyte response strength is largely determined in a stimulus-specific manner, requires the coordinated activation of neuronal ensembles, and is modulated by GLT-1 activity. This evidence implies that astrocytes are likely to be integral parts of neuronal cortical circuits underlying vision.

## Acknowledgements and Contributions

Rajeev R. Rykhie was instrumental in developing the methods and approach to imaging and comparing responses to natural movies and gratings in astrocytes; his work inspired these questions. Michael Goard initially built the two-photon system and made the awake imaging possible with innovative approaches to surgery and animal preparations. Jeremy Petravicz obtain the TetO-GLT-1 mouse lines and has been a constant source of insight and information regarding all things astrocytes. I would also like to thank the technicians in our lab, Stephanie Chou and Liaden Gunter, for their invaluable assistance with molecular assays and animal husbandry.

## 3.6 References


Allen N, Barres B (2009) Glia and Synapse Formation: An Overview. Encyclopedia of Neuroscience: Glia and Synapse Formation: An Overview:731–736.

Arriza JL, Fairman WA, Wadiche JI, Murdoch GH, Kavanaugh MP, Amara SG (1994) Functional comparisons of three glutamate transporter subtypes cloned from human motor cortex. The Journal of Neuroscience 14:5559–5569.

Asztely F, Erdemli G, Kullmann DM (1997) Extrasynaptic Glutamate Spillover in the Hippocampus: Dependence on Temperature and the Role of Active Glutamate Uptake. Neuron 18:281–293.

Attwell D, Buchan AM, Charpak S, Lauritzen M, MacVicar BA, Newman EA (2010) Glial and neuronal control of brain blood flow. Nature 468:232–243.

Azouz R, Gray CM (1999) Cellular mechanisms contributing to response variability of cortical neurons in vivo. The Journal of Neuroscience 19:2209–2223.

Bar M (2004) Visual objects in context. Nat Rev Neurosci 5:617–629.

Barlow H (2009) Redundancy reduction revisited. Network: Computation in Neural Systems 12:241–253.

Baudot P, Levy M, Marre O, Monier C, Pananceau M, Fregnac Y (2013) Animation of natural scene by virtual eye-movements evokes high precision and low noise in V1 neurons. Front Neural Circuits 7:206.

Bazargani N, Attwell D (2016) Astrocyte calcium signaling: the third wave. Nat Neurosci 19:182–189.

Bernardinelli Y, Randall J, Janett E, Nikonenko I, König S, Jones EV, Flores CE, Murai KK, Bochet CG, Holtmaat A, Muller D (2014) Activity-Dependent Structural Plasticity of Perisynaptic Astrocytic Domains Promotes Excitatory Synapse Stability. Current Biology 24:1679–1688.

Bjørnsen LP, Hadera MG, Zhou Y, Danbolt NC, Sonnewald U (2013) The GLT-1 (EAAT2; slc1a2) glutamate transporter is essential for glutamate homeostasis in the neocortex of the mouse. J Neurochem.

Bonder DE, McCarthy KD (2014) Astrocytic Gq-GPCR-Linked IP3R-Dependent Ca2+ Signaling Does Not Mediate Neurovascular Coupling in Mouse Visual Cortex In Vivo. The Journal of Neuroscience.

Borst A, Theunissen FE (1999) Information theory and neural coding. Nat Neurosci 2:947–957.

Bushong E, Martone M, Ellisman M (2003) Examination of the relationship between astrocyte

morphology and laminar boundaries in the molecular layer of adult dentate gyrus. J Comp Neurol 462:241–251.

Bushong E, Martone M, Jones Y, Ellisman M (2002) Protoplasmic astrocytes in CA1 stratum radiatum occupy separate anatomical domains. Journal of Neuroscience 22:183–192.

Carmignoto G, Gomez-Gonzalo M (2010) The contribution of astrocyte signalling to neurovascular coupling. Brain Res Rev 63:138–148.

Chapman B, Stryker MP (1993) Development of orientation selectivity in ferret visual cortex and effects of deprivation. The Journal of Neuroscience 13:5251–5262.

Cheung G, Sibille JX, xe9 R, mie, Zapata J, Cheung G, Sibille JX, xe9 R, mie, Rouach N (2015) Activity-Dependent Plasticity of Astroglial Potassium and Glutamate Clearance. Neural Plast 2015:1–16.

Cornell-Bell A, Finkbeiner S, Cooper M (1990) Glutamate induces calcium waves in cultured astrocytes: long-range glial signaling. Science.

Danbolt NC (2001) Glutamate uptake. Progress in Neurobiology 65:1–105.

Deitmer JW, Rose CR (2010) Ion changes and signalling in perisynaptic glia. Brain Res Rev 63:113–129.

Di Castro MA, Chuquet J, Liaudet N, Bhaukaurally K, Santello M, Bouvier D, Tiret P, Volterra A (2011) Local Ca(2+) detection and modulation of synaptic release by astrocytes. Nat Neurosci.

Ding F, O'Donnell J, Thrane AS, Zeppenfeld D, Kang H, Xie L, Wang F, Nedergaard M (2013) α1-Adrenergic receptors mediate coordinated Ca2+ signaling of cortical astrocytes in awake, behaving mice. Cell Calcium 54:387–394.

Dombeck DA, Khabbaz AN, Collman F, Adelman TL, Tank DW (2007) Imaging Large-Scale Neural Activity with Cellular Resolution in Awake, Mobile Mice. Neuron 56:43–57.

Eroglu C, Barres BA (2010) Regulation of synaptic connectivity by glia. Nature 468:223–231.

Fiacco TA, Agulhon C, Taves SR, Petravicz J, Casper KB, Dong X, Chen J, Mccarthy KD (2007) Selective stimulation of astrocyte calcium in situ does not affect neuronal excitatory synaptic activity. Neuron 54:611–626.

Gee JM, Smith NA, Fernandez FR, Economo MN (2014) Imaging Activity in Neurons and Glia with a Polr2a-Based and Cre-Dependent GCaMP5G-IRES-tdTomato Reporter Mouse. Neuron.

Haber M, Zhou L, Murai KK (2006) Cooperative astrocyte and dendritic spine dynamics at

hippocampal excitatory synapses. Journal of Neuroscience 26:8881–8891.

Haider B, Krause MR, Duque A, Yu Y, Touryan J, Mazer JA, McCormick DA (2010) Synaptic and Network Mechanisms of Sparse and Reliable Visual Cortical Activity during Nonclassical Receptive Field Stimulation. Neuron 65:107–121.

Hamilton NB, Attwell D (2010) Do astrocytes really exocytose neurotransmitters? Nat Rev Neurosci 11:227–238.

Haustein MD, Kracun S, Lu X-H, Shih T, Jackson-Weaver O, Tong X, Xu J, Yang XW, O'Dell TJ, Marvin JS, Ellisman MH, Bushong EA, Looger LL, Khakh BS (2014) Conditions and Constraints for Astrocyte Calcium Signaling in the Hippocampal Mossy Fiber Pathway. Neuron 82:413–429.

Haydon PG (2001) Glia: listening and talking to the synapse. Nat Rev Neurosci.

Hirase H, Qian L, Barthó P, Buzsáki G (2004) Calcium dynamics of cortical astrocytic networks in vivo. Plos Biol 2:e96.

Huang YH, Sinha SR, Tanaka K, Rothstein JD, Bergles DE (2004) Astrocyte glutamate transporters regulate metabotropic glutamate receptor-mediated excitation of hippocampal interneurons. Journal of Neuroscience 24:4551–4559.

Jackson JG, O'Donnell JC, Takano H, Coulter DA, Robinson MB (2014) Neuronal activity and glutamate uptake decrease mitochondrial mobility in astrocytes and position mitochondria near glutamate transporters. Journal of Neuroscience 34:1613–1624.

Jia H, Rochefort NL, Chen X, Konnerth A (2010) Dendritic organization of sensory input to cortical neurons in vivo. Nature 464:1307–1312.

Kanemaru K, Sekiya H, Xu M, Satoh K, Kitajima N, Yoshida K, Okubo Y, Sasaki T, Moritoh S, Hasuwa H, Mimura M, Horikawa K, Matsui K, Nagai T, Iino M, Tanaka KF (2014) In Vivo Visualization of Subtle, Transient, and Local Activity of Astrocytes Using an Ultrasensitive Ca2+ Indicator. Cell Reports 0:–.

Khakh BS, Mccarthy KD (2015) Astrocyte Calcium Signaling: From Observations to Functions and the Challenges Therein. Cold Spring Harbor Perspectives in Biology.

Khakh BS, Sofroniew MV (2015) Diversity of astrocyte functions and phenotypes in neural circuits. Nat Neurosci 18:942–952.

Kirischuk S, Héja L, Kardos J, Billups B (2015) Astrocyte sodium signaling and the regulation of neurotransmission. Glia:n/a–n/a.

Nishida H, Okabe S (2007) Direct astrocytic contacts regulate local maturation of dendritic spines. Journal of Neuroscience 27:331–340.

Ohki K, Reid RC (2007) Specificity and randomness in the visual cortex. Curr Opin Neurobiol 17:401–407.

Olsen ML, Khakh BS, Skatchkov SN, Zhou M, Lee CJ, Rouach N (2015) New Insights on Astrocyte Ion Channels: Critical for Homeostasis and Neuron-Glia Signaling. Journal of Neuroscience 35:13827–13835.

Olshausen BA, Field DJ (2004) Sparse coding of sensory inputs. Curr Opin Neurobiol 14:481–487.

Otsu Y, Couchman K, Lyons DG, Collot M, Agarwal A, Mallet J-M, Pfrieger FW, Bergles DE, Charpak S (2015) Calcium dynamics in astrocyte processes during neurovascular coupling. Nat Neurosci 18:210–218.

Pannasch U, Rouach N (2013) Emerging role for astroglial networks in information processing: from synapse to behavior. Trends in Neurosciences.

Paukert M, Agarwal A, Cha J, Doze VA, Kang JU, Bergles DE (2014) Norepinephrine controls astroglial responsiveness to local circuit activity. Neuron 82:1263–1270.

Perea G, Navarrete M, Araque A (2009) Tripartite synapses: astrocytes process and control synaptic information. Trends in Neurosciences 32:421–431.

Perez-Alvarez A, Navarrete M, Covelo A, Martin ED, Araque A (2014) Structural and Functional Plasticity of Astrocyte Processes and Dendritic Spine Interactions. The Journal of Neuroscience 34:12738–12744.

Petravicz J, Fiacco TA, Mccarthy KD (2008) Loss of IP3 receptor-dependent Ca2+ increases in hippocampal astrocytes does not affect baseline CA1 pyramidal neuron synaptic activity. Journal of Neuroscience 28:4967–4973.

Porter JT, McCarthy KD (1996) Hippocampal astrocytes in situ respond to glutamate released from synaptic terminals. The Journal of Neuroscience 16:5073–5081.

Reichenbach A, Derouiche A, Kirchhoff F (2010) Morphology and dynamics of perisynaptic glia. Brain Res Rev 63:11–25.

Rikhye RV, Sur M (2015) Spatial Correlations in Natural Scenes Modulate Response Reliability in Mouse Visual Cortex. Journal of Neuroscience 35:14661–14680.

Rose CR, Karus C (2013) Two sides of the same coin: Sodium homeostasis and signaling in astrocytes under physiological and pathophysiological conditions. Glia:n/a–n/a.

Rose CR, Verkhrastky A (2016) Principles of sodium homeostasis and sodium signalling in astroglia. Glia:n/a–n/a.

Rosenbaum R, Tchumatchenko T, Moreno-Bote R (2014) Correlated neuronal activity and its relationship to coding, dynamics and network architecture. Front Comput Neurosci 8:811.

Ruderman DL, Bialek W (1994) Statistics of natural images: Scaling in the woods. Phys Rev Lett 73:814–817.

Scanziani M, Hausser M (2009) Electrophysiology in the age of light. Nature 461:930–939.

Schummers J, Yu H, Sur M (2008) Tuned Responses of Astrocytes and Their Influence on Hemodynamic Signals in the Visual Cortex. Science 320:1638–1643.

Shadlen MN, Newsome WT (1994) Noise, neural codes and cortical organization. Curr Opin Neurobiol 4:569–579.

Shigetomi E, Bushong EA, Haustein MD, Tong X, Jackson-Weaver O, Kracun S, Xu J, Sofroniew MV, Ellisman MH, Khakh BS (2013a) Imaging calcium microdomains within entire astrocyte territories and endfeet with GCaMPs expressed using adeno-associated viruses. The Journal of General Physiology 141:633–647.

Shigetomi E, Jackson-Weaver O, Huckstepp RT, O'Dell TJ, Khakh BS (2013b) TRPA1 Channels Are Regulators of Astrocyte Basal Calcium Levels and Long-Term Potentiation via Constitutive D-Serine Release. Journal of Neuroscience 33:10143–10153.

Shigetomi E, Kracun S, Khakh BS (2010a) Monitoring astrocyte calcium microdomains with improved membrane targeted GCaMP reporters. Neuron Glia Biol:1–9.

Shigetomi E, Kracun S, Sofroniew MV, Khakh BS (2010b) A genetically targeted optical sensor to monitor calcium signals in astrocyte processes. Nat Neurosci 13:759–U143.

Shigetomi E, Patel S, Khakh BS (2016) Probing the Complexities of Astrocyte Calcium Signaling. Trends Cell Biol 26:300–312.

Sibille J, Pannasch U, Rouach N (2014) Astroglial potassium clearance contributes to short-term plasticity of synaptically evoked currents at the tripartite synapse. The Journal of Physiology 592:87–102.

Sibille J, Zapata J, Teillon J, Rouach N (2015) Astroglial calcium signaling displays short-term plasticity and adjusts synaptic efficacy. Front Cell Neurosci 9:189.

Simoncelli EP, Olshausen BA (2003) NATURAL IMAGE STATISTICS AND NEURAL REPRESENTATION. http://dxdoiorg/101146/annurevneuro2411193 24:1193–1216.

Smith SJ (1994) Neural signalling. Neuromodulatory astrocytes. Current Biology 4:807–810.

Takata N, Mishima T, Hisatsune C, Nagai T, Ebisui E, Mikoshiba K, Hirase H (2011) Astrocyte calcium signaling transforms cholinergic modulation to cortical plasticity in vivo. Journal of

Neuroscience 31:18155–18165.

Tanaka K, Watase K, Manabe T, Yamada K, Watanabe M, Takahashi K, Iwama H, Nishikawa T, Ichihara N, Kikuchi T (1997) Epilepsy and exacerbation of brain injury in mice lacking the glutamate transporter GLT-1. Science 276:1699–1702.

Theodosis DT, Poulain DA, Oliet SHR (2008) Activity-dependent structural and functional plasticity of astrocyte-neuron interactions. Physiological Reviews 88:983–1008.

Thrane AS, Thrane VR, Zeppenfeld D, Lou N, Xu Q, Nagelhus EA, Nedergaard M (2012) General anesthesia selectively disrupts astrocyte calcium signaling in the awake mouse cortex. P Natl Acad Sci Usa 109:18974–18979.

Tong G, Jahr CE (1994) Block of glutamate transporters potentiates postsynaptic excitation. Neuron 13:1195–1203.

Tong X, Shigetomi E, Looger LL, Khakh BS (2012) Genetically Encoded Calcium Indicators and Astrocyte Calcium Microdomains. Neuroscientist.

Ventura R, Harris KM (1999) Three-dimensional relationships between hippocampal synapses and astrocytes. Journal of Neuroscience 19:6897–6906.

Verkhratsky A, Nedergaard M, Hertz L (2015) Why are astrocytes important? Neurochem Res 40:389–401.

Wang F, Smith NA, Xu Q, Fujita T, Baba A, Matsuda T, Takano T, Bekar L, Nedergaard M (2012) Astrocytes Modulate Neural Network Activity by Ca2+-Dependent Uptake of Extracellular K. Sci Signal 5:ra26–ra26.

Wang X, Lou N, Xu Q, Tian G-F, Peng WG, Han X, Kang J, Takano T, Nedergaard M (2006) Astrocytic Ca2+ signaling evoked by sensory stimulation in vivo. Nat Neurosci 9:816–823.

Wilhelmsson U, Bushong EA, Price DL, Smarr BL, Phung V, Terada M, Ellisman MH, Pekny M (2006) Redefining the concept of reactive astrocytes as cells that remain within their unique domains upon reaction to injury. P Natl Acad Sci Usa 103:17513–17518.

Witcher MR, Kirov SA, Harris KM (2007) Plasticity of perisynaptic astroglia during synaptogenesis in the mature rat hippocampus. Glia 55:13–23.

Witcher MR, Park YD, Lee MR, Sharma S, Harris KM, Kirov SA (2010) Three-dimensional relationships between perisynaptic astroglia and human hippocampal synapses. Glia 58:572–587.

Xie AX, Sun M-Y, Murphy T, Lauderdale K, Tiglao E, Fiacco TA (2012) Bidirectional Scaling of Astrocytic Metabotropic Glutamate Receptor Signaling following Long-Term Changes in Neuronal Firing Rates. PLoS ONE 7:e49637.

Yu H, Farley BJ, Jin DZ, Sur M (2005) The Coordinated Mapping of Visual Space and Response Features in Visual Cortex. Neuron 47:267–280.

Zhao J, Wang D, Wang J-H (2012) Barrel cortical neurons and astrocytes coordinately respond to an increased whisker stimulus frequency. Mol Brain 5:12.

# Chapter 4: Effect of MeCP2 deficiency on $Ca^{2+}$ responses in astrocytes

## 4.1 Abstract

Rett syndrome (RTT) is a devastating neurodevelopmental disorder that primarily affects girls and arises primarily from sporadic mutations on the X-linked methyl-CpG binding protein 2 (MeCP2). Loss of function mutations in this ubiquitously expressed transcriptional regulator leads to imbalances in excitation and inhibition and disruption to neuronal circuit function. It was initially believed that MeCP2 was solely expressed in neurons and therefore disease phenotypes arose from loss-of-function mutations in these cells. However, recent work has implicated non-neuronal cell types as contributors to RTT pathophysiology. MeCP2 expression has been detected in astrocytes, and selective deletion or re-introduction of MeCP2 in astrocytes alone has been sufficient to induce or ameliorate pathological symptoms, respectively. Previously, we identified signaling pathways upstream of synaptic function that are impaired in MeCP2 mouse models, yet the downstream molecular and signaling effects resulting from a loss of MeCP2 function in astrocytes remains unknown. Here we report novel ways to measure signaling and astrocyte-specific proteins in a heterogeneous MeCP2-expressing population. We find that activated mTOR and AKT are reduced in astrocytes lacking MeCP2, while levels of cortical glutamate transporter 1 (GLT-1) are upregulated in astrocytes lacking MeCP2. We have recently shown that astrocytes in layer 2/3 of rodent visual cortex can respond to natural movies with robust and reliable microdomain $Ca^{2+}$ elevations and that this effect was influenced by the availability and function of GLT-1. Here, we report that the overall microdomain

area evoked during NMs is reduced in MeCP2$^{-/+}$ astrocytes and this finding is in line with reduced circuit function. These data identify novel, cell-specific effects in astrocytes lacking MeCP2 and offer insight on their signaling and circuit interactions.

## 4.2 Introduction

The majority of Rett Syndrome cases are caused by sporadic loss-of-function mutations in the gene encoding methyl-CpG binding protein 2 (MeCP2). The heterogeneity of cell types in the CNS complicates the understanding of the functional role of MeCP2. In particular, we do not have a clear idea how the lack MeCP2 regulation differentially affects cell populations in different brain regions or different types of cells across the brain. For example, mice with MeCP2 deleted from the hypothalamus show an increase in aggressive behavior as well as feeding behavior leading to obesity, while deletions in amygdala via viral-mediated delivery of Cre affected anxiety levels as well as normal social interactions (Fyffe et al., 2008; Adachi et al., 2009). Furthermore, circuit function requires balanced interaction between different cell types, and development and function of visual cortex is no exception. At the circuit level, lack of MeCP2 can disrupt proper development and function (He et al., 2014a; Krishnan et al., 2015).

Initial studies reported a lack of MeCP2 expression in glial cells. However, recent studies have firmly established expression in astrocytes. Wild type neurons co-cultured with MeCP2-null astrocytes developed aberrant dendritic morphologies akin to those seen in MeCP2-null neurons. Conversely, MeCP2-null neurons cultured with wild type astrocytes developed normal dendritic morphologies (Ballas et al., 2009;

Maezawa et al., 2009). Additionally, selective reactivation of MeCP2 expression in astrocytes improved development of dendritic morphology and may help stabilize disease symptoms (Lioy et al., 2011). This evidence strongly suggests that the loss of functional MeCP2 in astrocytes has a direct effect on the proper maturation of neurons and synaptic function that can contribute RTT pathogenesis. These studies highlight the complex role that MeCP2 plays; deficiencies in different cell populations can have vastly different effects and be responsible for the origins and progression of complex behaviors and phenotypes of RTT.

Signaling pathways have become a focal point in understanding the mechanisms contributing to disease phenotypes downstream of gene mutations (Sebastian-Leon et al., 2014; Sahin and Sur, 2015). Indeed, our own work has demonstrated that a reduction in the level of IGF1 has downstream effects on signaling pathways, synaptic maturation, and circuit function (Castro et al., 2014; Mellios et al., 2014). Importantly, the same pathways play critical roles in astrocytes and can modulate the expression of pivotal functional proteins such as glutamate transporters (Wu et al., 2010; Martinez-Lozada and Guillem, 2016). The role of astrocytes in RTT pathophysiology remains unclear, in particular their contributions *in vivo*. Therefore, an *in vivo* model of an astrocyte-specific MeCP2 loss-of-function would be paramount in furthering our understanding of non-neuronal contributions to RTT pathogenesis.

Here we develop ways to investigate the properties of astrocytes in the context of MeCP2 deficiency. We generated an astrocyte-specific reporter line that allowed us to visualize the full morphology both *in vivo* and *in situ*. Using these methods, we report the novel finding that astrocytes lacking functional MeCP2 expression have reduced

activated levels of mTOR and AKT as compared to neighboring astrocytes expressing MeCP2. This finding matches the decrease in similar pathway activation in neurons that we have reported and raises the possibility that MeCP2 may exert similar effects on signaling pathways in astrocytes. Surprisingly, we report that astrocytes completely lacking MeCP2 have increased levels of cortical GLT-1 protein in both $MeCP2^{-/y}$ males and $MeCP2^{-/+}$ females. Furthermore, we show that visually evoked responses in microdomains of layer 2/3 astrocytes are altered. Responses remain reliably activated by natural movies in both $MeCP2^{+/+}$ and $MeCP2^{-/+}$ animals. However, the size of regions with high activation is decreased in mutant animals in all stimulus conditions as compared to their $MeCP2^{+/+}$ littermates.

## 4.3 Methods

### *4.3.1 Mouse lines*

All experimental protocols were approved by the Animal Care and Use Committee at Massachusetts Institute of Technology and conformed to National Institutes of Health guidelines. Mecp2 heterozygous female mice and wild type (WT) littermates were obtained by breeding heterozygous females (Guy et al., 2001) (Jackson Labs, Maine; Stock#003890) with C57BL6/J male mice on the same background (Jackson #000664). Heterozygous females of ~3 months old were used for experiments. These were crossed with GFAP-tdTomato mice for astrocyte-specific (previously described, see Chapter 3).

### *4.3.2 Viruses*

Virus was constructed using the shortened hGFAP promoter to drive expression of the membrane-bound GCaMP5 (Lck-GCaMP5G, AddGene) in an AAV2.5 construct (Virovek). This vector was used with the GFAP-tdTomato transgenic line as previously described (see Chapter 3).

### *4.3.3 Western Blot Analysis*

Expression of GLT-1 was analyzed via Western blot. Neo-cortex from TetO-GLT-1 mouse brain slices was dissected and homogenized using RIPA buffer (150 mM NaCl, 1% Triton X-100, 0.5% sodium deoxycholate, 0.1% SDS, 50 mM Tris, pH 8.0) and protease inhibitor cocktail. Samples were then centrifuged at 13,200 rpm for 15 min at 4 °C. 10-15 mg of protein was loaded onto a 10% SDS-PAGE gel and analyzed via electrophoresis (BioRad, Hercules CA). Proteins were detected using an antibody against GLT-1 (guniea pig anti-GLT-1, 1:10,000, Millipore). β-actin (mouse-anti-β-actin 1:2000, Sigma) was used to confirm equal loading. Protein bands were visualized using fluorescently conjugated anti-mouse, or anti-goat antibodies (1:10,000 LiCor Biosciences, Lincoln, NE). Blots were scanned using an Odyssey Infrared Imager (LiCor Biosciences, Lincoln, NE). Quantification of protein expression was conducted using ImageJ (NIH) and expressed in relation to β-actin expression.

### *4.3.4 Immunohistochemistry*

Mice were overdosed with isoflurane and transcardially perfused with saline followed by 4% paraformaldehyde (PFA). The brain was extracted, placed in 1x PBS,

and then 50 µm sections were cut with a vibrotome (Leica VT1200, Germany). Sections were blocked in 10% goat serum and 0.1% triton in PBS for 60 minutes at room temperature on a shaker, and incubated overnight at 4°C in primary antibody for MeCP2 primary antibody (mouse anti-MeCP2, 1:500, M7443, Sigma), NeuN (mouse anti-Neun, 1:500, Milipore, MAB377), GFAP (rabbit anti-GFAP, 1:500, Sigma, G9269), and GLT-1 (guniea pig anti-GLT-1, 1:10,000, Millipore). Sections were then washed three times and incubated in secondary antibody for mouse (goat anti-mouse Alexa Fluor 647, 1:500, Molecular Probes, A-21235), rabbit (goat anti-rabbit Alexa Fluor 488, 1:500, Molecular Probes, A-11008), or goat (goat anti-guinea pig Alexa Fluor 488, 1:500, Molecular Probes, A11073). Sections were mounted on slides and coverslipped with Vectashield Hardset mounting media with DAPI (Vector Labs). Images of immuno-fluorescent sections were taken at 20X or 63X oil immersion objectives with a confocal microscope (Zeiss LSM5 Exciter). Care was taken to keep consistent image acquisition parameters across samples for intensity comparisons. Direct comparisons between MeCP2+ and MeCP2- cells with in the same sections were first made and normalized to intensities of the former before comparing across sections. Colocalization and overlap were quantified using ImageJ software (NIH).

### *4.3.5 Surgery*

Mice were anesthetized using isoflurane (3% induction, 1.5–2% during surgery). A custom-built metal head post was attached to the skull using dental cement (C&B-Metabond, Parkell), and a 3-mm-diameter craniotomy was performed over binocular V1 (2–3 mm lateral and 0.5 mm anterior to lambda). Care was taken not to rupture the

dura mater. The core body temperature was maintained at 37.5°C using a heating blanket (Harvard Apparatus). Mice were allowed to recover for 2–3 weeks to allow for adequate expression of the virus before imaging commenced.

### *4.3.6 Two-photon calcium imaging*

Mice were habituated to both imaging environment and visual stimulus prior to imaging sessions. During two-photon imaging sessions, awake animals were head-attached to custom-made stage for two-photon microscopy using a Prairie Ultima two-photon system (Prairie Technologies) driven by a Spectra Physics Mai-Tai eHP laser, passed through a Deep-See module (Spectra Physics / Newport). Excitation laser was tuned to 910 nm and passed through a 25x water-immersion objective (Olympus). Movies were acquired at ~7Hz frame rate.

### *4.3.7 Visual stimulation*

To assess the orientation selectivity and tuning of neurons, we presented oriented gratings on a 23" 1080p LCD monitor (Dell) using custom software (Network Visstim, Sur Lab) written in PsychToolbox-3 (Psychtoolbox.com) on a Windows 7 computer (Dell Precision) with a GeForce 8800 GTS 640MB graphics card (PNY). Gratings were optimized for cellular responsiveness using a contrast of 100%, spatial frequency of 0.002-0.256 cycles/degree, and a temporal frequency of 1-3 Hz. Gratings were then presented by stepping the orientation from 0-360 degrees in steps of 30 degrees, with each grating presentation being preceded for 6 seconds "off" followed by 2 seconds "on'.

Natural movies (n = 5) were selected from the van Hateren natural movie database. Gray scale values of each movie were discretized to 255 values and each frame was normalized to have equal mean luminance (mean of histogram = 128) and contrast (std. deviation of histogram = 32). To slow down the movie from its original 60Hz frame rate, we updated every three frames creating an effective frame rate of close to 20Hz. Movies were presented for 10s and were flanked by 4s gray screens (mean luminance = 128). See also Figure 6.

## 4.4 Results

### *4.4.1 Tools to label and visualize MeCP2-deficient astrocytes*

Our first goal was to establish ways to label and image astrocytes in an MeCP2-deficient background. In particular, measurements of cell-autonomous effects on proteins and signaling pathways is challenging since only few cell-specific proteins are known. Our previous study identified components of signaling pathways that are mis-regulated when MeCP2 is knocked out, and we sought to find ways to be able to measure corresponding effects in astrocytes. We took advantage of a transgenic line developed in collaboration with the Feng lab in which the red fluorescent reporter tdTomato is expressed in astrocytes. By crossing these lines with existing MeCP2 mouse models, we were able to probe effects on protein levels in MeCP2-null astrocytes and compare them with levels in adjacent, MeCP2-positive cells (Figure 1A). To do so, we first had to confirm that we could detect MeCP2 levels within astrocytes since levels of this protein have been shown to be much lower than in neurons (Figure 1B).

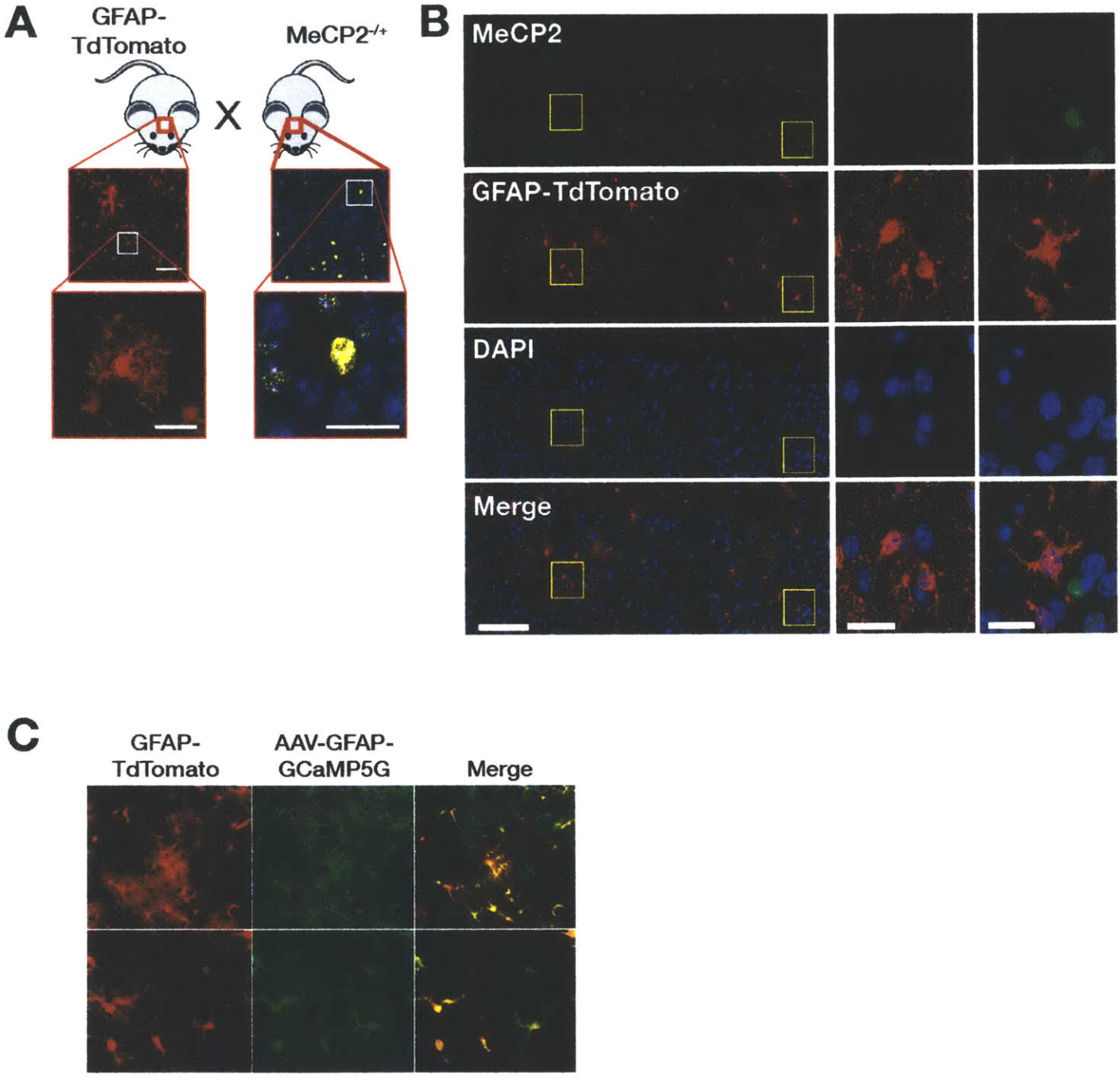


**Figure 1 – Visualizing astrocytes in mouse models of Rett Syndrome.** A.) The astrocyte-specific reporter line expressing tdTomato under the human GFAP promter was crossed with MeCP2 heterozygous females that would generate progeny with astrocytes labeled in red and about half of all cells lacking MeCP2 protein. B) Immunohistochemical analysis of cell specific cortical expression of MeCP2. Scale bars = 100 and 20 μm, respectively, for full image and insets. C) Images from two-photon in vivo imaging of progeny of animals from the crosses depicted in (A) with astrocytes expressing td-Tomato and viral-mediated expression of GCaMP5G.

We were also interested in visualizing functional activity in astrocytes and examined whether impaired neuronal circuits affected visually-evoked $Ca^{2+}$ responses in microdomains (MDs) of layer 2/3 astrocytes. We recently demonstrated that MDs of astrocytes, more so than somas, have robust $Ca^{2+}$ elevations in response to sensory information. In order to examine visually-evoked $Ca^{2+}$ elevations in astrocytes with the single-cell resolution necessary to record responses from MDs, we took advantage of our ability to endogenously label astrocytes in the live brain and employed vectors for cell-specific viral expression of genetically encoded calcium indicators (GECIs). Crossed with MeCP2 mouse models, we could now investigate the effect of MeCP2 loss-of-function on established sensory processing paradigms (Figure 1C).

### *4.4.2 Activated forms of signaling pathways have reduced levels in MeCP2 deficient astrocytes*

Several activators of signaling pathways involved in synaptic structure and function have been shown to be down-regulated in MeCP2 mutant animals (Cheng and Yeh, 2003; Greenberg et al., 2009; Castro et al., 2014; Li and Pozzo-Miller, 2014), yet analogous effects on these pathways in astrocytes have not been demonstrated. Using the methods developed and described within (Figure 1A-B), we set out to test the cell-specific effect on the lack of functional MeCP2 on the levels of activated signaling proteins. Downstream components of these signaling pathways, including mammalian target of rapamycin (mTOR) and protein kinase B (AKT), have both been shown to be altered in neurons of MeCP2 mutant mouse lines (Ricciardi et al., 2011; Jiang et al., 2013). We measured the colocalization of the phosphorylated versions of these

proteins within astrocytes that either expressed or lacked MeCP2 (Figure 2A-C). Analysis of the mean intensities of staining for these proteins revealed significantly reduced levels of both mTOR and AKT in astrocytes lacking functional expression of MeCP2, as compared to neighboring astrocytes that expressed MeCP2, similar to the effects observed in MeCP2-deficient neurons (Figure 2D, E).

### *4.4.3 Increased expression of glutamate transporter in MeCP2-deficient astrocytes*

We next sought to investigate the potential effect that the loss of functional MeCP2 expression might have on glutamate transporter expression. Several other disorders have been reported to have altered expression of GLT-1 and implicate a lack of glutamate uptake as a contributing factor to disease pathophysiology (Kim et al., 2011; Fontana, 2015). Transcriptional and translational control of GLT-1 in astrocytes is complex, but evidence exists that mTOR and AKT can modulated protein levels in cultures (Wu et al., 2010; Ji et al., 2011; Martinez-Lozada and Guillem, 2016). We found that colocalization of GLT-1 is elevated in astrocytes lacking MeCP2 in the cortex of female $MeCP2^{-/+}$ mice (Figure 2F). Because females express MeCP2 in a mosaic fashion in both neurons and astrocytes, and because cortical GLT1 is largely expressed in astrocytes, we measured GLT1 protein levels of $MeCP2^{-/y}$ male brains, which lack any functional MeCP2 in all cells. We found that GLT-1 levels are significantly increased in cortical whole-cell lysates at P28 (Figure 2G) in $MeCP2^{-/y}$ animals. Because GLT-1 is an important regulator of glutamate levels and our previous work indicates that it plays a role in astrocytic sensory processing, we next turned to analyzing visual responses of astrocytes in $MeCP2^{-/+}$ circuits.

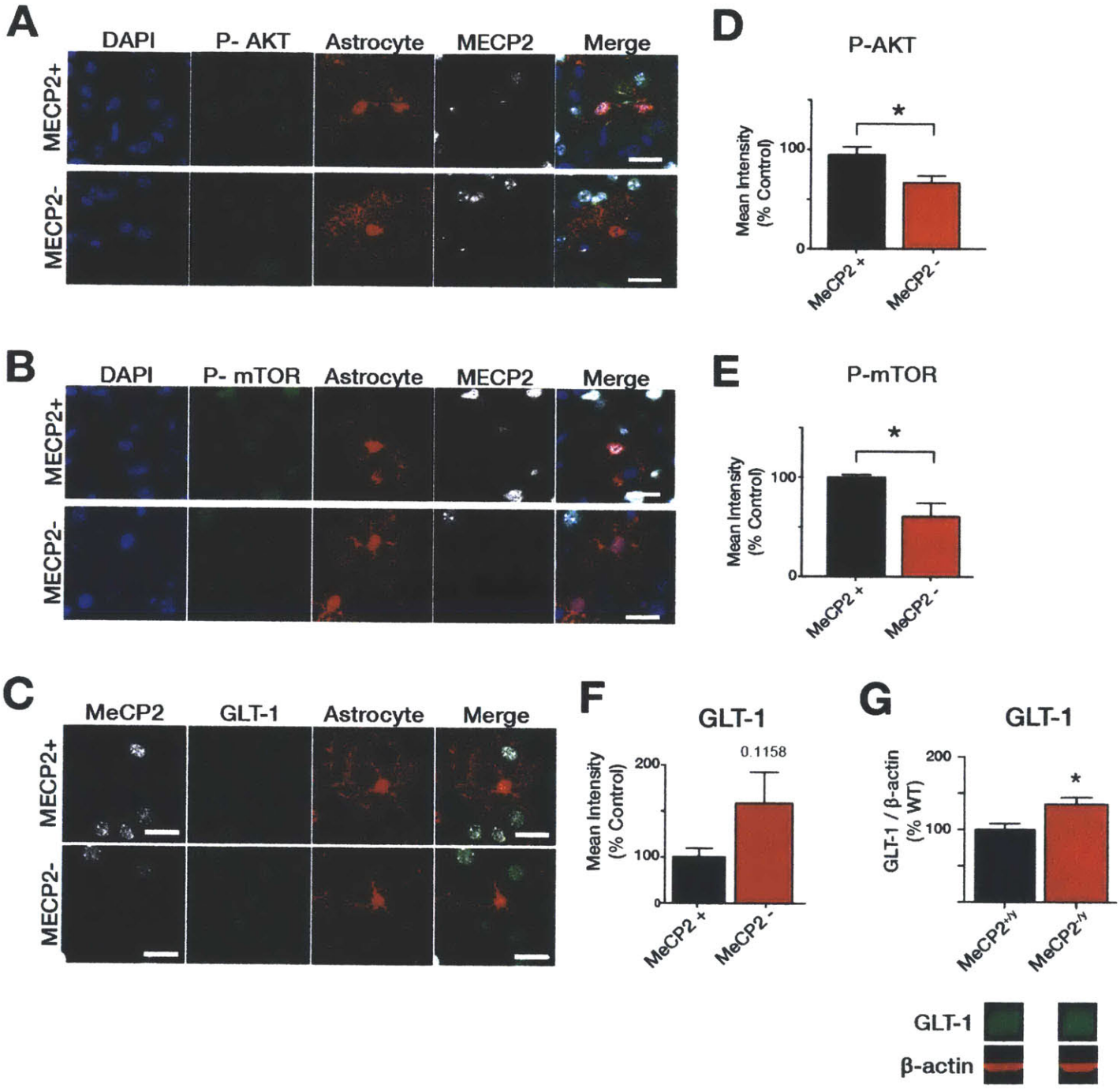


**Figure 2 – Modified level of signaling pathway and transporter protein levels in astrocytes of MeCP2$^{-/+}$ mice.** A-C) Antibody staining for MeCP2 (gray), signaling pathway proteins (A & B, green) and GLT-1 (C, green) in the cortex of MeCP$^{-/+}$ animals. Astrocytes expressing tdTomato (red). Scale bar = 20 μm. D-F) Quantification of mean intensity colocaliazation of P-AKT (D), P-mTOR (E), or GLT-1 (F) with MeCP+ and MeCP2- astrocytes shows a significant decrease in expression for P-AKT and P-mTOR at P28. GLT1 show increased levels. Student's t-test, * $p > 0.05$. For each genotype, n = 12 cells, 4 animals. G) Measurements of cortical whole-cell lysates of MeCP2$^{-/y}$ animals show increased GLT-1 expression. Bands for GLT-1 and internal control depicted below. Student's t-test, * $p > 0.05$. For each

### *4.4.4 Spatially correlated and temporally reliable $Ca^{2+}$ responses in astrocytes.*

We have previously demonstrated that MeCP2-deficient astrocytes exhibit altered synaptic transmission, which can have negative effects on circuit function (Chapter 2). Visually-driven excitatory and inhibitory conductances shape responses of primary cortex neurons, and influence reliability and signal-to-noise ratios. Visually-driven neuronal activity activates MDs of varying sizes in WT animals, with natural movies (NMs) evoking larger MD areas when compared to a drifting grating stimulus or during spontaneous activity (see Chapter 3). Figure 3A shows individual representative cells for which we generated maps of correlated neighboring pixels during spontaneous activity or in response to either NMs or drifting gratings for both MeCP2 heterozygous females ($MeCP2^{-/+}$) and MeCP2-positive litter mates ($MeCP2^{+/+}$). These maps allowed us to isolate regions composed of neighboring pixels with high signal correlations ($R>0.5$) and to assess the extent of this area within each cell (Figure 3B). We found that $MeCP2^{-/+}$ astrocytes had areas of visually-evoked MDs that were overall smaller, which may reflect reduced synaptic and visual drive in these animals. Furthermore, response to NMs was significantly greater in MDs of $MeCP2^{-/+}$ astrocytes than to either gratings or during spontaneous activity (Figure 4A). Comparisons with controls indicated that the MD areas evoked by NMs were significantly reduced in mutant animals (Figure 4B). Furthermore, the amplitude of these responses to the different conditions revealed significant differences: in $MeCP2^{+/+}$ animals, responses to NMs were significantly larger than during spontaneous activity or in response to

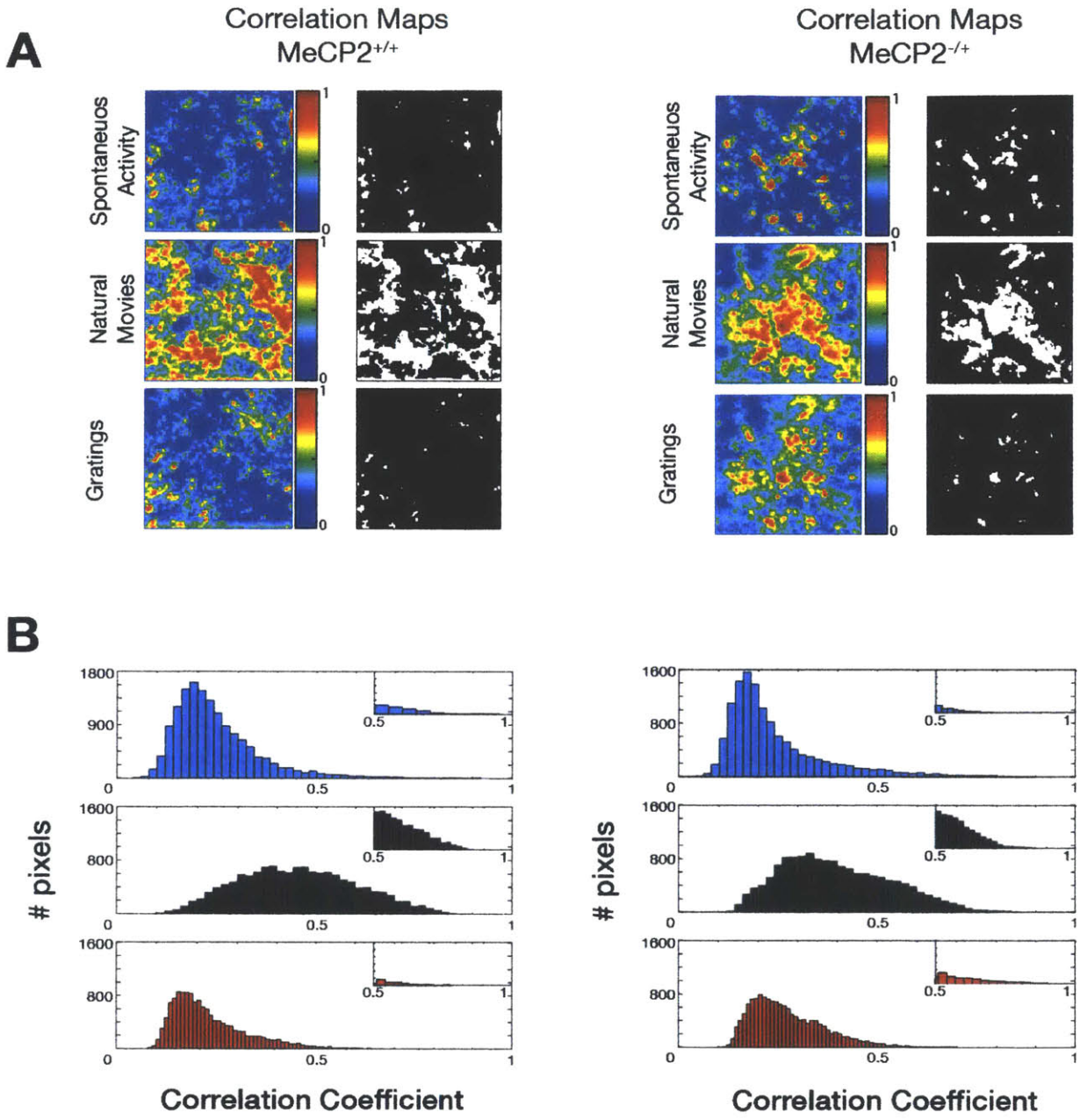


**Figure 3 – Spatially clustered responses in in astrocyte microdomains in MeCP2$^{-/+}$ mice.** A) Heat maps to spontaneous activity or in response to NM or drifting gratings for MeCP2$^{+/+}$ (left) and MeCP2$^{-/+}$ (right) depicting clusters of spatially correlated microdomains (left column) and same maps thresholded showing regions of pixels with significant correlations (R > 0.5, right column). B) Distribution of pixels with corresponding correlation values of representative maps in (A, left columns). Inset shows distribution for significant pixels (R > 0.5).

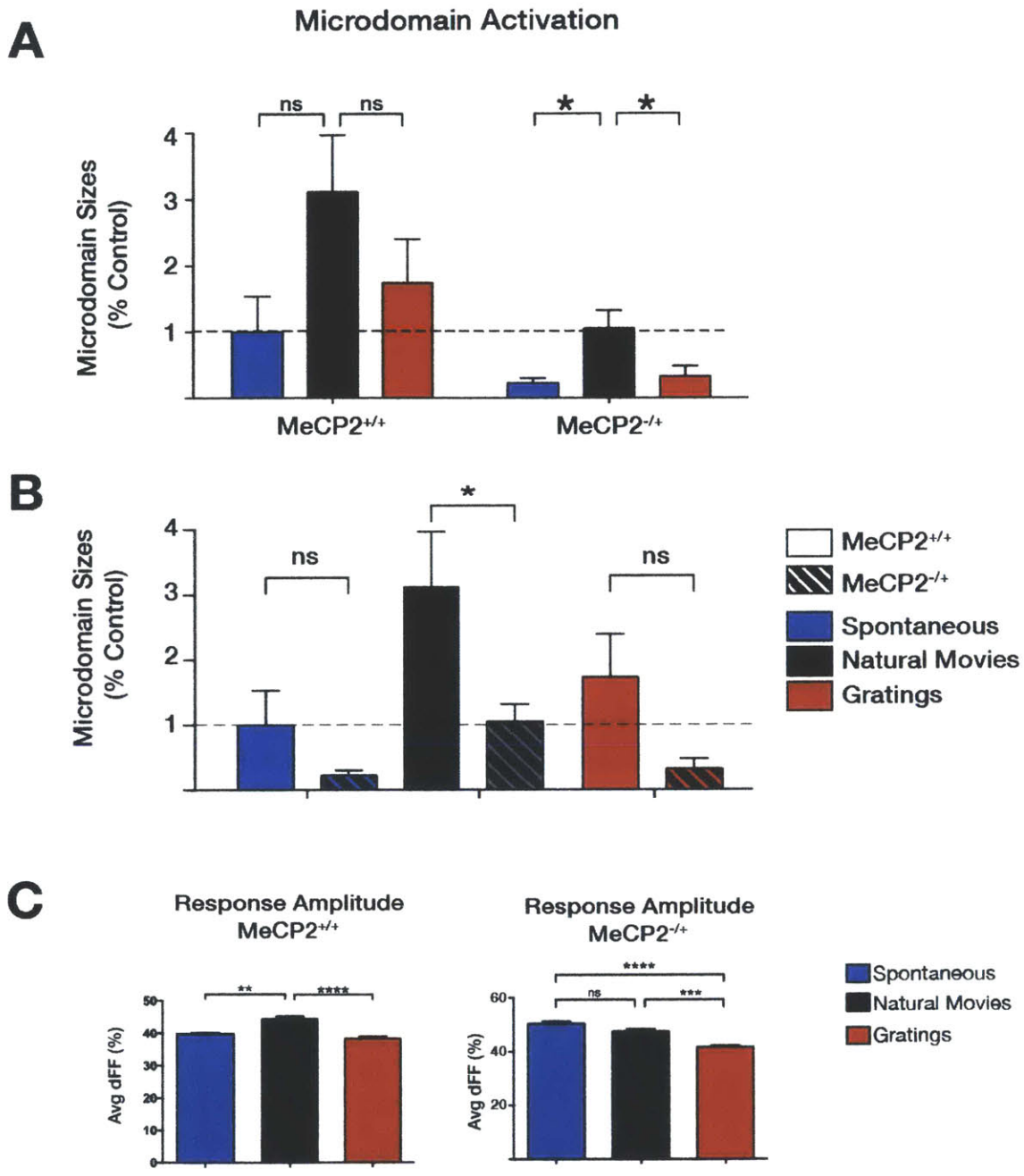


**Figure 4 – Microdomain sizes in MeCP2$^{-/+}$ mice during spontaneous activity or in response to NMs or gratings. and response amplitudes.** A) Overall activation of microdomains measured by the areas with significant signal correlations in maps to spontaneous activity, or response to NM or drifting gratings stimuli, depicted in Figure 3. n = 10 cells for each genotype. One-way ANOVA with Dunnet's multiple comparisons. *, $p < 0.05$. B) Same data as in A) but plotted to compare between conditions accross the genotypes shows significant difference in areas evoked by NMs. Two-way ANOVA with Sidak's multiple comparisons. *, $p < 0.05$. C) Average response amplitudes in regions of interest within correlated regions in microdomains. One-way ANOVA with multiple comparisons; **, $p < 0.01$; ***, $p < 0.001$, ****, $p < 0.0001$.

gratings, while MeCP2$^{-/+}$ mice had significantly smaller amplitudes to gratings, with no differences between spontaneous activity and NMs (Figure 4C).

Efficient processing of visual information requires the coordinated responses of ensembles of neurons, which we hypothesize is one of the driving forces in the increased activation of reliable responses in astrocytic MD. We next asked whether reported impairments of excitation and inhibition balance in MeCP2-deficient mouse models affected the reliability of astrocytic responses to natural movies. We compared the responses evoked by NMs to those of gratings (Figure 5A). In wild type animals we observed significant differences in the amount of reliable MD clustering elicited by NMs as compared to those evoked by drifting gratings, and a similar response was observed in both MeCP2$^{+/+}$ and MeCP2$^{-/+}$ animals (Figure 5B). Interestingly, the average slope of the power spectrum (PS) analysis for each cell did not differ between genotypes (Figure 5C), indicating similar areas with high temporal reliability in MDs of both MeCP2$^{+/+}$ and MeCP2$^{-/+}$ littermates. Due to X-linked inactivation, heterozygous females express functional MeCP2 in only about half of the cell populations. Since we could not differentiate *in vivo* between astrocytes that expressed MeCP2 and those that did not, we looked at the distribution of clustered reliable MDs and found no obvious bimodal effect, which could have indicated a bias towards one cell population or the other (Figure 5D).

## 4.5 Discussion

In this study, we use novel approaches to investigate the effect of the loss of MeCP2 on signaling proteins, glutamate transporters, and visually evoked $Ca^{2+}$ activity

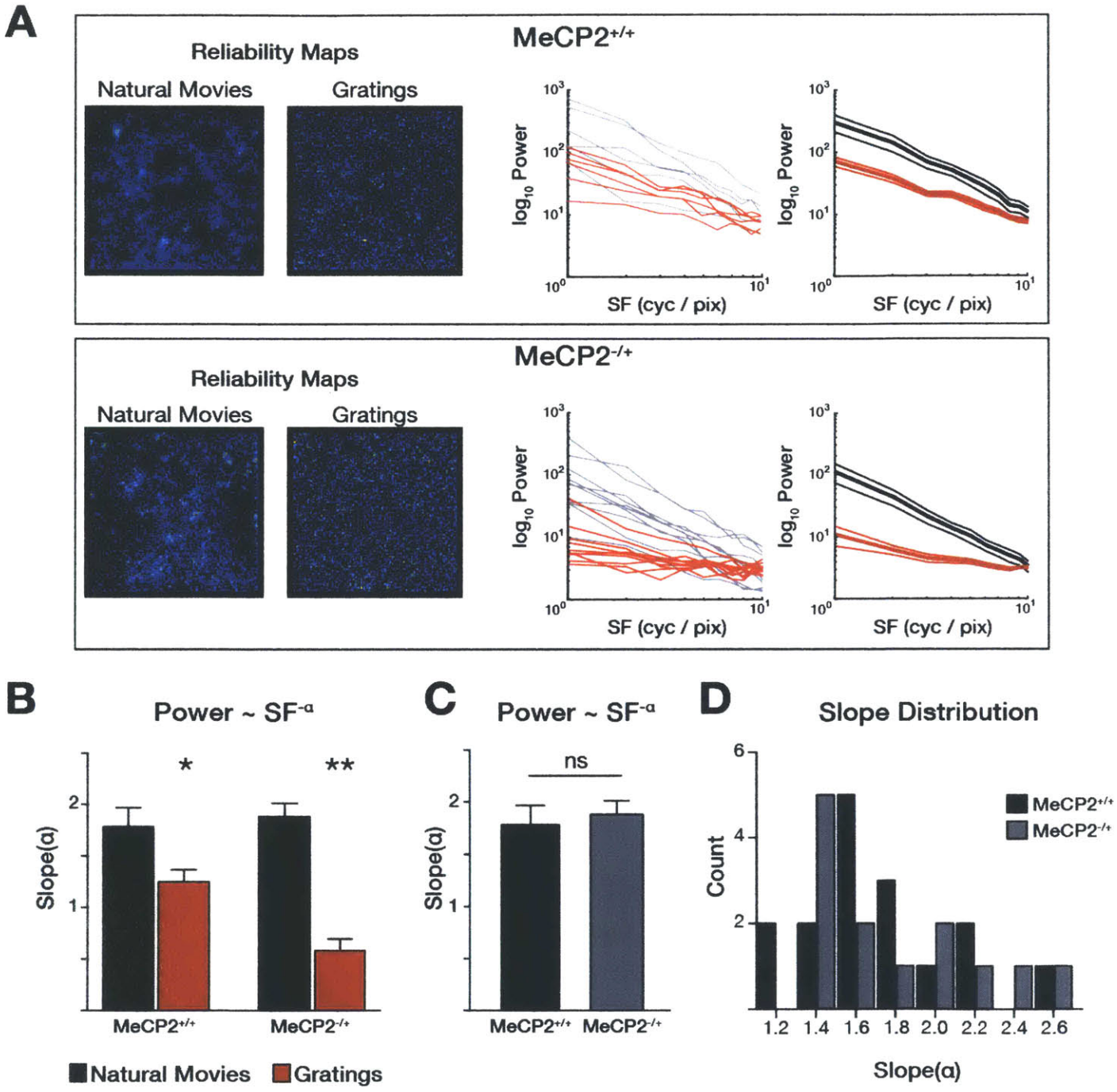


**Figure 5 – Temporally reliable response domains in MeCP2$^{-/+}$ mice.** A) Representative maps of clustering of relliable microdomains for NM and gratings (left) and power spectra for all recorded cells (black traces for NM and red for gratings). MeCP2 female litter-mate controls on top and hets below. B) The average of the slopes of the PS for NM and gratings (one-way ANOVA, * $p > 0.05$, ** $p > 0.01$) . C) Direct comparison of the slopes of the NM shows no significat diferences between genotypes (student's t-test). D) Frequency distrubiton of slope values shows normal distrbutions from all cells recorded. For MeCP2$^{+/+}$, n = 10 cells, 2 animals. for MeCP2$^{-/+}$, n = 10 cells, 3 animals.

in the microdomains (MD) of cortical astrocytes. We find that two key signaling proteins, mTOR and AKT, in astrocytes of female heterozygous MeCP2 mice have reduced levels of activation. Furthermore, we find that GLT-1 protein levels are increased in the cells lacking MeCP2. This increase is corroborated in measurements of cortical astrocytes of male $MeCP2^{-/y}$ mice which lack MeCP2 in all cells. We have previously reported that natural movies (NMs) evoke larger areas of reliable responses in astrocyte MDs. This activation is in part due to more reliable responses from larger number of neurons activated by NMs, and which we show is modulated by reducing the availability of GLT-1 in mature circuits (Chapter 3). In MeCP2 mouse models, we and others have found decreased excitatory synaptic transmission and reduced visual drive (Kang et al., 2013; Castro et al., 2014). Here, we investigated the activation of MDs in visual circuits impaired by the loss of MeCP2. We observe a reduction in the overall area of MDs expressing significant $Ca^{2+}$ responses in $MeCP2^{-/+}$ astrocytes, in line with deficits in overall circuit function. Our previous results (Chapter 3) demonstrated that reduction of GLT-1 levels in adult animals modulated reliable responses, whereas here we found no change in the sizes of reliably activated MDs between $MeCP2^{-/+}$ and $MeCP2^{+/+}$ mice. MeCP2 heterozygous mice represent a developmentally impaired model, and an important issue for astrocyte function lies in how the loss of MeCP2 and increase of GLT-1 impact synaptic and astrocyte development. These findings need further exploration to identify more precisely how the loss of MeCP2 affects astrocytic signaling and circuit function; however, these data contribute to the growing understanding of cell-specific mechanisms in RTT pathophysiology.

Astrocytes contribute to synaptogenesis through the release of soluble factors, first demonstrated in co-cultures of retinal ganglion cells (RGCs) and since then demonstrated in synapses of several neuronal subtypes (Pfrieger and Barres, 1997; Ullian et al., 2001; 2004; Kucukdereli et al., 2011). It has been demonstrated that this is achieved through the release of BDNF and thrombospondin (TSP), among other factors, as well as through contact-mediated signaling (Christopherson et al., 2005). Both the number of synapses and the stability of existing synapses are improved in the presence of astrocytes. It is around the time of synaptogenesis that astrocyte GLT-1 expression levels begin to increase. We and others have demonstrated that MeCP2 can regulated levels of BDNF and IGF-1, both of which are important activators of signaling pathways upstream of cellular maturation and protein synthesis (Li et al., 2013; Castro et al., 2014; Mellios et al., 2014). Data presented here corroborates that signaling molecules in MeCP2 deficient astrocytes are down regulated and the mouse models used suggest a developmental effect involving improper astrocyte protein expression, as observed with GLT-1. A recent *in vivo* study observed that the effects of a developmental loss of MeCP2 selectively in astrocytes resulted in much more severe phenotypes in mouse models than an adult knock-down of MeCP2 in astrocytes (Lioy et al., 2011). We have discovered that loss of MeCP2 leads to reduced levels of IGF-1 and that this loss is most profound earlier during development (Chapter 2). The effects of IGF-1 are most impactful during development and we have demosntrated that treatment with rhIGF-1 can activate signaling pathways and ameliorate some disease phenotypes. Here we show that impaired signaling pathway and altered glutamate

regulation reveal a potential mechanism by which astrocytes contribute to Rett Syndrome pathogenesis by inhibiting normal synaptogenesis and circuit development.

Many factors are known to contribute to the regulation of GLT-1 levels in astrocytes (Karki et al., 2015; Martinez-Lozada and Guillem, 2016). It is worth noting that studies of astrocyte cultures report GLT-1 expression can be induced by activation of PI3/AKT and mTOR pathway activation (Wu et al., 2010; Ji et al., 2011). Importantly, levels of GLT-1 are known to be very low in rat and mouse cultures without neurons present (Swanson et al., 1997; O'Shea et al., 2006; Ghosh et al., 2011). Neuronal activity *in vivo* contributes to increases in GLT-1 - this is especially evident during development when mRNA and protein levels increase during periods of synaptogenesis (Bar-Peled et al., 1997; Furuta et al., 1997). Evidence for neuronally induced regulation of GLT-1 identified nuclear-factor kB (NF-κB) as an important transcriptional regulator, and inhibiting NF-κB blocked neuronally dependent induction of GLT-1 (Yang et al., 2009; Ghosh et al., 2011). These studies imply that reduced neuronal activity or mTOR and AKT signaling would lead to reduction of GLT-1 levels. However, a recent study revealed that NF-κB signaling pathway is up regulated with the loss of MeCP2 function, and genetic attenuation of pathway activation improved aberrant dendritic morphology and improved the overall health of the animal (Kishi et al., 2016). Other factors converging on NF-κB can induce expression of GLT-1, and we believe future measurements using techniques outlined here would be informative in uncovering mechanisms contributing to GLT-1 dysregulation in RTT astrocytes.

Localization of GLT-1 on the surface of astrocytes is vital to their function and clustering has been observed in developing astrocyte processes near synapses (Zhou

and Sutherland, 2004; Benediktsson et al., 2012) . Diffusion across astrocyte membranes is reduced near glutamatergic synapses, and it is believed that surface trafficking of GLT-1 to active synapses is another mechanism by which synaptic transmission is regulated (Murphy-Royal et al., 2015). Mitochondria are also linked to areas of GLT-1 activity as well as buffering and regulation of $Ca^{2+}$ transients in astrocytic processes; however, the effect of MeCP2 reduction on this function is not known at this time (Jackson et al., 2014; Jackson and Robinson, 2015; Stephen et al., 2015). The clustering and trafficking of GLT-1 leading to the observed increase in GLT-1 protein levels after MeCP2 reduction requires further investigation.

Our own work and that of others has identified that loss of MeCP2 affects excitatory / inhibitory balance in cortical circuits, synaptic transmission, and visual drive (Durand et al., 2012; Castro et al., 2014; He et al., 2014b). While synaptic activity may be affected in MeCP2 deficient circuits, increased glutamate (Glu) uptake may be required in these mouse models. Microglia lacking MeCP2 can cause dendritic and synaptic damage by excessive Glu release and cerebrospinal fluid of RTT patients is reported to have elevated Glu levels (Lappalainen and Riikonen, 1996; Maezawa and Jin, 2010). Increased transporter levels on astrocytes may be a homeostatic response to such increases. One study revealed that cultured astrocytes from MeCP2-null brains exhibited more efficient Glu clearance, increased GLT-1 mRNA, and prolonged GLT-1 protein levels after exposure to Glu. Our observation of increased GLT-1 levels and potential effects on microdomain activation must be taken in the context of the feedforward and feedback or homeostatic impact of MeCP2 reduction on development of synapses and circuits (Zhou and Danbolt, 2013; Karki et al., 2015); however, these

findings implicate GLT-1 dysregulation as a contributor to reduced glutamate availability underlying circuit E/I imbalances.

With these emerging findings we have provided additional evidence for the role of astrocytes in Rett pathophysiology by showing that MeCP2: (1) regulates astrocyte signaling pathways, (2) leads to increased levels of GLT-1 selectively in MeCP2-null cells, and (3) implicates glutamate clearance in synaptic and circuit dysfunction. Our ability to visualize astrocytes *in situ* and *in vivo* are tools with which we can further probe mechanisms and cell-specific effects on sensory processing. Future work should aim to further elucidate the role of astrocyte specific loss of MeCP2 function, in particular by combining methods developed in this study with cell-specific knock-out. Additionally, the ability of rhIGF1 to ameliorate these deficits deserves careful examination.

## 4.6 References


Adachi M, Autry AE, Covington HE, Monteggia LM (2009) MeCP2-mediated transcription repression in the basolateral amygdala may underlie heightened anxiety in a mouse model of Rett syndrome. Journal of Neuroscience 29:4218–4227.

Ballas N, Lioy DT, Grunseich C, Mandel G (2009) Non-cell autonomous influence of MeCP2-deficient glia on neuronal dendritic morphology. Nat Neurosci 12:311–317.

Bar-Peled O, Ben-Hur H, Biegon A, Groner Y, Dewhurst S, Furuta A, Rothstein JD (1997) Distribution of glutamate transporter subtypes during human brain development. J Neurochem 69:2571–2580.

Benediktsson AM, Marrs GS, Tu JC, Worley PF, Rothstein JD, Bergles DE, Dailey ME (2012) Neuronal activity regulates glutamate transporter dynamics in developing astrocytes. Glia 60:175–188.

Castro J, Garcia RI, Kwok S, Banerjee A, Petravicz J, Woodson J, Mellios N, Tropea D, Sur M (2014) Functional recovery with recombinant human IGF1 treatment in a mouse model of Rett Syndrome. PNAS 111:9941–9946.

Cheng Q, Yeh HH (2003) Brain-derived neurotrophic factor attenuates mouse cerebellar granule cell GABAA receptor-mediated responses via postsynaptic mechanisms. The Journal of Physiology 548:711–721.

Christopherson K, Ullian E, Stokes C, Mullowney C, Hell J, Agah A, Lawler J, Mosher D, Bornstein P, Barres B (2005) Thrombospondins are astrocyte-secreted proteins that promote CNS synaptogenesis. Cell 120:421–433.

Durand S, Patrizi A, Quast KB, Hachigian L, Pavlyuk R, Saxena A, Carninci P, Hensch TK, Fagiolini M (2012) NMDA receptor regulation prevents regression of visual cortical function in the absence of Mecp2. Neuron 76:1078–1090.

Fontana ACK (2015) Current approaches to enhance glutamate transporter function and expression. J Neurochem 134:982–1007.

Furuta A, Rothstein JD, Martin LJ (1997) Glutamate transporter protein subtypes are expressed differentially during rat CNS development. The Journal of Neuroscience 17:8363–8375.

Fyffe SL, Neul JL, Samaco RC, Chao H-T, Ben-Shachar S, Moretti P, McGill BE, Goulding EH, Sullivan E, Tecott LH, Zoghbi HY (2008) Deletion of Mecp2 in Sim1-expressing neurons reveals a critical role for MeCP2 in feeding behavior, aggression, and the response to stress. Neuron 59:947–958.

Ghosh M, Yang Y, Rothstein JD, Robinson MB (2011) Nuclear Factor- B Contributes to Neuron-Dependent Induction of Glutamate Transporter-1 Expression in Astrocytes. The Journal of

Neuroscience 31:9159–9169.

Greenberg ME, Xu B, Lu B, Hempstead BL (2009) New Insights in the Biology of BDNF Synthesis and Release: Implications in CNS Function. The Journal of Neuroscience 29:12764–12767.

Guy J, Hendrich B, Holmes M, Martin JE, Bird A (2001) A mouse Mecp2-null mutation causes neurological symptoms that mimic Rett syndrome. Nature Genetics 27:322–326.

He L-J, Liu N, Cheng T-L, Chen X-J, Li Y-D, Shu Y-S, Qiu Z-L, Zhang X-H (2014a) Conditional deletion of Mecp2 in parvalbumin-expressing GABAergic cells results in the absence of critical period plasticity. Nat Comms 5:5036.

He L-J, Liu N, Cheng T-L, Chen X-J, Li Y-D, Shu Y-S, Qiu Z-L, Zhang X-H (2014b) Conditional deletion of Mecp2 in parvalbumin-expressing GABAergic cells results in the absence of critical period plasticity. Nat Comms 5:5036.

Jackson JG, O'Donnell JC, Takano H, Coulter DA, Robinson MB (2014) Neuronal activity and glutamate uptake decrease mitochondrial mobility in astrocytes and position mitochondria near glutamate transporters. Journal of Neuroscience 34:1613–1624.

Jackson JG, Robinson MB (2015) Reciprocal Regulation of Mitochondrial Dynamics and Calcium Signaling in Astrocyte Processes. Journal of Neuroscience 35:15199–15213.

Ji Y-F, Xu S-M, Zhu J, Wang X-X, Shen Y (2011) Insulin increases glutamate transporter GLT1 in cultured astrocytes. Biochemical and Biophysical Research Communications 405:691–696.

Jiang M, Ash RT, Baker SA, Suter B, Ferguson A, Park J, Rudy J, Torsky SP, Chao HT, Zoghbi HY, Smirnakis SM (2013) Dendritic Arborization and Spine Dynamics Are Abnormal in the Mouse Model of MECP2 Duplication Syndrome. Journal of Neuroscience 33:19518–19533.

Kang E, Durand S, LeBlanc JJ, Hensch TK, Chen C, Fagiolini M (2013) Visual Acuity Development and Plasticity in the Absence of Sensory Experience. Journal of Neuroscience 33:17789–17796.

Karki P, Smith K, Johnson J Jr, Aschner M, Lee EY (2015) Genetic Dys-regulation of Astrocytic Glutamate Transporter EAAT2 and its Implications in Neurological Disorders and Manganese Toxicity. Neurochem Res 40:380–388.

Kim K, Lee S-G, Kegelman TP, Su Z-Z, Das SK, Dash R, Dasgupta S, Barral PM, Hedvat M, Diaz P, Reed JC, Stebbins JL, Pellecchia M, Sarkar D, Fisher PB (2011) Role of Excitatory Amino Acid Transporter-2 (EAAT2) and glutamate in neurodegeneration: Opportunities for developing novel therapeutics. J Cell Physiol 226:2484–2493.

Kishi N, MacDonald JL, Ye J, Molyneaux BJ, Azim E, Macklis JD (2016) Reduction of aberrant NF-κB signalling ameliorates Rett syndrome phenotypes in Mecp2-null mice. Nat Comms 7:10520.

Krishnan K, Wang B-S, Lu J, Wang L, Maffei A, Cang J, Huang ZJ (2015) MeCP2 regulates the timing of critical period plasticity that shapes functional connectivity in primary visual cortex. P Natl Acad Sci Usa:201506499.

Kucukdereli H, Allen NJ, Lee AT, Feng A, Ozlu MI, Conatser LM, Chakraborty C, Workman G, Weaver M, Sage EH, Barres BA, Eroglu C (2011) Control of excitatory CNS synaptogenesis by astrocyte-secreted proteins Hevin and SPARC. PNAS 108:E440–E449.

Lappalainen R, Riikonen RS (1996) High levels of cerebrospinal fluid glutamate in Rett syndrome. Pediatr Neurol 15:213–216.

Li W, Pozzo-Miller L (2014) BDNF deregulation in Rett syndrome. Neuropharmacology 76 Pt C:737–746.

Li Y, Wang H, Muffat J, Cheng AW, Orlando DA, Lovén J, Kwok S-M, Feldman DA, Bateup HS, Gao Q, Hockemeyer D, Mitalipova M, Lewis CA, Vander Heiden MG, Sur M, Young RA, Jaenisch R (2013) Global transcriptional and translational repression in human-embryonic-stem-cell-derived Rett syndrome neurons. Cell Stem Cell 13:446–458.

Lioy DT, Garg SK, Monaghan CE, Raber J, Foust KD, Kaspar BK, Hirrlinger PG, Kirchhoff F, Bissonnette JM, Ballas N, Mandel G (2011) A role for glia in the progression of Rett's syndrome. Nature.

Maezawa I, Jin L-W (2010) Rett syndrome microglia damage dendrites and synapses by the elevated release of glutamate. Journal of Neuroscience 30:5346–5356.

Maezawa I, Swanberg S, Harvey D, LaSalle JM, Jin L-W (2009) Rett syndrome astrocytes are abnormal and spread MeCP2 deficiency through gap junctions. Journal of Neuroscience 29:5051–5061.

Martinez-Lozada Z, Guillem AM (2016) Transcriptional Regulation of Glutamate Transporters: From Extracellular Signals to Transcription Factors. Advances in Pharmacology.

Mellios N, Woodson J, Garcia RI, Crawford B, Sharma J, Sheridan SD, Haggarty SJ, Sur M (2014) β2-Adrenergic receptor agonist ameliorates phenotypes and corrects microRNA-mediated IGF1 deficits in a mouse model of Rett syndrome. PNAS 111:9947–9952.

Murphy-Royal C, Dupuis JP, Varela JA, Panatier A, Pinson B, Baufreton J, Groc L, Oliet SHR (2015) Surface diffusion of astrocytic glutamate transporters shapes synaptic transmission. Nat Neurosci.

O'Shea RD, Lau CL, Farso MC, Diwakarla S, Zagami CJ, Svendsen BB, Feeney SJ, Callaway JK, Jones NM, Pow DV, Danbolt NC, Jarrott B, Beart PM (2006) Effects of lipopolysaccharide on glial phenotype and activity of glutamate transporters: Evidence for delayed up-regulation and redistribution of GLT-1. Neurochemistry International 48:604–610.

Pfrieger FW, Barres BA (1997) Synaptic efficacy enhanced by glial cells in vitro. Science 277:1684–1687.

Ricciardi S, Boggio EM, Grosso S, Lonetti G, Forlani G, Stefanelli G, Calcagno E, Morello N, Landsberger N, Biffo S, Pizzorusso T, Giustetto M, Broccoli V (2011) Reduced AKT/mTOR signaling and protein synthesis dysregulation in a Rett syndrome animal model. Human Molecular Genetics 20:1182–1196.

Sahin M, Sur M (2015) Genes, circuits, and precision therapies for autism and related neurodevelopmental disorders. Science 350:aab3897–aab3897.

Sebastian-Leon P, Vidal E, Minguez P, Conesa A, Tarazona S, Amadoz A, Armero C, Salavert F, Vidal-Puig A, Montaner D, Dopazo J (2014) Understanding disease mechanisms with models of signaling pathway activities. BMC Systems Biology 2014 8:1 8:1.

Stephen TL, Higgs NF, Sheehan DF, Awabdh Al S, Lopez-Domenech G, Arancibia-Carcamo IL, Kittler JT (2015) Miro1 Regulates Activity-Driven Positioning of Mitochondria within Astrocytic Processes Apposed to Synapses to Regulate Intracellular Calcium Signaling. The Journal of Neuroscience 35:15996–16011.

Swanson RA, Liu J, Miller JW, Rothstein JD, Farrell K, Stein BA, Longuemare MC (1997) Neuronal regulation of glutamate transporter subtype expression in astrocytes. The Journal of Neuroscience 17:932–940.

Ullian E, Christopherson K, Barres B (2004) Role for glia in synaptogenesis. Glia 47:209–216.

Ullian EM, Sapperstein SK, Christopherson KS, Barres BA (2001) Control of synapse number by glia. Science 291:657–661.

Wu X, Kihara T, Akaike A, Niidome T, Sugimoto H (2010) PI3K/Akt/mTOR signaling regulates glutamate transporter 1 in astrocytes. Biochemical and Biophysical Research Communications 393:514–518.

Yang Y, Gozen O, Watkins A, Lorenzini I, Lepore A, Gao Y, Vidensky S, Brennan J, Poulsen D, Won Park J, Li Jeon N, Robinson MB, Rothstein JD (2009) Presynaptic regulation of astroglial excitatory neurotransmitter transporter GLT1. Neuron 61:880–894.

Zhou J, Sutherland ML (2004) Glutamate transporter cluster formation in astrocytic processes regulates glutamate uptake activity. Journal of Neuroscience 24:6301–6306.

Zhou Y, Danbolt NC (2013) GABA and Glutamate Transporters in Brain. Frontiers in Endocrinology 4:165.